Analysis of Composites Recycling and Thermal Oxidative Treatments On Carbon Fibre

BY

Joseph Paul Heil

Thesis submitted to the University of Nottingham for the degree of

Doctor of Philosophy

January 2016

Abstract

The process of carbon fibre composite recycling has been analysed and broken down into the thermal-kinetic behaviours of the constituent components of the composite and the reduction in mechanical properties of the recycled carbon fibres. Carbon fibre recycling has been a commercial operation since 2009 and the subject of extensive research for the last 10-15 years, with many years before that looking at glass fibre composites. However, very little work has been published regarding the optimization of the recycling process or a scientific explanation as to how the mechanical properties of the fibres are affected by the recycling.

This research hypothesises that the tensile strength and elastic modulus are intimately linked to the microstructural changes that happen to the fibre as a result of its exposure to the hot oxidising environment used for carbon fibre recycling. To investigate this hypothesis a lab-scale carbon fibre recycling operation was built using a tube furnace and gas flow controllers. Carbon fibre-epoxy composites were recycled between 550^{o}C and 650^{o}C in varying oxygen concentrations between 0% and 21% for up to forty minutes to find recycling results representative of what is used commercially. Once this time, temperature, oxygen concentration parameter space was established, sized virgin fibres were recycled under these same conditions. Raman, XRD, XPS and single filament tensile testing were used to characterise the fibres before and after recycling. High strength and intermediate modulus fibres from both Hexcel and Toray were studied. Fibre type, fibre manufacturer, time, temperature, and oxygen concentration were used as factors in a design of experiments. Microstructural parameters, tensile strength, and elastic modulus were measured as responses. The microstructure of the recycled fibres was found to change in unpredictable ways. Temperature and the interaction of temperature with

oxygen concentration were the most significant terms in the design of experiments. Time was not a significant factor on its own. AS4 and IM7 fibres from Hexcel were discovered to have an acute sensitivity to high temperatures and oxygen concentrations compared to T700 and T800S fibres from Toray.

To better understand the recycling process itself a thermal-kinetic model is utilized to describe the oxidative decomposition of the composite. The recycling process is broken down into three reactions: pyrolysis, char oxidation, and fibre oxidation. TGA and DSC were used to characterise each of these reactions. The model uses a 1D finite difference method to predict the heat and mass flow through the composite over time. Temperature, composition of the composite, and mass flux are calculated for and between each of the model's discrete layers. Any intermediate result may be printed to a text file for viewing or supplementary analysis. Most of the model parameters are based on user input, which makes the model a flexible and powerful tool for investigating carbon fibre composite recycling. The user defines the thickness and composition of the composite system of interest as well as the recycling time and operating temperature.

Different resin systems can be studied as well as different thermal recycling methods by changing parameters in the model such as the heat transfer coefficient and defining what happens to the fibre once all the resin has been removed from it. For example, in the fluidised bed process the fibre leaves the recycling atmosphere, but for a belt furnace, fibre stays in the furnace for the entire duration of the process. The model is used to determine how long it takes for the pyrolysis and char oxidation reactions to occur which then tells how long a fibre is exposed to the recycling atmosphere for a process of a fixed duration.

Table of Contents

Nomenclature

ANOVA – Analysis of Variance

BET - Brunauer-Emmett-Teller

CF – Carbon Fibre

CFRP- Caron Fibre Reinforced Plastic

COV – Coefficient of Variation

DOE – Design of Experiments

HS – High Strength

HTT- Heat Treatment Temperature

IM – Intermediate Modulus

PAN – Polyacrylonitrile

rCF – Recycled Carbon Fibre

rCFRP – Recycled Carbon Fibre Reinforced Plastic

SEM – Scanning Electron Microscopy

SFTT – Single Fibre Tensile Test

SM – Standard Modulus

TEM – Transmission Electron Microscopy

TGA – Thermogravimetric Analysis

XPS – X-ray Photoelectron Spectroscopy

XRD – X-Ray Diffraction

1. Introduction

Use of carbon fibre composites is a rapidly growing as they offer phenomenal strength to weight ratios and design flexibility. However, concerns over the life cycle of carbon fibre composites (CFRP) limits the adoption of CFRP into new products. Composite structures often outlast the life cycle of the device they are used in and due to their energy and materials intensive construction, users are reluctant to simply dispose of the composite structure. Additionally, European Union legislation such as the End-of-Life Vehicles directive (ELV) (directive 2000/53/EC)[1] and Landfill Directives (directive 1999/31/EC)[2], places limits on how much material can be landfilled or incinerated in addition to recommendations on how much material should be recycled or reused. The ELV mandated that by 2006 at least 85% of a vehicle's materials shall be reused or recovered and that reuse and recycling shall be used to re-use or recover 80% of the vehicle by weight. Additionally, in 2015 reuse and recovery targets were set to increase to 95% reuse and recovery and 85% reuse and recycling. The Landfill Directive restricted the amount of biodegradable material, including composites, that can be landfilled to 35% of the 1995 levels by 2006 [2]. Pimenta and Pinho suggest that the cost to legally landfill composites can be a substantial motivator for recycling [3]. Carbon fibre recycling provides an avenue to manage the environmental impact of using CFRP. Carbon fibre recycling is the reuse of dry fibre or the reuse of cured materials in new materials or the process of removing the resin matrix to recover the more valuable carbon fibre. At present the amount of composite waste that is recycled is at most 10%, in part because the recycled fibres are most often not as strong as they were originally.

Loss of fibre strength and stiffness as a result of carbon fibre composite recycling has been documented by many organisations for multiple different types of recycling processes [3, 4]. Trying to optimise a recycling process for a given feedstock has been met with relative success by several organisations. The success is relative because the result is always a compromise. For example Adherent Technologies combined their vacuum cracking and wet chemical breakdown processes to handle ‘next generation’ composite materials such as the Boeing 787 fuselage, but the combined process ran much slower than either of the individual processes on their own [5]. ELG Carbon Fibre Ltd. cite excellent tensile strength retention of their fibres but at lengths of 80-100 µm [6]. The University of Nottingham demonstrated a fluidised bed recycling process that could handle end of life materials with metal and honeycomb contamination as well as manufacturing scrap, but the strength retention suffers (50% for 25 mm long fibres [7] and 75% for 10 mm long fibres [8]). So far no one has tried to understand what physical or chemical change damages the fibre and how that change is imparted by the recycling process. The work presented here will evaluate the mechanical properties, microstructure, and surface chemistry of recycled fibres in order to develop relationships between recycling conditions and the structure and chemistry of the fibres; the work also evaluates the relationships between the structure and chemistry of the fibres and their mechanical properties. The link between the structure and chemistry and mechanical properties is valuable since it is recycling process independent.

Recycling processes can broadly be classified as mechanical, thermal, or thermo-chemical. Thermal processes have shown the most potential for scale up to processing rates needed for commercial viability [3, 4]. Therefore a thermal process will be pursued in this work. When a composite is thermally recycled there are several reactions that take place to remove the polymer matrix. First, at low temperatures (150^{o}C-250^{o}C for epoxy) the matrix undergoes devolatilization where gases trapped during the manufacturing process and adsorbed species escape. From 250^{o}C – 450^{o}C there is additional devolatilization of low molecular weight species in the resin. 150^{o}C-250^{o}C is where most of the devolatilization occurs, however some species may require higher temperatures. The next stage is pyrolysis which begins most noticeably between 450^{o}C – 500^{o}C, but sustained temperatures of less than 550^{o}C are ineffective for recycling. At temperatures between 250^{o}C and 450^{o}C both pyrolysis and devolatilization occur but it can be difficult to determine which if either reaction is dominant. Pyrolysis means in the absence of oxygen, but a pyrolysis stage is assigned to polymer decomposition even in an oxidative atmosphere [7]. During pyrolysis polymer chains break into shorter lengths, and eventually cover the surface of the fibre in char: a carbon rich, dense, and unreactive material. Pyrolysis on its own, even at elevated temperatures, will not produce clean fibres [9], but vacuum pyrolysis has been shown to be an effective method of carbon fibre recycling [10]. During the final step of recycling the char undergoes oxidation where oxygen reacts with the carbon in the char to form CO_2 and other gases. Oxidation effectively cleans the fibre, however there is nothing stopping the fibre from also being oxidised, which results in damage and loss of mechanical properties. In a vacuum pyrolysis process, the atmospheric pressure is so low that low molecular weight species volatilize with minimal heating. Higher molecular weight polymer chains, such as those that make the epoxy resin, cleanly volatilize and can easily be collected as a liquid fuel or sent to an afterburner for gas treatment, as opposed to forming char on the fibre surface. To further explore how carbon fibre recycling removes the resin matrix of a composite to leave only fibres, a thermal–kinetic model for composite recycling was written in the Java programming language.

Microstructure is a term for describing how a material is organised at an atomic level (~10-100 nm [11]). The microstructure of carbon fibre describes the formation and quality of graphite planes, the organization of these planes with respect to each other (like how well they stack and in which direction), and how these planes are aligned with respect to the fibre axis. Different types of carbon fibres have slight differences in crystal quality, size and orientation, and interplanar spacing which should be responsible for the differences in properties between types of carbon fibre. Structural differences between PAN and Pitch precursor or between Intermediate Modulus and High Strength fibres are well documented, but the difference between two fibres of the same type like Toray T800S and Hexcel IM7 cannot necessarily be predicted as it depends on the manufacturing process [12].

The work presented in this thesis has four main sequential components: determination of appropriate recycling conditions, simulated thermal recycling of fibres using an approach developed with a tube furnace, carbon fibre composite recycling model development, and model validation.

To determine the appropriate recycling conditions for the second component of this study, carbon fibre epoxy composites were recycled in a tube furnace under a range of time, temperature, and oxygen concentrations. The composites were made from Toray T700 carbon fibre and Umeco MTM 57 or Umeco MTM 44 resin films. T700 is the strongest fibre in Toray’s high strength/ standard modulus range and is used in industrial and recreational applications [13]. MTM 57 and MTM 44 are both epoxy resins, but MTM 44 has a higher glass transition temperature and is more suited for aerospace compared to MTM 57 which is more commonly used for automotive and industrial applications [14, 15]. MTM 44 represents a structural aerospace grade resin with a 180ºC cure temperature while MTM 57 is a 120ºC cure and would be used for automotive structures. The structural chemistry of MTM 44 and MTM 57 is proprietary and no further information than that in the product data sheets about the differences between MTM 44 and MTM 57 was available. Once an appropriate set of conditions was established, a Design of Experiments (DOE) based on the first component of work was used to build an understanding of how processing conditions influenced a wide range of structural, mechanical, and chemical properties of the recycled fibres during the second stage of this work.

In the third stage of this work, an innovative model for composite recycling was developed that uses the kinetics of the oxidation reactions that occur during recycling to determine mass loss and temperature distribution of a piece of composite as it undergoes recycling. The model is a tool to virtually study and optimise thermal recycling processes. Different processes such as The University of Nottingham's fluidised bed or ELG's belt furnace can be represented with the model by changing just a few input parameters. A huge advantage of the model over a physical experiment is the ability to change things like material type and thickness, temperature, or process time which may not be practical or possible to change. In the fourth component of this work the thermal-kinetic model is compared to weight loss and temperature distributions of composites tested in the lab.

A review of carbon fibre structure and its impact on thermal and mechanical properties is presented in the next chapter along with an overview on the state of carbon fibre recycling. Section 3 reviews the experimental methodology and how certain general procedures may have been refined and optimized for testing carbon fibre. A more detailed explanation and justification of the experimental studies is found in sections 4 and 5. Results from recycling solely fibres are reviewed in sections 6 - 8. The development and validation of the thermal model are found in sections 9 and 10, respectively. Conclusions from the entire study are presented in the final section.

2. Literature Review

2.1 Structure of Carbon Fibres

During the 1970s and into early 1980s (the early days of the carbon fibre industry), carbon and graphite fibres were interchangeably used to describe polymer derived carbon fibres. However, significant differences between polymer precursor *carbon* fibres and pitch precursor *graphite* fibres are found in their crystal structure and other physical properties. For example the thermal conductivity of Polyacrylonitrile (PAN) based fibres ranges from 8-105 W/m·K while for pitch based fibres it is around 1000 W/m·K [12]. Similarly, the crystal size in PAN fibres is 1.4-3.92 nm and for pitch fibres it is 10.25-17 nm [16]. Using the terms, carbon and graphite, interchangeably would thus be quite confusing when discussing developments in carbon fibre technology.

For polymeric carbon fibres, a promising description of the structure uses graphite planes as the fundamental building blocks. The unit cell of graphite is shown in Figure 1. These unit cells form small graphite like sheets such as those seen in Figure 2. The crystalline sheets are linked together with amorphous material (the squiggles in Figure 2) which provide very little strength or stiffness.

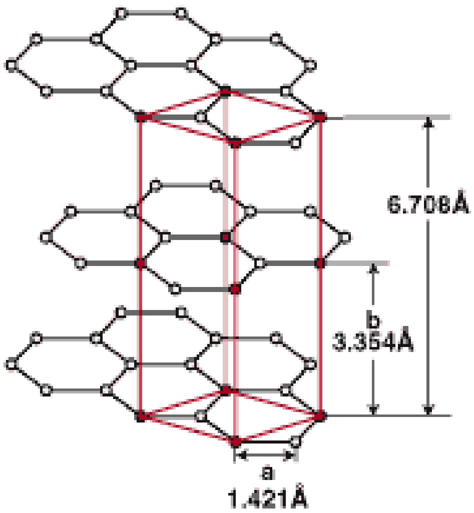

Figure 1 Unit cell of graphite [17]

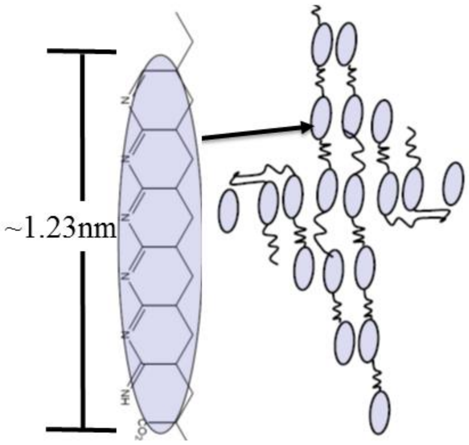

Figure 2. Crystalline and Amorphous regions in fibrils[18]

Figure 3 helps to show the hierarchy of the carbon fibre structure. The assembly of lamella units in Figure 2 form a fibril which has many fibre-like properties but is actually a subassembly of a fibre as shown in Figure 3. These assemblies are what constitute a crystal in terms of XRD analysis; Figure 3 shows the orientation of graphite crystals with respect to the fibre and also various measures of crystal size.

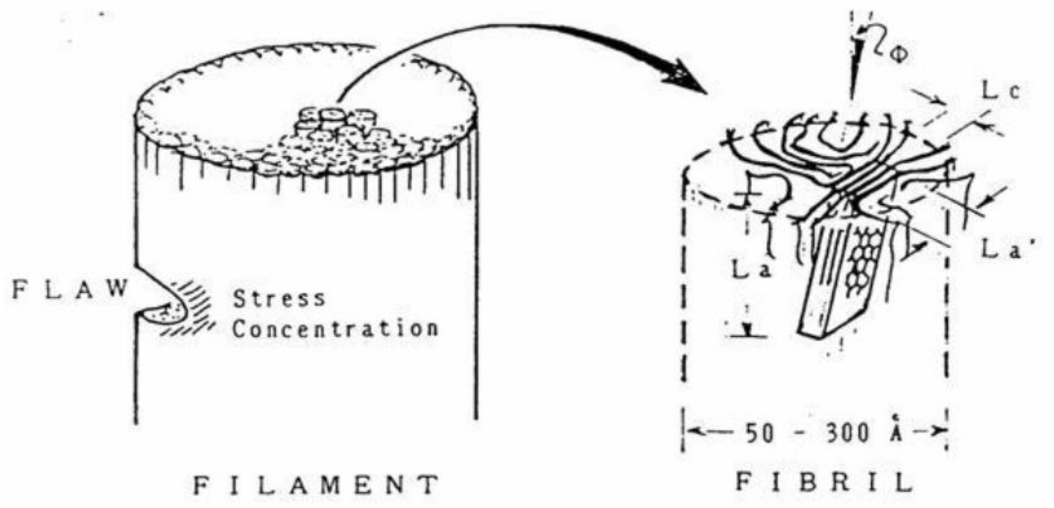

Figure 3. Scale of carbon fibre structures [18]

The commonly cited structural model of PAN carbon fibres as proposed by DJ Johnson [19] is sheets of graphite bent around the C-axis of the fibre (Figure 4). Even though Figure 4 was created before the availability of the X-ray data informing the depiction in Figure 2, it arguably takes into account the amorphous regions seen in Figure 2 and shows how graphite sheets could imperfectly pack into a fibril.

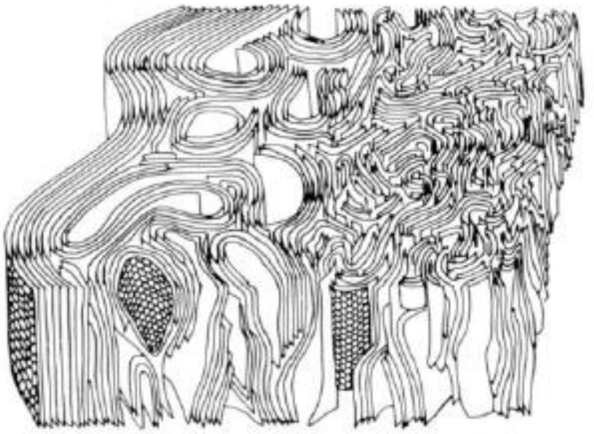

Figure 4 Schematic three-dimensional representation of structure in PAN-based high modulus carbon fibres. Fibres of lower modulus will have a more disordered structure [19].

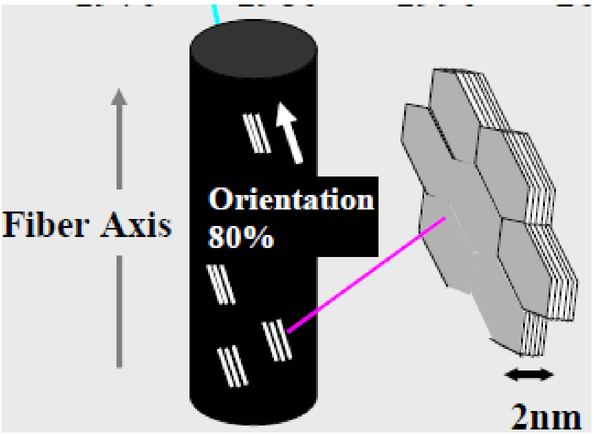

Figure 5 Incorporation of graphite planes in carbon fibre [20]

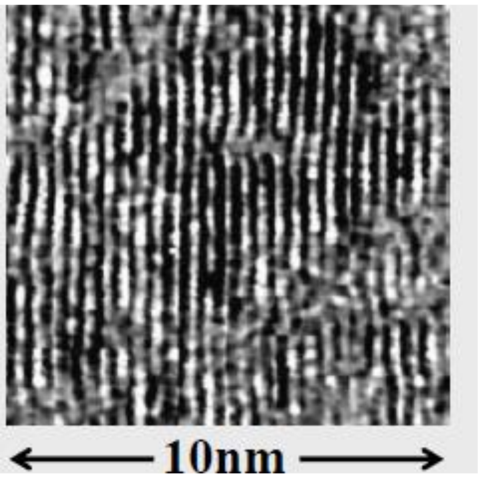

Figure 6 TEM of cross sectional view of graphite planes [20]

At the macro scale, fibrils are not discrete units and the surface of carbon fibre appears homogenous. The lamellae within a fibril are oriented at an angle with respect to the fibre axis as shown in Figure 3 and in the simplified diagram in Figure 5. Figure 6 is a TEM micrograph showing how the graphite planes in a fibril actually look.

Carbon fibres are commonly available in three different ranges of elastic moduli, each having increasingly higher carbon content and alignment of the graphite planes with respect to the fibre axis. High Strength (HS) and Intermediate Modulus fibres (IM) are 93% - 95% carbon, while High Modulus (HM) fibres, especially pitch based carbon fibres, are 99+% carbon. Residual atoms from the polymerization make up the remaining content and are predominantly oxygen and nitrogen. The increased carbon content results in more C=C bonding lending extra stiffness to the fibre. However, XRD clearly shows enhanced crystal orientation in HM fibres versus SM and IM fibres, which also explains the increase in elastic modulus.

High Strength carbon fibres have an elastic modulus in the range of 200-250 GPa [21]. A few products of this type of fibre are Sigrafil C30, Hexcel AS4, Toray T700, and Cytec T300H. Intermediate modulus carbon fibres have an elastic modulus in the range of 280-300 GPa [21]. Two examples of this type of fibre are Toray T800S and Hexcel IM7. Figure 7 shows IM fibres also have higher strength than HS fibres; while HM fibres sacrifice strength for additional stiffness.

PAN high modulus carbon fibres have an elastic modulus in the range of 350-600 GPa [21], and pitch HM and ultra high modulus fibres have elastic moduli from 600-900 GPa [12]. A few products of this type of fibre are Grafil HR-40 and Toray M46J as polyacrylonitrile based fibres and Dialead K139 and Carbonic HM 70 as pitch based fibres.

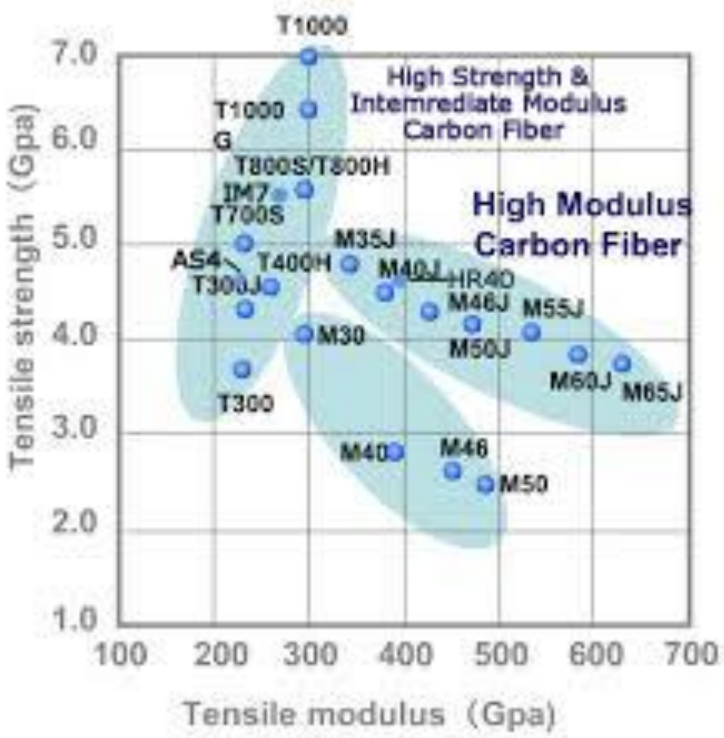

Figure 7. Tensile Strength and Modulus of PAN carbon fibre [22]

The heat treatment temperature and drawing conditions the fibre experiences during carbonization and graphitization influences the microstructure developed in the fibre. The microstructure then controls the fibre's tensile strength and elastic modulus. Figure 8 shows the microstructure of a carbon fibre becomes increasingly homogeneous as the heat treatment temperature is increased. The effect of heat treatment on tensile strength and modulus are shown in Figure 9 and Figure 10. At 1100K the temperature is short of temperatures needed for carbonization, resulting in the development of structure with an insufficient degree of carbon purity. Additionally, the range over which the structure is coherent is quite limited. Based on [20] and Figure 8, SM fibres are probably heat treated at around 1700K which results in a structure with a high degree of carbon purity, but with average crystal size. From [23] temperatures in the realm of 2000K are used to additionally purify the carbon structure and to coax the aromatic structure to coalesce into the sheet structure found in IM fibres. However, Figure 9 uses more recent data and suggests IM fibres are treated to 1700K and SM fibres would be less than that. The differences between Figure 8 and Figure 9 suggest technological advances have enabled lower HTT to produce the same level of stiffness and crystal development in PAN than higher HTT previously did in the 1980's. A knock-on effect has been fibres produced today have higher strength to stiffness ratios than originally possible.

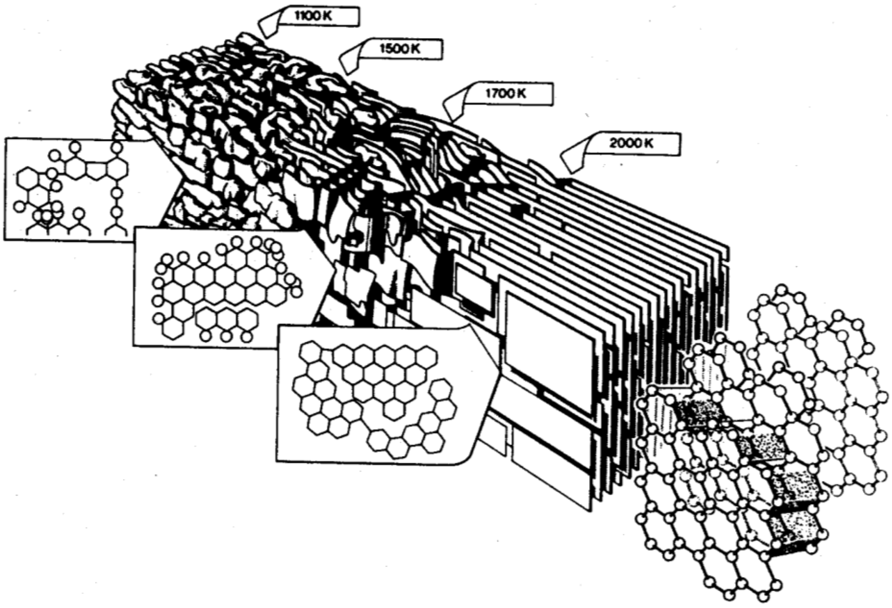

Figure 8 Structure of PAN based carbon fibre during different points during carbonization and graphitization [23]

SM and IM fibres have their graphite planes oriented similarly with respect to the fibre axis, but IM fibres have a larger crystal size. High modulus fibres are graphitized at 3000K or more in an effort to grow the crystal size and perfect the sheet-like structure.

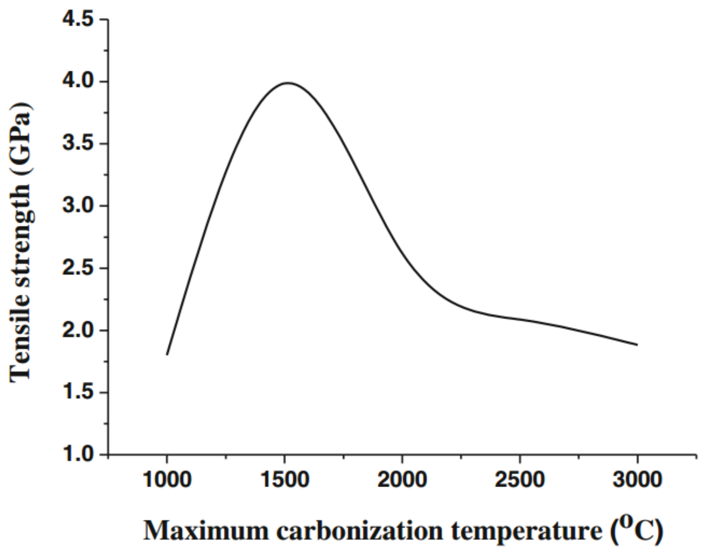

Figure 9. Tensile Strength as a function of HTT [12]

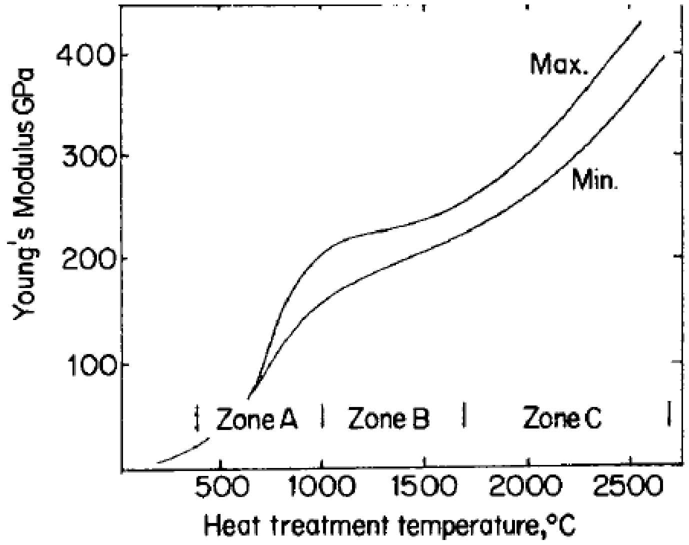

Figure 10. Elastic Modulus as a function of HTT [24]

The structural models shown in Figure 8 and Figure 11 were developed in the 1970s and 1980s when carbon fibres were classified as Type I, Type II, or Type III. Type I had the highest heat treatment temperature resulting in the stiffest fibre, but with a tensile strength lower than type II fibres. Type III fibres were only partially carbonized so their elastic modulus was inferior compared to Types I and II. As discussed in section 2.2, the larger crystal size in Type I fibres compared to Type II fibres made them fail at lower stresses than Type II carbon fibres. However, today

IM fibres are often stronger than SM fibres. There are several possibilities for this observation: structural models developed in the 1970s and 1980s do not explain modern carbon fibres well enough, today's IM fibres have purer polymer precursors than SM fibres resulting in a decreased flaw density, or there are additional structural factors that determine the tensile strength and elastic modulus (but that are still consistent with the available structural models).

The most universal attribute for classifying carbon fibres is their elastic modulus. The elastic modulus of a material describes its stiffness or resistance to deformation. A more scientific definition of elastic modulus is that the elastic modulus is a measure of the stress needed to displace a plane of atoms by once lattice space [25]. Working from this definition, both the structure and chemistry of a material play a role in establishing the elastic modulus of a material.

2.2 Strength of Carbon Fibre

As discussed previously, higher heat treatment temperature helps form larger and more collated crystals. Large continuous crystal regions in carbon fibre closely resemble those in single crystal graphite, so in theory the strength and stiffness of carbon fibres should increase with crystal size. Two factors limit the strength of carbon fibres. Firstly, higher alignment of graphite planes means less mechanical interlocking is available, such as that shown in Figure 11. This leaves the tensile strength of the fibre increasingly limited by the weak Van Der Waals forces impeding the sliding of graphite sheets. Defects are the second limiter of strength. Defects very broadly can mean impurities in the precursor [26], kinks or bends in the graphite sheet structure like those evident in Figure 4, or amorphous material between crystalline regions which was previously shown in Figure 2.

The tensile strength of carbon fibres has been correlated to their structural arrangement and defects by Reynolds and Sharp [27]. The theoretical tensile strength of a material can be evaluated using the Orowan-Polamyi Equation

$$\sigma = \frac{E\gamma_a^{1/2}}{a} \tag{1}$$

where E is young's modulus, γ_a is the surface energy, and a is the interplanar spacing. Reynolds and Sharp adapt the well-known Griffith criteria

$$\sigma^2 = \frac{2E\gamma_a}{\pi C} \tag{2}$$

to account for presence of defects, where the elastic modulus, E, is dependent on the misorientation of graphite planes with respect to the fibre axis, and C is the critical crack size.

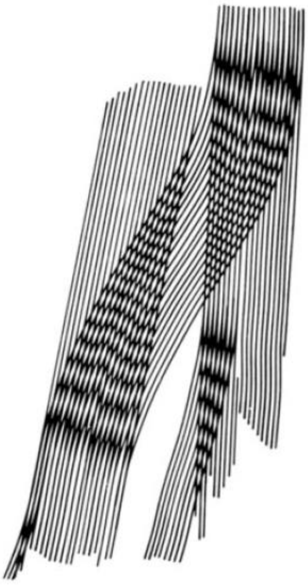

Figure 11. Schematic of longitudinal structure in PAN carbon fibres[19]

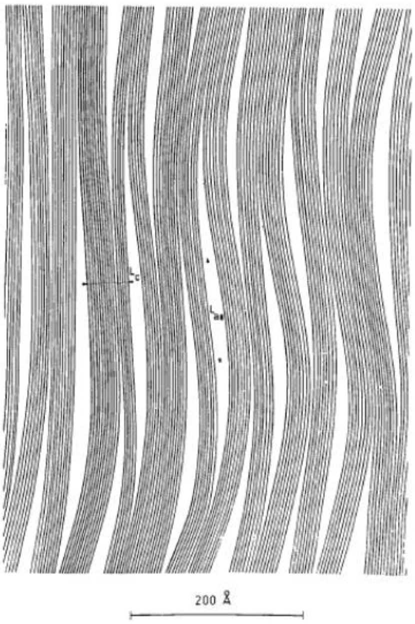

Figure 12. Wrinkled microfibrils

Reynolds and Sharp argue that because of the interlinked ribbon structure of carbon fibre (for example Figure 11), failure of carbon fibres cannot be explained using dislocation theory; instead it should be described with respect to the progressive unbending of curved ribbons, yielding via local shear deformation, and slippage [27]. When tensile stress is applied to misoriented crystallites, they build up shear stress. Perfect solids can release this strain energy via cracking, but carbon fibres must release this energy through the rupture of basal planes. The rupture of a basal plane can cause a crack to form and propagate across and through planes. One of two following criteria must be met for the described failure to happen [27].

Condition 1. Crystallite size in the propagation direction must be greater than the critical flaw size.

Condition 2**.** A crystallite must be sufficiently continuous to its neighbours such that a crack can propagate across surfaces.

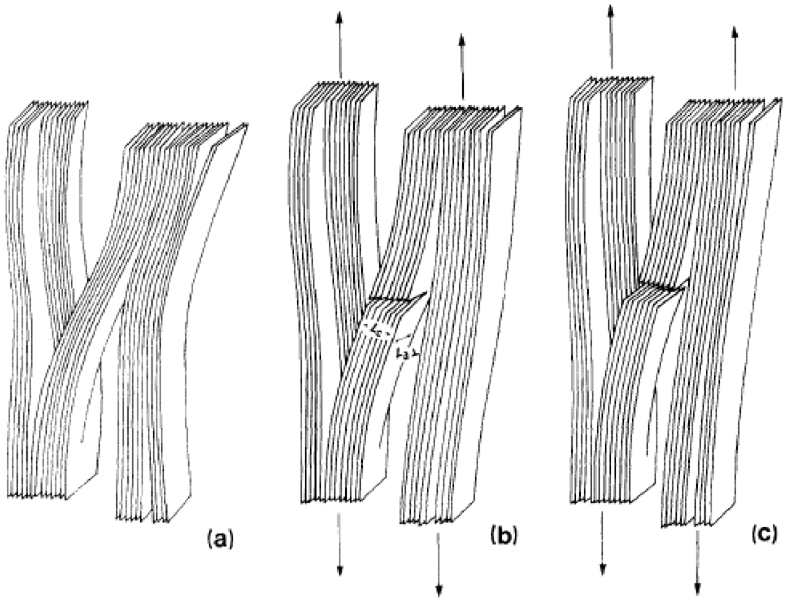

Figure 13 Reynolds-Sharp mechanism of tensile failure. *(a)* Misoriented crystallite linking two crystallites parallel to the fibre axis. *(b)* Tensile stress exerted parallel to fibre axis causes layer plane rupture in direction *Lc,* crack develops along *Lc* and *La, (c)* Further exertion of stress causes complete failure of misoriented crystallite. Catastrophic failure occurs if the crack exceeds the critical size in *Lc,* or *La* directions. [27]

D.J. Johnson has done extensive TEM work to determine the accuracy and applicability of Reynolds and Sharp's work. Johnson's work confirms that Reynolds and Sharp captured the fundamentals of tensile failure. In 1980 Johnson [28] investigated Type I carbon fibres and determined the strength-limiting defects were internal defects containing misoriented crystallites within the outer skin region of the fibres. In subsequent work [19, 29] the importance of the difference between Type I and Type II fibres and the role of internal versus surface flaws was no longer stressed. Johnson's shift of emphasis suggests either inconclusive experimental methodology or wider applicability of Reynolds-Sharp failure than Johnson originally thought. In 1983 Bennett, Johnson, and Johnson [29], taking advantage of advances in TEM since the time of Reynolds and Sharp, were able to measure the structural properties of failed fibres to determine how well the Reynolds-Sharp theory actually works. In Bennet et al.'s [29] work, the size and orientation of crystallites surrounding the failure regions were studied. Based on the weakest-link approach, the fibres should fail at the largest defect (in this case, holes), but Bennett et al. found this to not always be true. Based on Reynolds-Sharp failure, the crystallites surrounding a failure point must be large (to satisfy Condition 2) and have a large misorientation with respect to the fibre axis. However, this proved to be not always true; sometimes the crystallites near the failure region were aligned nearly parallel to the fibre axis. Equally many times in support of Reynolds and Sharp's method of determining tensile strength, the severely misoriented crystallites were about 20^{o} off-axis, resulting in theoretical fibre properties being quite close to the tensile properties of the fibres used [29]. The difficulty in using the Reynolds-Sharp failure to predict tensile strength is that *local* rather than average orientation of the graphite crystals must be measured.

2.3 Carbon Fibre Recycling Activities

Carbon fibre recycling has been attempted or investigated by many organisations, most notably: North Carolina State University (NCSU), The University of Nottingham (UoN), Imperial College London (ICL), University of Leeds, Adherent Technologies, Firebird Advanced Materials, Materials Innovation Technologies-Recycled Carbon Fibre (eMIT-RCF), and ELG- Carbon Fibre (ELG). The two most significant commercial carbon fibre recycling operations are run by Carbon Conversions (formerly eMIT-RCF) [30, 31] and ELG [32, 33]. Carbon Conversions process waste streams from aerospace (e.g., uncured prepreg), high end sporting goods sectors, and fibre manufacturers, braiders, and weavers [34]. They have well-developed relationships with Boeing, Trek Bicycle, and Oracle racing. Carbon Conversions's facility in Lake City, South Carolina is sized to handle 1.4-2.3 million kilograms of CFRP waste a year. The fibre recovered from this waste is used in a wetlay RotoFormer™ process and a Three Dimensional Engineered Preform (3-DEP®) process to make new goods using recycled fibre. Examples include an out-of-autoclave moulding tool for VX Aerospace, C07 Corvette upper plenum, lower protective bumper on a hybrid urban commuter buses, and sidewalls for commercial aircraft offering 25%-35% weight savings compared to glass-phenolic panels commonly used [35].

ELG Carbon Fibre has been working on carbon fibre recycling since 2008 (then under the name Milled Carbon) and in 2009 commissioned a new facility housing a 21 m long pyrolysis belt oven capable of handling 2,000 tonnes of CFRP waste per anum [36]. ELG Carbon Fibre is in a prime position to receive all the composites manufacturing scrap in the UK and through its parent company, ELG, the distribution and transportation facilities are there to make it happen and possibly include lucrative European CFRP waste as well. Most recently ELG has started to work with Long Fibre Thermoplastic (LFT) industry suppliers to develop a pellet product containing recycled fibres 6-10 mm in length [34]. Previously ELG's primary product was milled and random chopped fibre. A significant difference between ELG and Carbon Conversions is how they process incoming scrap. Carbon Conversions sort the waste and keeps track of the fibre pedigree which is useful for maximizing mechanical properties and assuring their customers of fibre quality. ELG lets their waste streams mix and documents the mechanical properties that can generally be expected from their products [37]. ELG's 'pyrolysis' process reportedly has the ability to act as a two stage process: first, pyrolysis then second, an oxidation operation that includes the ability to operate under reduced oxygen content environments through the use of nitrogen or recycled waste gases [32].

Through projects funded by The Boeing Company, North Carolina State University studied the properties of recycled carbon fibres from 2005-2011 [38-42]. Since 2002 University of Nottingham has developed two carbon fibre recycling processes and has subsequently studied the properties of carbon fibres recovered from these processes as well as composites made from these recycled carbon fibres [4, 8, 43-50]. Imperial College London starting in 2009 has developed mechanical models to predict the strength of composites made from recycled carbon fibre [51-53]. There are two areas of focus from these models. The first is scaling single fibre tensile properties to the mechanical properties of a bundle and the second is considering the toughening effect these bundles have on composites. The degree of toughening is influenced by bundle strength, fibre to matrix interfacial strength, and bundle geometry. University of Leeds was a partner in the Fibrecycle project which examined co-mingling thermoplastic PET and manufacturing virgin carbon fibre scrap to make composite laminates [54, 55]. Adherent Technologies and Firebird Advanced Materials have not released any details related to commercialising recycling processes. Adherent Technologies built two solvent-based and one pyrolysis-based carbon fibre composite recycling processes [56, 57]. In 2009 Adherent combined their vacuum pyrolysis and low pressure/ low temperature solvent processes to successfully recycle state-of-the-art 2nd generation aircraft composites coming from the fuselage barrel of Boeing's 787 Dreamliner [58]. Adherent produced high quality fibres using this combined process, but felt it was too slow to be worth a commercialisation pathway [5]. Firebird Advanced Materials earned an Air Force Phase II Small Business Innovation Research grant to build a microwave pyrolysis carbon fibre recycling process [59]. The technology had great potential for recycling thick laminates, but in practice the process could be difficult to control and fibre quality was highly dependent on the type of composite recycled. Throughout the published work on carbon fibre recycling, there is extensive data on specific recycling processes and in limited cases, the same recycling process is used, but different recycling conditions or material feedstock are incorporated. Efforts to correlate recycling process conditions to fibre properties have been extremely limited at best. The most relevant effort has come from L.O. Meyer, while at The Hamburg University of Technology, in a study seeking to optimize pyrolysis as a carbon fibre recycling process [9]. Raman spectroscopy was used to provide information about the presence of pyrolytic carbon and possible damage to the carbon fibre, but the Raman measurements were not complemented with any other quantitative technique such as X-ray diffraction or single filament tensile testing.

Meyer chose to study carbon fibre recycling by using TGA to alter the time, temperature, and gas atmosphere to examine the effects of changing process parameters on fibre quality. SEM and Raman were then used to evaluate the recycled fibers. Meyer determined that the carbon fibre recycling process is much more sensitive to temperature when air, as opposed to nitrogen, is used. Beyond 30 minutes, no time dependency of the pyrolysis process was found when using nitrogen. In air the polymer matrix was not removed at a process temperature of 400°C, but at 600°C SEM revealed noticeable damage to the fibres. Choosing 500°C as an operating temperature and air for the gaseous environment, the degree of fibre degradation could loosely be controlled by exposure time [9]. In the temperature range of 400°C to 550°C the build-up of pyrolytic char from the decomposition of the polymer matrix was less in an inert nitrogen atmosphere than in an oxygenated atmosphere. However, at temperatures below 550°C, the inert atmosphere does not remove pyrolytic char no matter how long the exposure time. The presence of pyrolytic char was initially postulated from examination of TGA weight loss curves and was later confirmed by Raman spectroscopy. Raman uses laser light to identify the vibrational modes in a material which helps to identify elements or compounds that make up the material [60]. For carbon the dominate modes are from sp2 bonding (graphite/ g-band) and sp3 bonding (diamond/disorder/ d-band). Raman is reviewed more thoroughly in section 3.2. Meyer's use of Raman showed fibres recycled in nitrogen (as opposed to air) to have a smaller ratio of the disorder band to the graphite band, indicating less pyrolytic char. From data offered by SEM and Raman, the optimal recycling conditions were either ramping to 600°C at 10°C/min in air or ramping to 500°C at 10°C/min in air and dwelling at temperature for two hours.

Meyer subsequently conducted a batch recycling experiment using the facilities at Refibre (Roslev, Denmark). At Refibre a two-step recycling process was used. The first step used a two hour isothermal dwell at 550^{o}C in nitrogen to remove as much of the organic polymer matrix as possible. Since decomposition of the polymer matrix is an exothermic process, the temperature of the fibres can be difficult to control. Knowing that oxidation of the carbon fibres is extremely temperature dependent, the risk of damage to the fibres was minimized by letting the most exothermic part of the recycling process happen under inert conditions. After the initial pyrolysis stage, the composite was allowed to cool to 200^{o}C before undergoing partial oxidation at 550^{o}C. Neither the duration nor oxidising conditions were disclosed. From Meyer's TGA experiments, the Raman spectra of fibres recycled at 500^{o}C in nitrogen for two hours show separate disorder (D band) and graphite (G band) peaks, but the peaks rapidly broaden at less than their full intensity. No Raman spectra for fibres recycled at 550^{o}C or 600^{o}C in nitrogen were available for comparison. Raman spectra for fibres heated to 700^{o}C in nitrogen at 10^{o}C/min had clearly defined peaks quite similar to the spectrum of the 'ideal', as determined from TGA experiments, recycling condition of ramping to 600^{o}C at 10^{o}C/min in 21% O_2. The fibres recycled at Refibre had 96% strength retention as measured by the Weibull scale parameter [9]. The method for determining the Weibull shape and scale parameters was not indicated. While the tensile strength of the fibres recycled at Refibre is quite encouraging, the pyrolysis procedure used was quite different than any of the conditions Meyer studied with TGA, SEM, and Raman to optimize pyrolysis as a carbon fibre recycling process. In Meyer's work it is not clear how the information gathered from the TGA experiments influenced the conditions used for the batch recycling work at Refibre. The two step process is a clear departure from the TGA work but is a logical way to control fibre damage during the recycling process by only using oxygen when oxygen is needed.

Most of the recycling literature focuses on thermal processes and shows they have been identified for larger scale trials. From the studies by Meyer and Adherent Technologies, a pyrolysis stage where the oxygen concentration is zero has been shown to be advantageous but adds process complexity and increases the time it takes to recycle a batch of CFRP. When ELG (then Recycled Carbon Fibre, ltd) first scaled up their process to the 21 m belt furnace, the importance of temperature uniformity became obvious [41]. Carbon Conversions annealing oven for carbon fibre recycling and Milled Carbon’s patent application [32] suggest the ability to work in a reduced oxygen atmosphere is also advantageous. These bits of knowledge from the literature were prevalent when designing the tube furnace recycling rig for this study (section 5.1.1) and when establishing the recycling conditions (section 5.2). Research by Firebird Advanced Materials indicates that resin chemistry can have a dramatic impact on temperatures needed during the recycling process and the need to control the oxidation rates at high temperatures. Using two different resins also came from learning from the experience Adherent Technologies had of changing from working on epoxy resins used on military aircraft in the 1990s to working with thermoplastic toughened next generation epoxies used in the latest commercial aircraft like the Boeing 787.

Many aspects of the carbon fibre composite recycling process are explored more thoroughly in this study than inprevious research. Specific interests were the ideal range of operating temperatures plus the pros and cons of each temperature, the use of reduced oxygen content atmospheres, how fibres are damaged during recycling, and how differently various fibres and resins respond to the recycling process. The strength and stiffness, surface oxygen concentration, and microstructure are all explored to see how recycling changes them and if the surface and or structural properties of the fibre can be related to its tensile strength and elastic modulus.

3. Characterisation Techniques

3.1 Scanning Electron Microscopy (SEM)

SEM was used to examine the shape and texture of the fibres as well as any debris or char deposited on the fibre. Energy Dispersive Spectroscopy (EDS) was used to identify what elements were present in material on the fibre surface. A Philips XL30 field emission SEM equipped with an Oxford Instruments INCA microanalysis system fitted with an Si(Li) detector and ultra-thin window was used. Imaging conditions were 5 keV accelerating voltage using an Everheart-Thornley secondary electron detector. For elemental identification with EDS, the accelerating voltage was set to 10 keV and a 30 s collection time was used to acquire 75,000-100,000 counts over a 0-5 keV X-ray energy range. Small portions of multiple fibre tows around 2 cm in length were extracted and placed on an SEM sample stub. The fibres were secured to the sample stub by graphite tape at the top and bottom so that the middle portion of fibre was clearly visible against the metal sample holder.

Figure 14 gives an example of the image quality possible when using the EDS set-up. While intricate fibre detail is not clear, both the fibre and debris on the fibre are clearly seen. This setup allows an image to be captured of the exact area under X-ray analysis.

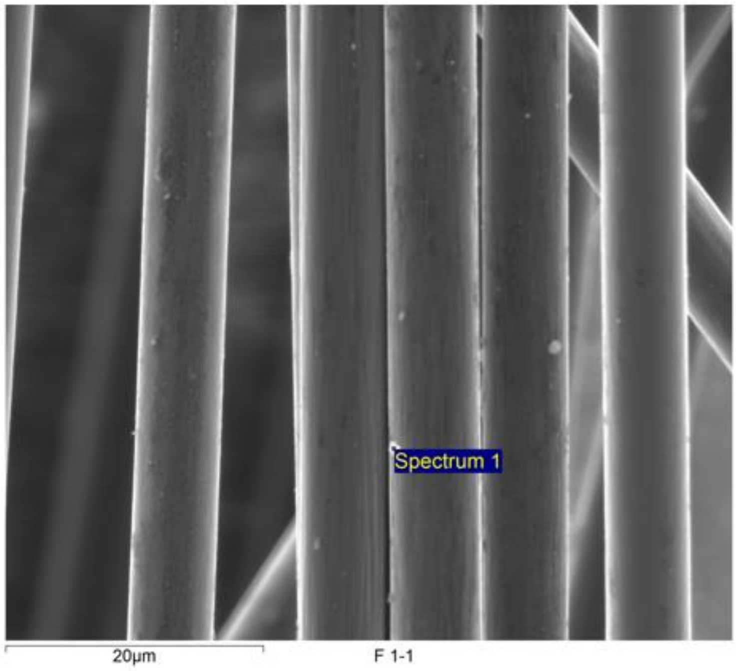

Figure 14. Micrograph of AS4_30min_600C_15.5%O_2 with location of EDS analysis marked

Figure 15 shows the energy distribution of the X-ray analysis and the associated elements for each peak. Multiple elements may be associated with an energy range. In this situation choosing the correct element for each energy range is down to context of the material being recycled including its processing and handling history as well as consideration of elements that frequently appear together such as in ionic salts.

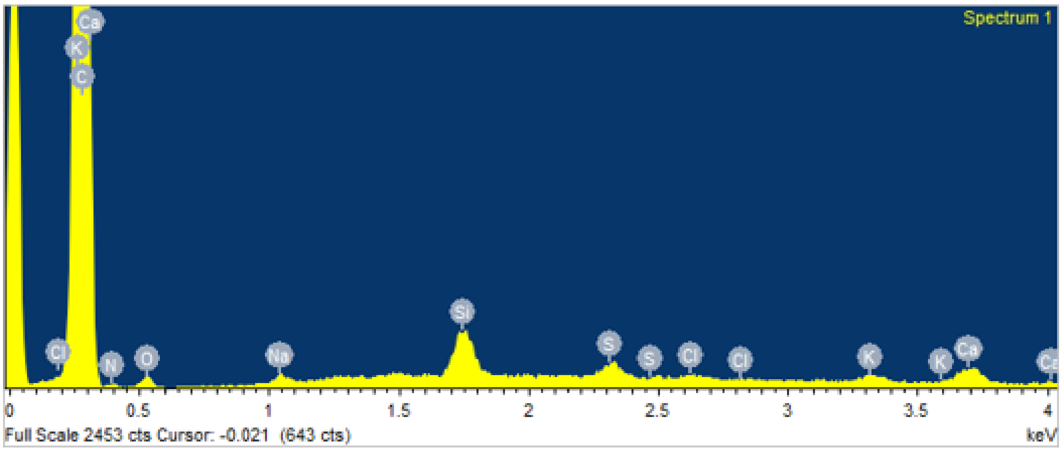

Figure 15. EDS Spectrum of area marked in Figure 14

3.2 Raman Spectroscopy

Raman Spectroscopy is used to measure the relative proportions of order and disorder in the crystal structure of carbon fibre. Crystalline boundaries and deformed carbon ring structures contribute to the disorder peak (D-peak). SP2 resonance bond structure, like that found in graphite, contributes to the order peak (G-peak). The area ratio of disorder to order (A_D/A_G) is typically inversely proportional to crystal size as measured by X-ray Diffraction [61]. A Horiba LabRAM Raman spectrometer coupled to an optical microscope was used. The spectrometer was calibrated against the first order peak for silicon and against the laser wavelength used (532 nm). A tow or a section of a tow of carbon fibre was placed on the microscope stage and then brought into focus with an Olympus 50X objective in place. The 50X objective remained in place when using the laser. Trial samples were used to establish optimal settings of: 25% filter, 1050 µm hole size, 1400 cm^{-1} grate setting, 180 s exposure time, two exposures, and a scan range of 850 cm^{-1} to 1850 cm^{-1}. Spectra were exported as a text file which could then be imported into Microsoft Excel. A peak fitting macro was used to set a linear baseline and perform curve fitting with pseudo-Voigt functions on the: I (~1330 cm^{-1}), D (1350-1370 cm^{-1}), D" (~1500 cm^{-1}), and G (1575-1582 cm^{-1}) peaks [62]. An example of the peak fitting is shown in Figure 16. The raw measured spectrum is shown in black and the sum of each of the curves, detailed above, is shown in purple. The D’ peak at 1620 cm^{-1} is commonly found in highly ordered samples, but no such peak was found for the fibres considered in this study.

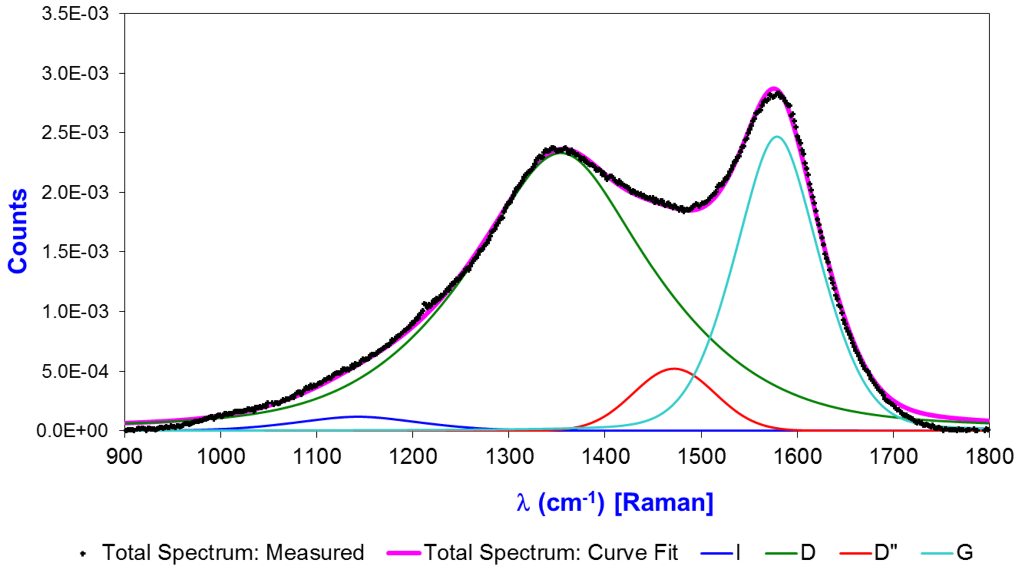

Figure 16. Raman peak fitting on a tow of carbon fibre

Spectra for two areas on each of three tows were collected and the parameters $FWHM_D$, $FWHM_G$, and A_D/A_G were considered in analysis [63, 64]. Measurements on small bundles of 5-10 filaments were compared to the corresponding measurement on tows to see if smaller bundles would produce sharper spectra with increased peak separation. As indicated by Figure 17 and Table 1, the difference in spectra based on the different sample geometries is not significant.

.

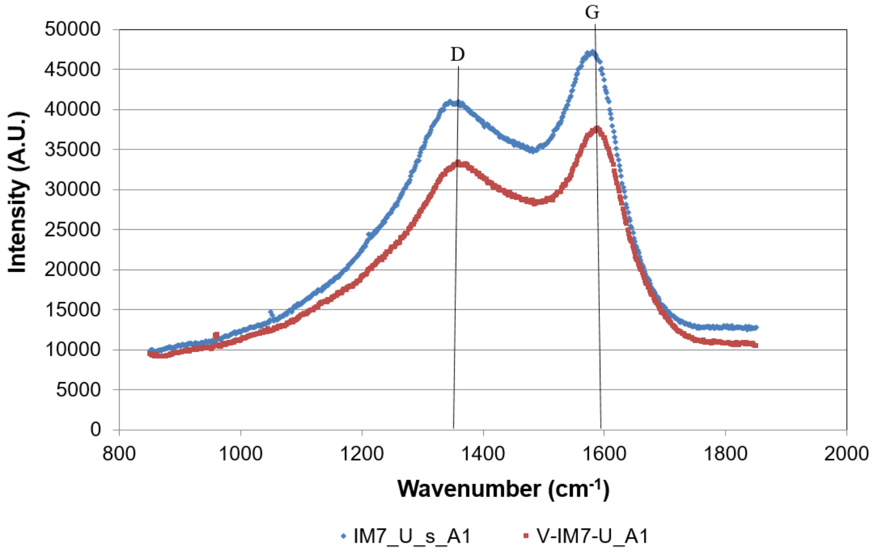

Figure 17. Overlay of Raman spectra for a tow and a small bundle of unsized IM7 fibre

Table 1. Average disorder ratios for a tow and a small bundle of unsized IM7 fibre

Sample	Ad/Ag	Ad/AT
IM7_U (tow)	2.44 ± 0.03	1.86 ± 0.06
IM7_U_s (bundle)	2.33 ± 0.01	1.86 ± 0.01

3.3 XRD

X-ray diffraction is another method used to interpret the crystalline structure of carbon fibre. Crystal size in the cross-section plane is calculated from the (10) and (11) collection of peaks. Crystal thickness is calculated from the (002) peak. Orientation of graphite crystallites with respect to the fibre axis is measured using a transmission method where 2Θ is set to the angle where (002) appears in reflection and the sample is rotated through the chi (Χ) axis as pictured in Figure 18. The orientation of the crystallites is proportional to the full width at half-maximum (FWHM) of the resulting peak. A Siemens D500 diffractometer was used collect powder diffraction patterns of the (002), (10), and (11) peaks in reflection. Powder diffraction was chosen over transmission because the peak positions are more reliable in reflection, peak shifting could be corrected using silicon as a reference, and peak broadening due to imperfect sample preparation is less. Peak broadening in transmission mode is unavoidable since the many 100s or few thousand filaments, extracted from a tow, will lie in multiple focus planes at once. In this case, peak broadening occurs because each filament does not satisfy the Bragg criteria [65] at the same 2Θ as all the other filaments. Additionally, the signal to noise ratio is often lower in transmission mode since X-rays must pass through the fibre bundle. A Bruker D8 Discover diffractometer is used in transmission mode for the azimuthal scan of the (002) peak to measure crystallite orientation. Table 2 lists the scan parameters used.

Table 2. Scan Settings for XRD Studies

Peak	Step Size (2Θ)	Dwell Time (s)	Range (2Θ)/(Χ)
(002)	0.02	4	16-32
(10)	0.02	8	38-52
(11)	0.02	10	72-88
Azimuthal (002)	0.05	16	-3-+90

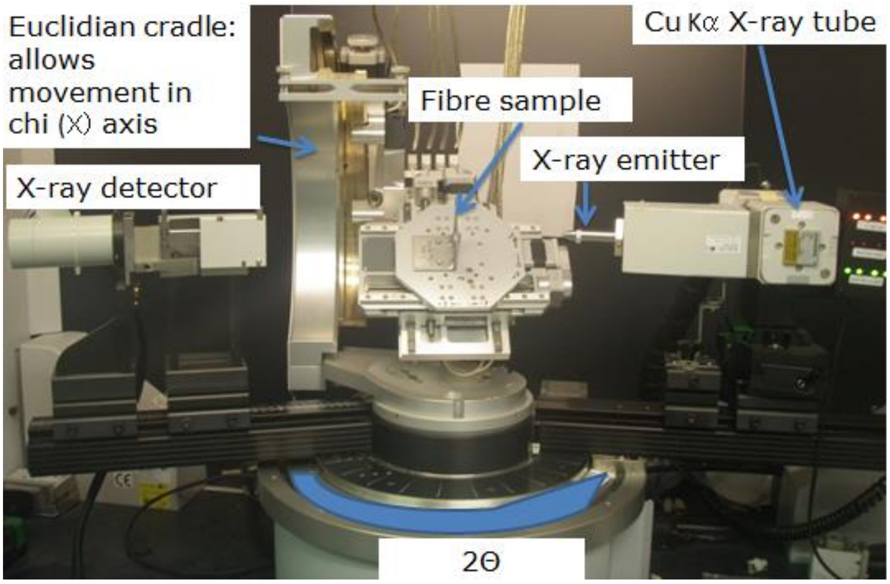

Figure 18. XRD setup for orientation analysis

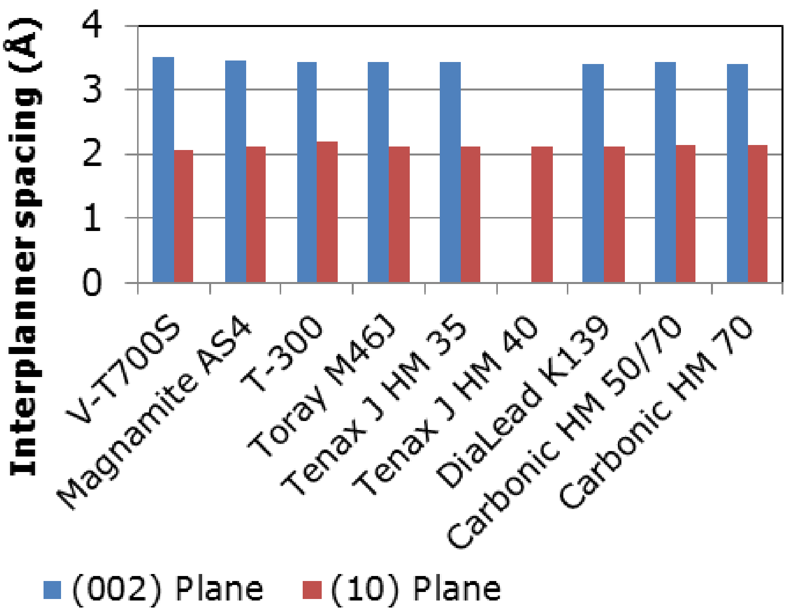

Figure 19. Interplanar spacing measured by XRD of PAN high strength and high modulus fibres as well as high modulus pitch virgin carbon fibre

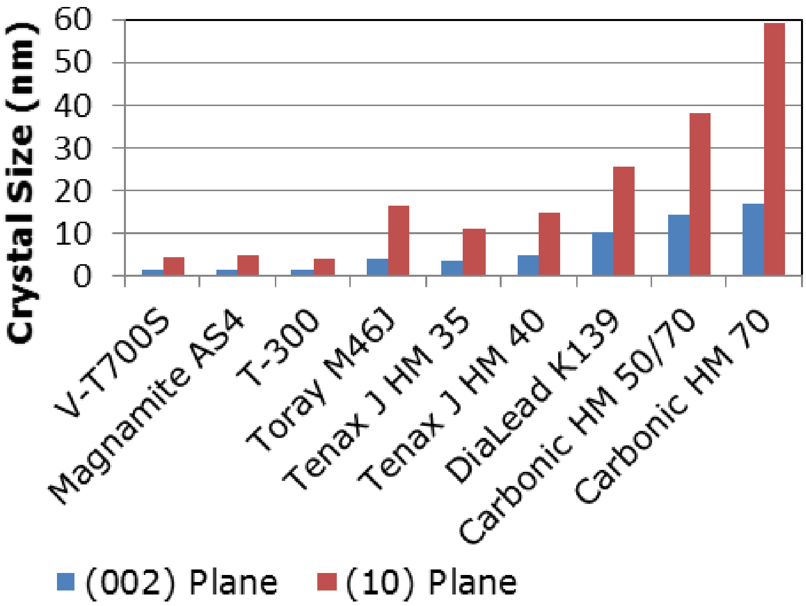

Figure 20. Crystal size measured by XRD of PAN high strength and high modulus fibres as well as high modulus pitch virgin carbon fibre

In Figure 19 and Figure 20 interplanar spacing and crystal sizes for Toray M46J, Dialead K139, and V-T700S based carbon fibres were compared to results found in the literature against the same type of fibres [16, 66]. Carbonic HM 50 and HM 70 are pitch based high modulus fibres, Tenax J HM 35 and HM 40 are PAN based high modulus fibres, while T-300 and AS4 are high strength PAN based fibres. As expected, with increasing graphitic character peak widths and interplanar spacing decrease while crystal size increases.

3.4 Single Fibre Tensile Test (SFTT)

Universal Testing Machines (UTM) from Instron, Tinus Olsen, and Shimadzu were reviewed against the desired capabilities of fibre testing equipment and a specially designed fibre testing system from Dia-Stron, ltd was bought to enhance UoN's single fibres tensile testing capabilities. The unique features of the Dia-Stron equipment compared to a conventional UTM are: integrated fibre diameter measurement, higher accuracy and resolution load cell at low levels of load, higher axial alignment of the fibre with the testing axis and less sample handling. In collaboration with Dia-Stron, CERSA-MCI, who makes laser diffraction units for measuring fine wire, was able to adapt their LDS0200 laser diffraction unit specifically for Dia-Stron. As can be seen in Figure 21, the LDS0200 is integrated into a single platform with the tensile testing unit, LEX820, and a sample transport system, MLS200. For reliable laser diffraction measurements, the fibre must be perfectly straight and presented at a 90^o angle to the laser beam. The fibre potentially has three degrees of alignment with respect to the laser beam: pitch, roll, and yaw. Any yaw movement of the fibre is constrained by being glued in the wells of the plastic sample tabs. A fibre being rolled with respect to the laser beam does not prevent it from being at a 90^o angle. In order to compensate for the fibre possibly being at a non-level pitch, the LDS0200 is connected to a stepper motor allowing the LDS0200 to rotate $\sim\pm5^o$ ensuring the laser beam intersects the fibre at 90^o. The LEX 820 and LDS0200 are positioned orthogonally to each other so that the LEX 820 can place the fibre under tension to satisfy the requirement for fibre straightness. Dia-stron's control software records the diameter measurement as well as the load-extension data gathered during a tensile test.

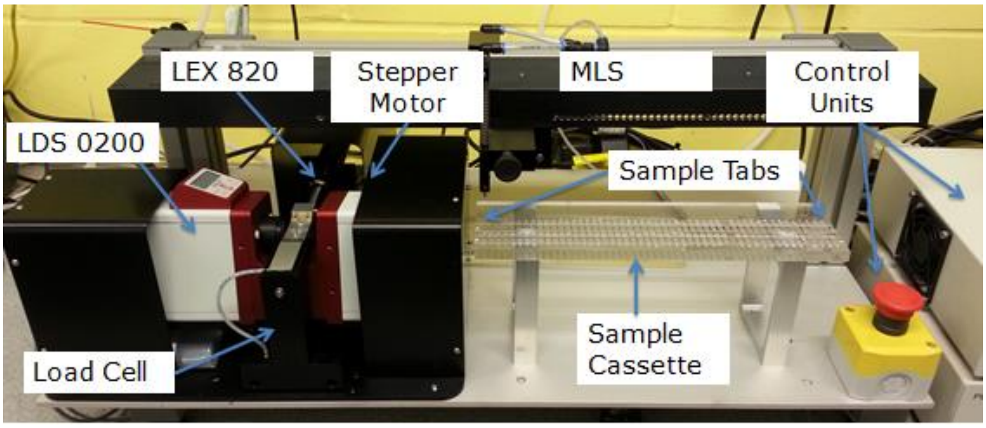

Figure 21. Dia-Stron tensile testing setup

BS/ISO 11556 "Carbon Fibre- Determination of the tensile properties of a single-filament" was used as a procedural guide. The calibration of the load cell was checked and found to be accurate to within 0.6% of the force reading throughout the expected loading range, satisfying the requirement for 1% force accuracy. The load cell used was Futek FSH00103 with a capacity of 22.2 N and a force resolution of 0.49 mN. A large capacity (relative to average fibre breaking loads which were on the order of 0.08 N to 0.1 N) load cell was selected to reduce the system compliance. Dymax 3193 UV curing adhesive was used to bind the fibres to the plastic tabs as seen in Figure 21. How Dymax 3193 was selected is discussed in section 3.4.1. Cross-sectional area was determined from laser diffraction assuming circular cross-section, which is true for the virgin fibres considered. Compliance of the system was determined according to Annex A of BS/ISO 11556 using gauge lengths of 4 mm, 12 mm, and 20 mm, with the compliance being determined from 10 filaments mounted at each gauge length. For each fibre sample tested the system compliance was calculated. The compliance corrected elastic modulus was calculated only for samples tested at 20 mm gauge lengths according to Method B in BS/ISO 11556.

To determine the true gauge length and breaking strain, a method was devised to correct the extension data for slack. No standard method for doing so is available. The method chosen extrapolates a best fit line found between 20% and 60% of the breaking load to the pre-tension load of 0.59 cN (0.5 gf) and determines the extension at that load to be the amount of slack. The method then subtracts this slack from the extension data and recalculates strain. 20% to 60% of the breaking load was chosen since that is the method used to determine elastic modulus in JIS 7601 “Standard Test Methods for Carbon Fibres”. A pre-tension load was used to get the sample tabs moving towards the front face of the sample pocket before collecting data, thus avoiding collecting noisy stick-slip movement that may interfere with the analysis. 0.59 cN was chosen as a sufficiently low load that no damage would likely be done to the fibre and would also be below the 20% breaking load point used in the slack correction algorithm. These data reduction and analysis procedures were not originally written into the Dia-Stron software. Through a collaborative working relationship between UoN and Dia-Stron, UoN helped Dia-stron add and test the necessary data analysis features in their software. A macro written in VBA uses the analysis summary provided by Dia-Stron’s software to calculate the dL/dF values needed to determine compliance. Then the compliance corrected elastic modulus is easily and quickly determined through the use of pre-setup worksheet formulas in Excel. Unless otherwise noted, at least 60 filaments were tested at the 20 mm gauge length to determine tensile strength and elastic modulus. Tests that showed any of the following: slipping in the grips, the slipping of two fibres past each other, exceedingly high (>20 cN) or low (<2 cN) break loads, and exceeding high (>400 GPa) or low elastic (<100 GPa) modulus (without compliance correction) were not included in the final analysis.

Table 3. Number of single fibres included in tensile strength and elastic modulus analysis and compliance measured for each sample.

Fibre Sample	Filaments in Analysis	Compliance (mm/N)
V-T700	59	0.305
T7_20min_550C_10%O_2	56	0.256
T7_40min_550C_10%O_2	59	0.438
T7_20min_550C_21% O2	62	0.257
T7_40min_550C_21% O_2	71	0.228
T7_30min_600C_15_5%O_2	85	0.256
T7_20min_650C_10%O_2	58	0.485
T7_40min_650C_10%O_2	59	0.261
T7_20min_650C_21% O_2	62	0.212
T7_40min_650C_21%O_2	65	0.157
V-AS4	66	0.178
AS4_20min_550C_10%O_2	61	0.282
AS4_40min_550C_10%O_2	63	0.209
AS4_20min_550C_21% O_2	57	0.223
AS4_40min_550C_21% O_2	25	0.192
AS4_30min_600C_15.5%O_2	30	0.115
AS4_20min_650C_10%O_2	7	0.268
AS4_40min_650C_10%O_2	9	0.178
AS4_20min_650C_21% O_2	N/A	N/A
AS4_40min_650C_21% O_2	N/A	N/A
V-T800S	57	0.303
T8_20min_550C_10%O_2	56	0.299
T8_40min_550C_10%O_2	59	0.233
T8_20min_550C_21% O2	59	0.253
T8_40min_550C_21% O2	65	0.457
T8_30min_600C_15.5%O_2	52	0.340
T8_20min_650C_10%O_2	43	0.149
T8_40min_650C_10%O_2	67	0.200
T8_20min_650C_21% O2	54	0.01
V-IM7	58	0.405
IM7_20min_550C_10%O_2	63	0.345
IM7_40min_550C_10%O_2	40	0
IM7_20min_550C_21% O_2	48	0.312
IM7_40min_550C_21% O_2	29	0.340
IM7_30min_600C_15.5%O_2	39	0.011
IM7_20min_650C_10%O_2	13	0.077
IM7_40min_650C_10%O_2	35	0.003
IM7_20min_650C_21% O_2	N/A	N/A
IM7_40min_650C_21% O_2	N/A	N/A

Sometimes single fibres were so fragile that even after preparing 100 fibres, not even 50 successful tests were made. In these situations further sample preparation and testing was considered futile. Table 3 shows the number of fibres included in the final tensile strength and elastic modulus analysis as well as the system compliance determined for each fibre sample. Samples with N/A were too heavily damaged by the recycling conditions for testing.

Carbon fibres were provided in tow format and portions of the tows were randomly selected from which to extract the single fibres needed for the test. Virgin fibre was available as a tow wound on a bobbin. Three 6-8 cm lengths of tow were cut from the bobbin to supply the fibres needed. The lengths were not cut sequentially but instead one was cut from each of the first three meters of material. Four 6-8 cm lengths of virgin fibre were put aside for each recycling condition. The cuts were made sequentially on the bobbin of virgin fibre but each sequential section was put aside for a different recycling condition. When it came to picking single fibres for testing; fibres were taken from across three different tows. Each tow was sectioned by sliding tweezers down the tow in the fibre direction. These small sections were then further coaxed apart with brushing motions from fingers and tweezers until single filaments could be easily extracted. If more material was needed another section would be removed from each tow as needed. For fibres recovered from a composite, a range of tows were selected so that the top, middle, and bottom of the central mass of the composite were represented.

The Weibull distribution was originally published by Waloddi Weibull in 1951 as “A Statistical Distribution Function of Wide Applicability” [68]. The Weibull distribution is defined by three parameters: scale (σ_o), shape (β), and threshold (δ). The scale parameter is the value that corresponds to the 63.2% percentile of the Weibull distribution. The shape parameter gives an indication of the amount of spread in the data, where a larger shape parameter indicates a less deviation in the data. Below the ‘threshold’ value the probability for an event occurring is zero. Setting δ=0 reduces the complexity of the Weibull distribution and the Weibull distribution is often used in a simplified two parameter form. There must be a physical reason to choose a non-zero value for the threshold parameter; doing so unnecessarily will often reduce the goodness of fit to the data being studied [69]. In this work δ was set to zero as no previous life cycle data was available from which to suggest otherwise. Further discussion of Weibull including probability plots for all samples tested is included the Appendix.

Median rank estimates were used to compute failure probabilities [67] to determine the Weibull scale and shape parameters. The Weibull shape and scale parameters were calculated by writing a Visual Basic for Applications (VBA) macro for Excel. Weibull was used alongside the arithmetic average and standard deviation for tensile strength to provide a second estimate of these properties and because Weibull statistics are hugely advantageous for making failure analysis predictions with small sample sizes [67]. Given the many thousands of filaments in a tow of carbon fibre, even as many as 60 tests on single filaments is quite a small sampling.

3.4.1 Glue Selection

For the Dia-Stron setup, a glue that was easy to use, quick to cure, bonded well to the fibres and the sample tabs, and had low compliance was the most desirable. When using the paper card method on conventional universal test machines, epoxy is used to glue the fibre to the card. Dia-Stron presented the option of using a UV curing glue and three options were considered: Dymax 3094, Dymax 3193, and Delo Katiobond AD640. These UV curing glues came in cartridge form and could easily be dispensed using a plunger and syringe tip attached to the cartridge. In addition to the UV curing glues a range of household glues were also tested including: Loctite super glue, Araldite rapid cure, Araldite standard cure, and J-B Weld 2 part epoxy. Table 4 summarises the attributes of the glues considered. Araldite and J-B weld were difficult to apply to the fibres while they were in the sample tabs as a bulk mixture was made and then separately applied to the small 2 mm x 2 mm well in the sample. The glue was very viscous on application making it difficult to only apply enough to fill the well in the sample tab and then cleanly remove the applicator without disrupting the sample or spilling glue. Glues that needed a 24 hour cure were left overnight and the full 24 hour cure may not have been reached. Needing to leave a batch of fibres 24 hours to cure would have slowed down the testing process immensely as only 50 fibres could be prepared per day unless additional sample trays were bought at a significant expense.

Table 4. Glues considered for tensile testing

Glue	Chemistry	Cure Time	Cure Method
Dymax 3094	Acrylated Urethane	30 s	UV-A light
Dymax 3193	Acrylated Urethane	30 s	UV-A light
Delo Katiobond AD 640	Epoxy	30 s+24 hrs	UV-A light + ambient
Araldite Standard (2 part)	Epoxy	14 hrs	Ambient
Araldite Rapid (2 part)	Epoxy	2 hrs	Ambient
J-B Weld (2 part)	Epoxy	15-24 hrs	Ambient
Loctite Super Glue	Cyanoacrylate	24 hrs	Ambient

Dymax 3193 and 3094 as well as Delo-Katiobond AD 640 were used across a range of 8 different virgin and recycled carbon fibre samples and the system compliance for each sample was calculated for each glue. An average compliance for the glue was then taken as average of all the system compliances. Evaluating the glue’s performance over a variety of different fibres was considered acceptable since this would reflect the actual use of the glue as opposed to choosing the best glue for each fibre sample. Compliances for the Araldite, J-B Weld and Loctite glues were just determined from testing virgin T700 fibres. Table 5 shows the test results for the glues except for Loctite Super Glue where all the fibres pulled out of the glue during testing. The two compliance test results for Delo Katiobond are for just the UV cure and then the UV cure plus curing overnight. Based on this analysis Dymax 3193 was the best glue, although not significantly better than Dymax 3094. Dymax 3193 was then provisionally used for all fibre samples being tensile tested. A few months after the compliance study, Dymax no longer supplied 3094 in small quantities so Dymax 3193 was used for all further testing as well.

Table 5. Compliance Results

Glue	Compliance (mm/N)
Dymax 3094	0.262±0.099
Dymax 3193	0.220±0.054
Delo Katiobond AD 640	1.06 /0.399
Araldite Standard (2 part)	0.315
Araldite Rapid (2 part)	0.810
J-B Weld (2 part)	0.315
Loctite Super Glue	N/A

3.5 Thermogravimetric Analysis (TGA)

TGA was used to observe mass loss over time of cured resin film, and composite samples. Ramp rates, isotherm temperatures, and dwell times were adjusted as needed for each experiment. A TA instruments SDT 600 was used with a nitrogen purged measurement cell and clean dry air in the sample/furnace chamber. The SDT 600 is also able to measure heat flow in and out of the sample similarly to DSC. 550°C isothermal runs were conducted with composite material in order to identify the range over which pyrolysis, char oxidation, and fibre oxidation reactions occur. Further experiments were carried out on cured resin film; where each sample was heated at a given heating rate from room temperature to 750°C. The resin film was cured by placing the film with its backing paper in an air circulating oven which was then heated from room temperature to the isothermal cure temperature for the resin (120°C for MTM 57 and 180°C for MTM 44). The resin was left in the oven for the time indicated in its cure profile (1 hour for MTM 57 and 2 hours for MTM 44). After the allotted cure time the resins were left to remain in the oven for an additional 2 hours for post curing (120°C for MTM 57 and 180°C for MTM 44). Both resins bubbled up on the backing paper forming half dome droplets of cured resin. As many droplets as possible were packed into a TGA crucible to get as much resin mass as possible. For both MTM 44 and MTM 57 resin films, six different ramp rates were used (5, 10, 20, 30, 40, and 50°C/min). Friedman's Method [70] was used to analyse the data from the non-isothermal sample runs in order to determine the kinetic parameters needed for the thermal-kinetic modelling.

3.5.1 Friedman's Method

Friedman's method is a way of using TGA to determine the activation energy, pre-exponential constant, and reaction order for reactions that fit the form

$$\left(\frac{-1}{w_o}\right)\left(\frac{dw}{dt}\right) = Ae^{-Ea/RT} f\left({}^{w}\!/_{w_o}\right) \qquad 3$$

Where w_o is the initial mass, dw/dt is the weight loss over time, A is the pre-exponential factor, R is the universal gas constant in J/mol·K, T is the temperature in Kelvin, and $f(w/w_o)$ is a function of weight loss. The kinetic details for fibre oxidation was taken from literature [71]. Taking the log of both sides of Equation 3 gives a linear function:

$$\ln\left[\left(\frac{-1}{w_o}\right)\left(\frac{dw}{dt}\right)\right] = \frac{-E_a}{RT} + \ln(A) + \ln\left(f\left({}^{w}\!/_{w_o}\right)\right) \qquad 4$$

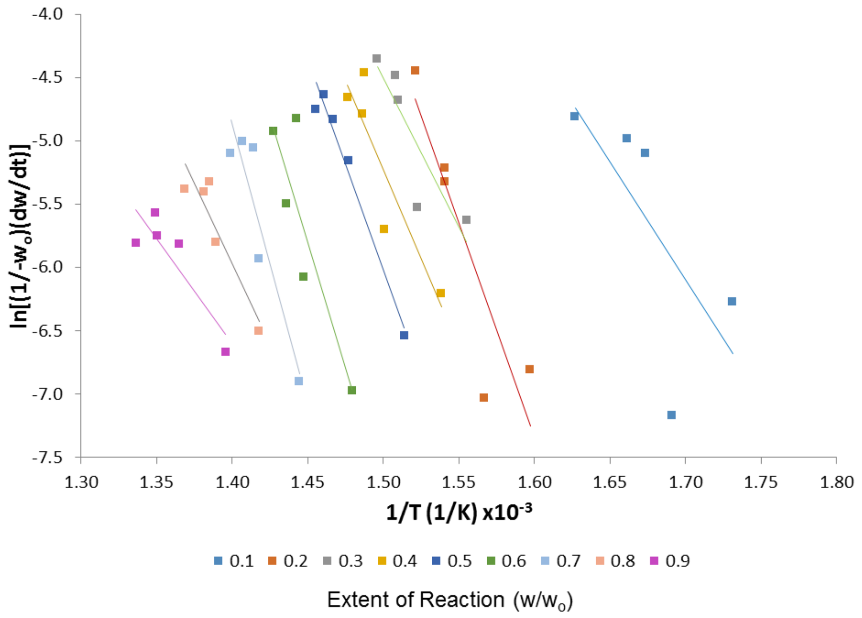

Figure 22. Determination of activation energy for MTM 44 pyrolysis reaction

After linearizing the kinetic equation, the next step in the Friedman method is to consider the same value of (w/w_o) over multiple heating rates and calculate the $ln[(-1/w_o)(dw/dt)]$ for each heating rate. Plotting these points with $ln[(-1/w_o)(dw/dt)]$ as the Y-axis and $1/T$ as the X axis gives $-E_a/R$ as the slope and the Y-intercept as $ln(A*f(w/w_o))$. For pyrolysis and char oxidation, w/w_o must be plotted from 0 to 1 for both reactions individually. An example of this is shown in Figure 22 where each series is the collection of points taken from the same (w/w_o) value but at different heating rates. The plotting procedure is then repeated for multiple (w/w_o) values. For each (w/w_o) series, E_a and A$f(w/w_o)$ can be determined. So far the only kinetic parameter that has been determined is E_a and A still needs to be calculated. To do this the form of $f(w/w_o)$ must be known; and in Freidman's original work the form was assumed to be

$$f\left(\frac{w}{w_o}\right) = \left(\frac{w - w_f}{w_o}\right)^n \quad \mathbf{5}$$

where w is the weight of the material at any instant in time, w_f is the final weight of the material after decomposition and w_o is the original mass of material. By multiplying Equation 5 by A on both sides and taking the log on both sides, the form of the equation is again convenient to plot as a linear function.

$$\ln\left[Af\left(\frac{w}{w_o}\right)\right] = \ln A + n * \ln\left(\frac{w - w_f}{w_o}\right) \quad 6$$

The left hand side of Equation 6 is the same term used as the Y-intercept in Equation 4. Figure 23 shows the decomposition data plotted according to Equation 6 using an X-axis of ln$((w\text{-}w_f)/w_o)$, a slope of n (where n is the reaction order), and ln$A$ as the Y-intercept. In this case the different (w/w_o) series are all grouped together into a common data set.

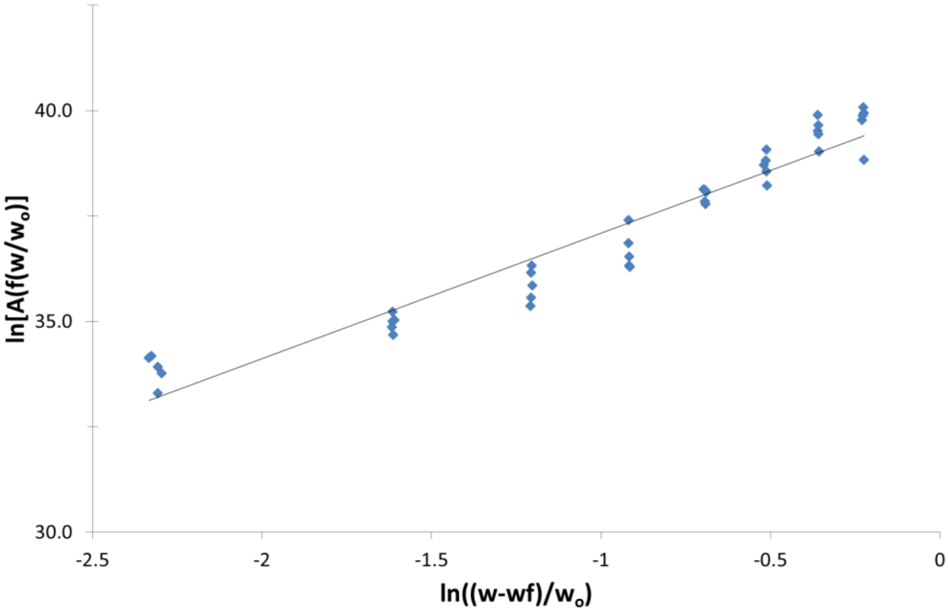

Figure 23. Determination of preexponential factor (A) and reaction order (n)

Table 6. Kinetic Constants for MTM 44

Reaction/Parameter	Pre-exponential Factor (A) (1/s)	Activation Energy (Ea) (J/mol·K)	Reaction Order (N)
Pyrolysis	$2.522\text{x}10^{17}$	271,022	2.97
Char Oxidation	303,000	120,576	1.02

Table 7. Kinetic Parameters for MTM 57

Reaction/Parameter	Pre-exponential Factor (A) (1/s)	Activation Energy (Ea) (J/mol·K)	Reaction Order (N)
Pyrolysis	1.24×10^{6}	8,881	1.18
Char Oxidation	9.27×10^{8}	165,684	1.69

3.6 X-Ray Photoelectron Spectroscopy (XPS)

X-Ray Photoelectron Spectroscopy (XPS) is used to identify elements and their chemical and electronic state on the surface of a material. In XPS an X-ray beam is used to excite the electrons of atoms on and near the surface of a substrate material. When these electrons relax to a lower energy state, they release energy in the form of a characteristic photon. The energy of the photon identifies the element being excited. Studying the energy distribution and amounts of photons allows further identification of the material under study to the point where compositional, electronic, and chemical bonding information is determined. A Kratos Analytical Axis Ultra XPS with a spot size of 300 μm x 700 μm of monochromated Al K-α radiation was used to collect spectra. Three areas were analysed for each fibre sample. A complete scan was conducted on each carbon fibre sample, and the elemental peaks were identified along with their atomic percentages. Shirley backgrounds were applied to carbon (1s), oxygen (1s), nitrogen (1s), and sodium (1s) peaks when present. Fibre bundles were taped to an aluminium sample bar and spectra were collected from areas without tape underneath to prevent contributions from the carbon tape appearing as part of the sample spectrum.

3.7 Brunauer-Emmett-Teller method for surface area (BET)

A measure of surface area is possible by the use of gas adsorption techniques. The Brunauer-Emmett-Teller (BET) method is commonly used. The BET method expands the Langmuir Theory for monolayer adsorption to multilayer adsorption. In order for multilayer adsorption to work, then at equilibrium, the evaporation rate of the i^{th} layer must be the same as the condensation rate as the $i+1$ layer. In the BET derivation the assumption is made that the evaporation and condensation properties in the second and further adsorbed layers are the same as if they were in the liquid state. The volume of adsorbed gas can then be related to the assumed volume of a complete monolayer of gas (v_m), the saturation pressure of the gas (p_o), the pressure of the gas (p), and a constant (C) as per equation 7. The more familiar form of the BET equation is shown in its linearized form as equation 8 and is only valid in the low pressure regime such that $p << p_o$ [72].

$$v = \frac{v_m C p}{(p_o - p)\left(1 + (c-1)\, p/p_o\right)} \tag{7}$$

$$\frac{p}{v\left(p_o - p\right)} = \frac{1}{v_m C} + \frac{c-1}{v_m C}\frac{p}{p_o} \tag{8}$$

This low pressure regime is commonly taken in the relative pressure (p/p_o) range of 0.05-0.3; however, the more important criteria is that the BET plot is linear and therefore the pressure range of 0.05-0.3 may not always work. The constant C is related to the difference in the heat of adsorption of the first layer and the heat of liquefaction of the second and subsequent layers. C must not be negative [73]. To reach the saturation pressure of the gas, the sample and gas must be cooled. This is typically done with liquid nitrogen which brings the temperature down to 77K. A plot of $\frac{p}{v\left(p_o - p\right)}$ against $\frac{p}{p_o}$ gives a line with a slope $s = \frac{C-1}{v_m C}$ and intercept $i = \frac{1}{v_m C}$. The total surface area can then be determined using equation 9, where W_m is the weight of a monolayer of adsorbed gas, N is Avogadro's number, A_{cs} is the adsorbate (gas that gets adsorbed) cross sectional area, and M is the molecular weight of the adsorbate. *Wm* is defined as the reciprocal sum of the slope and intercept *(1/(s+i))* of the BET equation. The specific surface area of the sample is then simply the total surface area divided by the sample weight [74]. Figure 24 shows the BET plot of one of the virgin T700 fibre samples. The plot is confined to the typical low pressure range of 0.05 – 0.35 p/p_o and also shows the regression of the BET equation through 21 relative pressure points. The Y-axis label is the Micrometrics version of $\frac{p}{v(p_o - p)}$ where the Y-axis is a measure of the weight of gas adsorbed, not its volume.

$$S_t = \frac{W_m N A_{cs}}{M} \qquad 9$$

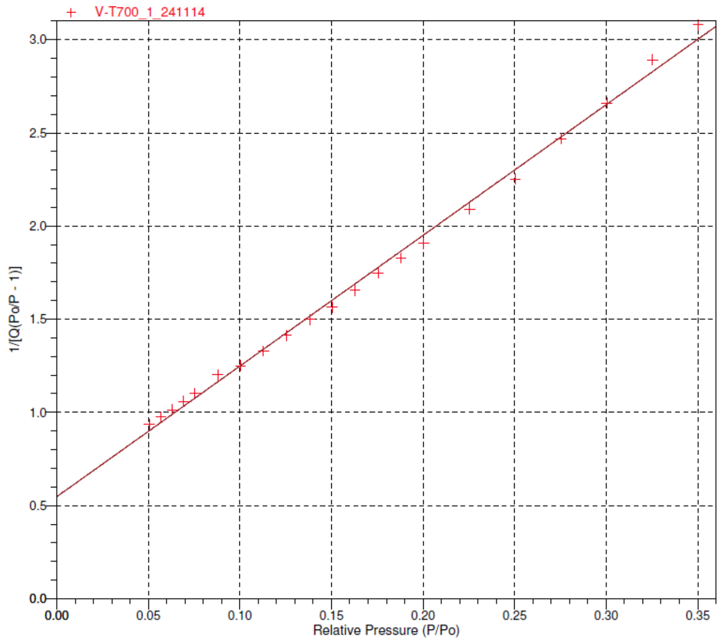

Figure 24. Example BET plot

In practice, the adsorbate sample is weighed and placed in a glass tube or bulb which is also weighed. The sample is then dried and conditioned by heating and pulling vacuum on it while flushing it with a dry inert gas such as nitrogen or helium. This is to remove water and any other adsorbed gasses. In this work samples were conditioned by heating them to 200°C for 3 hours while under vacuum and flushing with dry nitrogen. After conditioning, the sample is allowed to cool to room temperature and weighed with the glass tube to determine its dry weight. A stopper is often placed on the glass tube to keep air from readsorbing onto the sample. The sample and glass tube are then returned to the BET machine for analysis. Before analysis begins, the sample is again put under vacuum until its outgassing rate is sufficiently low (this rate is set by the manufacturer of the equipment). To complete the BET analysis, the adsorbate gas is metered into the glass tube with the sample. Only a small amount of gas is let in at a time. Some of this gas adsorbs onto the sample. The gas is left to adsorb onto the sample for a preset equilibration period during which the relative pressure is measured. If the pressure drops below the preset pressure more gas is let in. This procedure is repeated over and over again at increasing relative pressures of the adsorbate gas. To get the gases to adsorb onto the sample, the gas and sample are cooled. A dewar of liquid nitrogen usually surrounds the glass sample tube and the reference pressure, P_o, tube. For this study a multipoint point BET was used, meaning 11^+ different relative partial pressure points were measured and then the BET equation was regressed though these points. The most common adsorbate gas is nitrogen, but krypton is used for materials with extremely low surface areas [75]. The software on the BET machine is preloaded with the adsorption cross section and additional information about the adsorbate gas for temperatures of 77K (liquid nitrogen), and room temperature.

Filler rods were used to reduce the amount of free volume in the sample tube. Reducing the free volume decreases the number of unadsorbed adsorbate gas in the sample tube which means the pressure measurement is more due to adsorbed gas molecules rather than unadsorbed ones just sitting in the sample tube. For samples with a large surface area the measurement due to unadsorbed gas is negligible. Krypton is useful for analysis of materials with a low surface area because krypton's saturation pressure at 77K is 2.6 Torr compared to ~760 Torr for nitrogen, meaning about 300 times fewer krypton than nitrogen molecules fit in the free volume of the sample cell [75].

3.8 Transmission Electron Microscopy (TEM)

Virgin fibres were used to develop the TEM sample preparation procedure. Small portions of the virgin fibre tow were dispersed in the Embed 812 epoxy embedding medium. Embed 812 was selected as a replacement for Polarbed 812 which was used by Derurbergue and Oberlin when studying high modulus carbon fibres from Toray by TEM [76]. Once embedded the fibres were cut to 80 nm thick cross-sections using a diamond blade on a Leica EM UC6/FC6 - cryoultramicrotome. Micrographs were collected at 110 keV accelerating voltage on a FEI Tecnai 12 Biotwin TEM. Fibres from the 80 nm thick sections frequently pulled out of the resin or fragmented during the cutting process. Thicker 100 nm and 200 nm sections were cut so the fibres were more likely to cut cleanly. These sections were prepared with the intention of thinning using a Focused Ion Beam. However equipment downtime lead to this method of sample preparation being shelved.

4. Materials and Methods

The principal materials used in the study are T700, T800S, IM7, and AS4 carbon fibres, MTM 44 and MTM 57 resin films, and BMS8-276 prepreg, however additional fibres or composites were used to obtain experimental parameters for the thermal kinetic model or to verify the procedures developed for Raman and XRD.

Further details of the fibres used are presented in Table 8. The additional notes field is used to indicate the precursor material, the classification of the fibre, and any additional clarification as for the reason of its use. The T700, T800S, AS4, and IM7 fibres were 'recycled' as just fibres in a tube furnace under 9 different time, temperature, and oxygen concentrations. These fibres were then characterised to try to identify any changes in structure and any correlation between recycling conditions and mechanical properties.

Table 8. Information about fibres used in this work[1]

Fibre	Manufacturer	Sizing	Additional Notes
T700	Toray	Epoxy 50C 1.0 wt%	PAN / HS
T800S	Toray	Epoxy 10E 0.5 wt%	PAN / IM7
AS4	Hexcel	1.0 wt%	PAN / HS
IM7	Hexcel	0.9 wt%	PAN / IM
T600	Toray	Epoxy 50C 1.0 wt%	PAN / HS used for reference in Raman and XRD work
M46J	Toray	Epoxy 50A 1.0 wt%	PAN / HM used for reference in Raman and XRD work
Dialead K139	Mitsubishi Rayon	Not available	Pitch / HM used for reference in Raman and XRD work

1. Sizing data collected from fibre data sheets [77-83]

The two resins used in this work were obtained from UMECO which is currently owned by Cytec Advanced materials. The MTM 44 and MTM 57 resin films were used to make T700 unidirectional laminates for initial recycling trials. Four samples of this MTM44-T700 composite were recycled in the tube furnace to see the difference between composites recycling and just recycling fibre. The hope was to develop an oxidation severity model that would link oxidation severity to mechanical properties. The thermal-kinetic model could then in turn predict the degree of oxidation a fibre would see during a given composites recycling operation. MTM 44 and MTM 57 resin films were also examined using TGA to determine their kinetic degradation properties. MTM 44 kinetic degradation data was used in the thermal-kinetic model. The resin for BMS8-276 was not made available by Boeing.

Table 9. Resin Film Properties

Resin	Glass Transition Temperature (T_g) (ºC)	Cure Temperature (ºC)	Post Cure Temperature (ºC)	Cured Resin Density (g/cm^3)
MTM 57	125	120	120	1.22
MTM 44	190	130	180	1.18

A tool was designed and built to layup and mould composites made from T700 fibre and MTM 57 or MTM 44 resin films. As shown in Figure 25, carbon fibre in the form of a continuous tow is wrapped onto the tool forming a layer of unidirectional reinforcement. Resin film is pressed into the fibre layer and the backing paper removed, leaving the laminate ready for another layer of resin or fibre.

Figure 25. Tool for layup and moulding of composites

Layers of carbon fibre and resin film are stacked to create a laminate-like construction with the necessary fibre volume fraction. By knowing the linear density, size content of the carbon fibre and the number of tows that will fit on the tool, the areal weight of the fibre layer is calculated. The calculated fibre areal weight is used along with the specified resin areal weight to determine the number of layers of fibre and resin needed to achieve a fibre volume fraction in the range of 0.50-0.55. Fibre volume fraction is determined from fibre weight fraction using equation 10 where w_f is fibre weight fraction, w_m is resin (i.e. matrix) weight fraction, ρ_f is the fibre mass density, and ρ_m is the specified cured resin density. Fibre mass density is calculated using Helium Pycnometry. The spacing between pins was chosen so that tows would overlap in the slightest, preventing gaps in the fibre layout.

$$V_f = \frac{w_f / \rho_f}{w_f / \rho_f + w_m / \rho_m} \tag{10}$$

To cure the laminate the entire tool and laminate layup were vacuum bagged and cured in an air circulating oven following the cure cycles described below.

MTM 57:

- Apply vacuum at room temperature
- Heat laminate to 120°C at a rate of 2°C/min
- Maintain temperature for 3 hours
- Cool to 60°C at 2°C/min
- Remove vacuum

MTM 44:

- Apply vacuum at room temperature
- Heat laminate to 130°C at a rate of 2°C/min
- Maintain temperature for 4 hours
- Cool to 60°C at 2°C/min
- Remove vacuum
- Remove laminate from tool
- Pre-heat oven to 130°C
- Load laminate in to oven
- Heat to 180°C at 0.3°C/min
- Maintain temperature for 2 hours
- Cool at 2°C/min to 70°C

BMS8-276 is a prepreg material made by Toray to a Boeing propriety specification. This material is used in the primary structure of the Boeing 787 Dreamliner. The prepreg is epoxy based, with a high T_g (assumed to be similar to MTM 44) and with a fibre weight content of 67%. The fibre used is Toray T800S. The prepreg was supplied by Boeing as a tape 250 mm wide. 6 mm thick laminates of BMS8-276 were made by stacking 30 plys thick and curing with an autoclave. The curing cycle used is listed below:

1. Apply full vacuum (0.75 bar minimum)
2. Pressurize the autoclave to 5.8 bar
3. Once the autoclave is fully pressurized, heat to 180°C at 2.7°C/min (71 minute ramp)
4. Hold at temperature for 120 minutes
5. Cool under pressure until the temperature reaches 60°C
6. Release pressure and remove part

The physical and thermal properties of BMS8-276 were used when developing the thermal-kinetic model. The fibre content of BMS8-276 was determined by TGA. A laminate of BMS8-276 was used to determine the heat transfer coefficient and thermal conductivity that are used in the thermal-kinetic model.

5. Testing Strategy

In this study a novel fibre characterisation program was developed. Previous testing programs have paid more attention to the parameters of the recycling method rather than the entire process which includes what the composition of the composite is, how much of it is fed through the recycling process at a time, control, uniformity, and measurability of the recycling method, and comprehensive testing of the recovered fibres. Along with carefully controlling and designing the entire recycling process, this study wanted to understand how the recycling process changed the structure or chemistry of the fibres and how these changes then correspond to differing tensile strengths and elastic moduli of recycled fibre.

Firstly, composites handlayed from resin film and bobbins of carbon fibre tow were recycled using a tube furnace under a variety of time, temperature, and oxygen concentration conditions. Out of these conditions a narrower range was selected that made sure enough resin was removed from the composite such that the fibres could be separated out into bundles or plys while at the same time limiting the conditions so the fibre would not be ‘overcooked’. Additionally, the conditions were limited to those that would be practical to reproduce on full size recycling rigs.

The outcomes of this research will need to be applied on full size recycling facilities if it is to truly advance the field of carbon fibre recycling. By the time this study was being conducted, the carbon fibre composite recycling community had invested so much time and money into designing and manufacturing state of the art recycling equipment, that the recycling conditions used in this study were kept within the range that could be achieved by this equipment. If this study were to show recycled fibres with very poor mechanical performance, then subsequent work could relax the need for the recycling conditions to be comparable to that achievable on pilot and commercial scale fibre recycling rigs.

A design of experiments for recycling just fibres on their own was constructed around temperature, time, and oxygen concentration of the recycling atmosphere. More exact details regarding the tube furnace used for recycling is found in section 5.1 while the DOE is explained in section 5.3.

Out of the DOE, relationships between recycling process parameters and the structure of the fibre were explored as well as the strength and stiffness of the fibre. The microstructural analysis was carried out to understand more fundamentally and mechanistically what causes the strength and stiffness of the fibres to change. If this could be understood then it might be possible to tailor the recycling process to emphasise one property over the other. By focusing on reclaiming fibres with either a high strength or high stiffness retention then the recycling process might be able to be run more quickly or more cost effectively compared to when it is run to recover fibres with both high strength and stiffness retentions. Knowing how the recycling process changes the mechanical properties of the fibre also allows composites to be recycled under a certain set of conditions based on the intended end use of the recovered fibres, meaning they can be sold at a higher value than fibres recycled to almost meet all needs.

The final component of the testing program was to develop a thermal kinetic decomposition model for composite recycling. This model provides an invaluable framework for ‘simulating’ the recycling process. In this ‘simulation’ the composite material and or the processing conditions can be changed and the effects of this change evaluated. By using this model the time-temperature profile of the fibres in the composite is known. This time temperature profile is then compared to the lab scale recycling work on just fibres (sections 6 and 7) which is used to determine the expected change in mechanical properties. Further details on the model development and use are detailed in sections 9 and 10.

5.1 Lab Scale Carbon Fibre Recycling

5.1.1 Recycling Furnace Construction

In order to study the effect of recycling process parameters on fibre quality, a recycling rig where the temperature, oxygen concentration, and process time could be carefully controlled and measured was needed. A Carbolite CTF tube furnace was purchased to provide the core piece of equipment to build a recycling rig around. Provisions were made for gas tight endcaps with thermocouple glands, data logging, the ability to mix air with nitrogen, and an oxygen meter to determine the actual oxygen content of the gas being delivered to the tube furnace. N-type thermocouples were used to measure the temperature inside the worktube, while a rigid 3 mm diameter K-type thermocouple was used to push and pull the sample tray within the furnace as well as measure the sample tray temperature. The sample tray was constructed from stainless steel and is shown in Figure 26. The tray was 40 mm wide at the base, 50 mm wide at the top, 70 mm long, and 10 mm high with a screened in front and rear to allow for air flow through the sample. Data logging and PID control was achieved through a Eurotherm Nanodac controller with three thermocouple channel inputs in addition to a fourth built-in thermocouple to measure the temperature of the furnace between the work tube and the heating coils. The subsequent section details how the experimental setup evolved to its final state as shown in Figure 27.

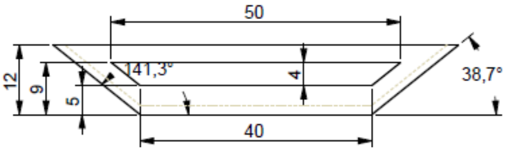

Figure 26. Sample Tray

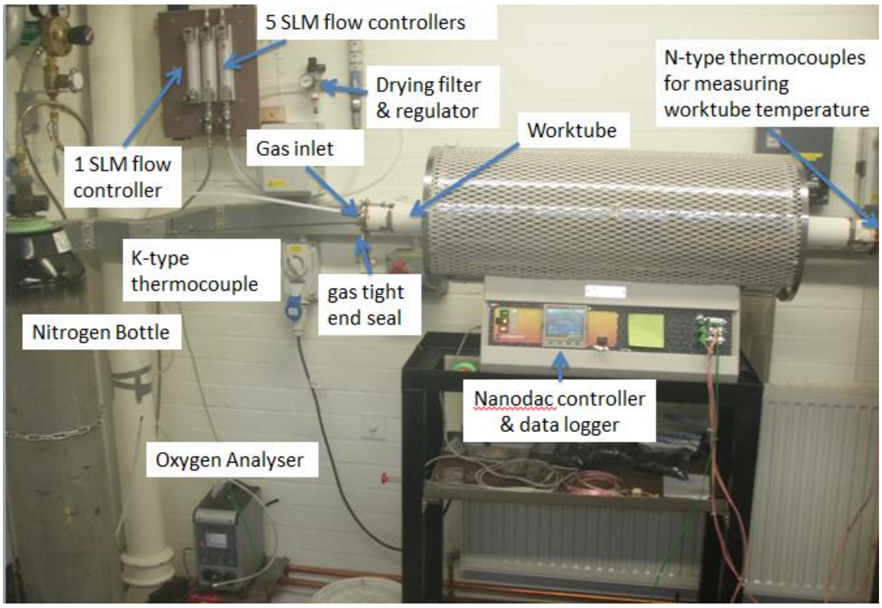

Figure 27. Carbon fibre recycling tube furnace

Initially oxygen for the process was provided by the building's central air line metered by a 5 Standard Litre per Minute (SLM) air flow controller prior to being mixed with nitrogen and run to the furnace. Dry oxygen free nitrogen was supplied from a bottle and also connected to a 5 SLM flow controller before being mixed with air and sent to the furnace. The air supply turned out to have an unstable flow rate, probably varying according to the overall demand across the building. To make the air supply useable, a drying filter and pressure regular was installed between the airline and the flow controller. Regulating the house air supply down to 1.5 bar from ~7 bar resulted in a stable flow rate. The nitrogen bottle was also regulated to 1.5 bar. The use of flow controllers on the air and nitrogen supplies allowed for the oxygen concentration in the gas stream delivered to the tube furnace to be accurately varied between 0 and 21% O_2 while maintaining an overall flow of 5 SLM. One reason for using 5 SLM was to ensure the air to fuel ratio during recycling would always be in excess. The more important reason for selecting 5 SLM was to ensure accurate and repeatable oxygen concentrations in the air–nitrogen mixture. The flow controllers used were accurate in the range 0.6-5.0 SLM and had marked increments at every 0.2 SLM between 0.6 SLM and 5.0 SLM. An overall flowrate of 5 SLM ensured that any limit to the precision or accuracy at which the flow controllers could be set to deliver the exact concentration of oxygen in the air-nitrogen mixture was not a problem since small deviations in the flow controller setting was insignificant compared to the total gas flow. An oxygen analyser was used to check that the settings on the flow controllers actually delivered the intended oxygen concentration.

Temperature uniformity measurements along the length of the worktube were conducted as part of the commissioning process. These measurements, as seen in Figure 28, showed poor temperature uniformity at a gas flow rate of 5 SLM, but acceptable temperature uniformity, ±6°C over 4 cm either side of centre, using a flow rate of 1 SLM. The Servomex 580A oxygen analyser used during the T700 DOE broke beyond repair and a new Servomex Servoflex MiniMP oxygen analyser was purchased as a replacement. Unfortunately, accurate measurement of the oxygen content required greater than 1 SLM flow rate to the oxygen analyser. Figure 29 shows gas flow rates of 1 SLM to the oxygen analyser fall outside of the expected error range, whereas a flow rate of 5 SLM is within the error bounds. The high oxygen content error bound was calculated assuming the air flow controller was set one increment too high and the nitrogen flow controller set one increment too low. The low boundary assumed the opposite. To maintain temperature uniformity and to provide a high enough flow rate to the oxygen analyser, nitrogen and air were mixed at a combined flow of 5 SLM and this flow was then split to the oxygen analyser and to the tube furnace. The supply going to the tube furnace was passed through a third flow controller to limit the flow to 1 SLM. The oxygen analyser calibration and temperature uniformity of the tube furnace were rechecked with the revised gas distribution method. Oxygen analyser calibration was perfect at 0% oxygen (only N_2) and 21% O_2, and within 0.1% of expected oxygen concentrations when mixing air and nitrogen. The temperature uniformity was still within +/-6°C. Figure 30 shows how the air and nitrogen supplies are mixed to the desired oxygen content and then passed to the recycling tube furnace.

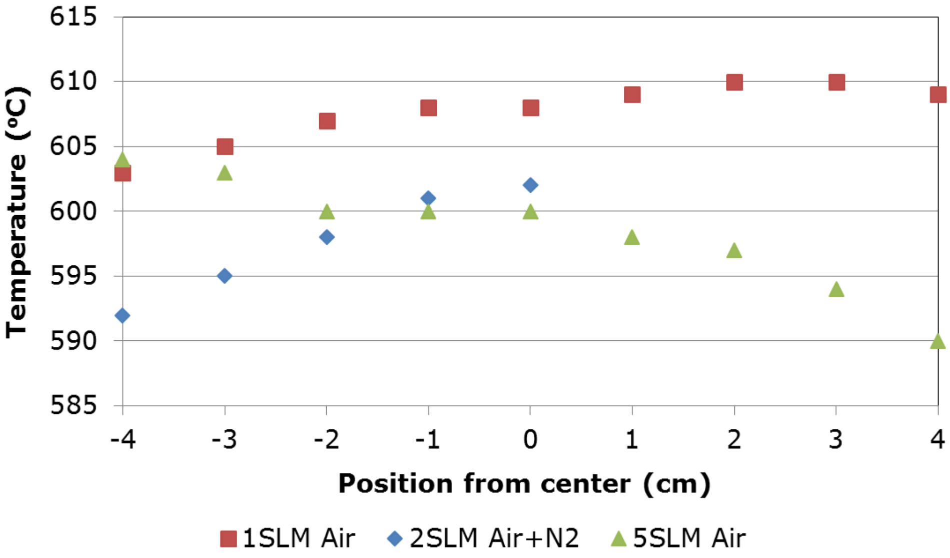

Figure 28. Effect of flow rate on temperature uniformity

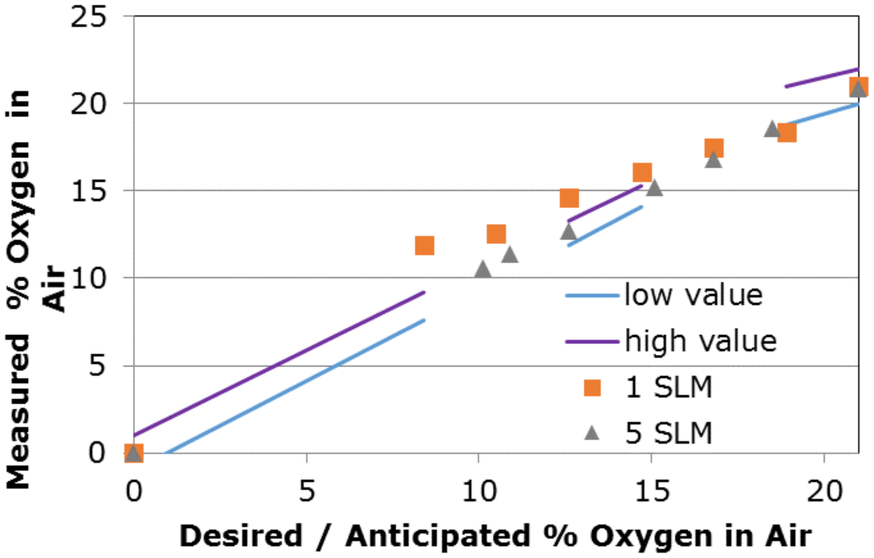

Figure 29. Effect of flow rate on oxygen measurement

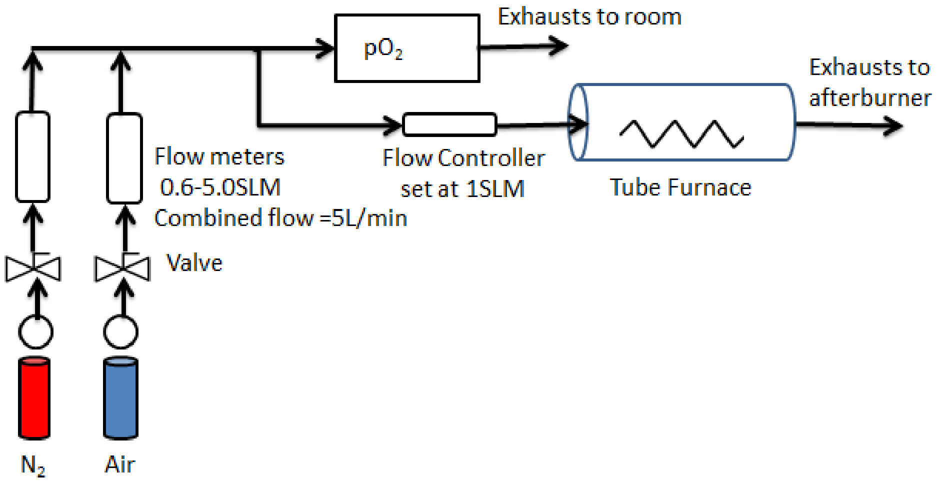

Figure 30. Gas delivery to recycling tube furnace

5.1.2 Operation

To conduct a recycling run a control program is loaded and enabled. Each recycling control program has five parts differing only in the dwell time and temperature setpoint. The steps of each recycling program are:

1 Heating to temperature
2 Inserting the sample
3 Sample equilibration
4 Dwell
5 Cool down

The time and temperature settings were determined from initial composites recycling work discussed in section 5.2. The PID loop is driven off of the “T/C_CH3” input, which corresponds to an N-type thermocouple positioned in the worktube about 5cm from centre. To avoid erroneous measurements this thermocouple is positioned so that it does not touch the sample tray or the worktube walls. In the “T/C CH4” input is another N-type thermocouple positioned alongside the thermocouple in CH3. When the temperature of these two thermocouples is similar, the measurement is valid. If one thermocouple measures much differently from the other thermocouple, then one thermocouple is probably touching the sample tray or the worktube walls. When this happened the setup would be corrected before continuing the run.

Step 1 ensures the furnace is at the desired temperature (550°C, 600°C, or 650°C). Step 2 occurs when the measured temperature inside the worktube is within 2°C of the setpoint. Step 2 tells the furnace to dwell at the current setpoint for one minute. During step 2 the sample tray is pushed into the tube furnace, but not all the way to the centre hot zone. After one minute step 3 starts and allows five minutes for the sample tray to equilibrate to the setpoint temperature. Inserting the sample tray actually cools the worktube; if the temperature in the worktube drops too much, then the PID control loop overcompensates causing a large thermal gradient across the walls of the worktube (in Figure 31 the difference between the “Furnace Temperature” line and the “T/C_CH4 line”). This large thermal gradient then causes the temperature to uncontrollably rise during step 4 (In Figure 31 the “SampleTray Temp” line rises to 560°C even though the PID loop is being driven off of “T/C_CH3” which has exceeded the “Furnace Setpoint”). To avoid the temperature of the worktube dropping too much, the sample tray is pushed to the hot centre zone in increments. During step 3 the temperature of the worktube is allowed to drop 5°C. If a temperature drop of more than 5°C is registered, the equilibration timer is set to pause until the temperature is back in range. An equilibration period of greater than five minutes is thus possible, but preferably avoided to maximise consistency of treatments. Once the five minute equilibration period has passed step 4 is activated. Step 4 tells the furnace to dwell at the current setpoint temperature for a given time (20, 30, or 40 minutes). At the conclusion of the step 4, step 5 engages and sets the temperature setpoint to 200°C which effectively turns off the heating. At this point the sample tray is pulled back to the cold end of the worktube and allowed to cool to

200°C or less before being removed from the furnace. At 200°C there is not enough thermal energy for the oxygen in the air to attack the carbon. After each run the logged data is reviewed to determine the actual treatment time and the range of temperatures the sample was exposed to. Small deviations (±5%) from the desired time are allowed. After running about 25% of the samples, a target temperature range, found in Table 1, was set to ensure consistency across all samples.

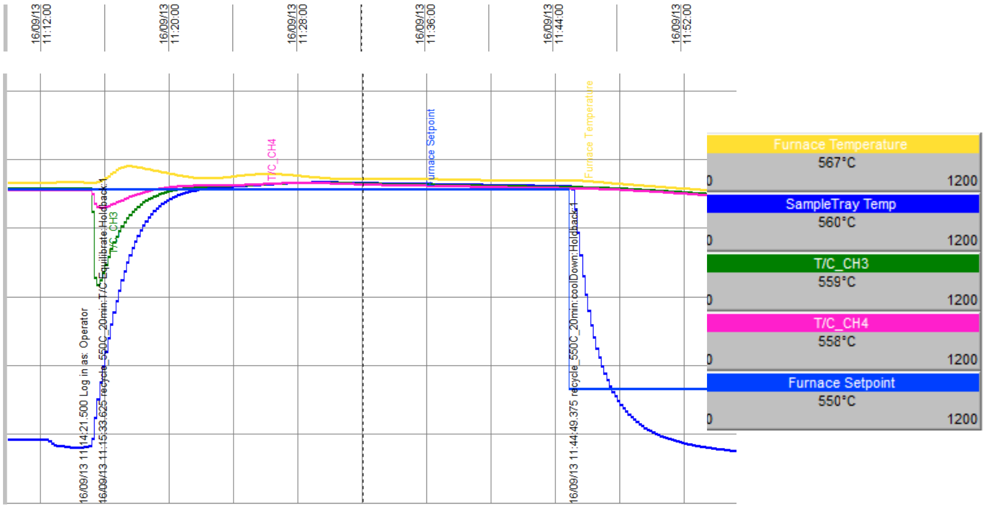

Figure 31. Example data log with thermal overrun

In Figure 31 at 11:15-11:16 a large drop in temperature for ‘T/C_CH3’ is seen along with a peak in the ‘Furnace Temperature’ curve. This behaviour results from the sample tray being pushed all the way into the central hot zone at once. Around 11:22 when ‘T/C_CH3’ and ‘T/C_CH4’ approach the ‘Furnace Setpoint’ temperature, the PID loop turns on the heating elements and the furnace temperature increases again. This rise in furnace temperature provides enough thermal inertia that even over the next 12 minutes the ‘SampleTray’ temperature is much greater than the ‘Furnace Setpoint’ temperature.

Table 10. Target temperature range for recycling runs

Desired Temperature (°C)	Target Temperature Range (°C)
550	542-548
600	597-600
650	644-648

5.2 Initial Recycling Work

Figure 32 shows the recycling process conditions used in initial work to define the useful parameter space for a design of experiments. Two ply unidirectional composites were fabricated with Toray T700 fibre and either Umeco MTM 44 or Umeco MTM 57 resin films with an intended fibre volume fraction of 0.5-0.55. The fibre bundles recovered from each condition were given a pass or fail rating based on their handling characteristics. A fibre bundle would receive a fail rating if it was stiff (indicating not enough removal of resin or too much charring), if the fibre bundles could not be separated into plys, or if within a ply the fibres did not easily separate. Fibre bundles that were given a pass rating were soft to the touch, separated easily both interlaminarly and within the ply, and could easily blow away given a slight air current.

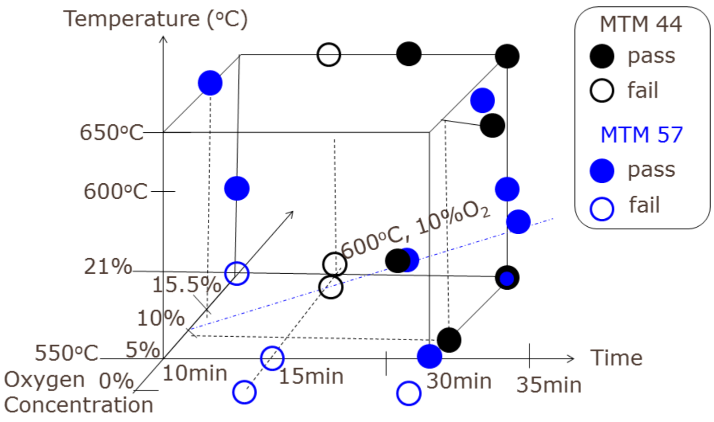

Figure 32 Recycling conditions tested to define DOE parameter space

The levels chosen for the time, temperature, and oxygen concentration factors are influenced by two goals: 1) to be representative of commercial scale recycling processes and 2) for there to be enough change in fibre properties that these changes can be accurately and reliably measured. The fluidised bed recycling rig operates using air (21% oxygen) and a temperature of 550^{o}C. The US and World Patent filed by, at the time Recycled Carbon Fibre Ltd., but now ELG-RCF, reports a two-step process. The first stage uses a reduced oxygen environment, preferably less than 16% oxygen, at temperatures in the 300^{o}C to 500^{o}C range with residence times of three to fifteen minutes [84]. During the first stage, resin that is not volatilized forms a char structure that is extremely stable at low temperatures and reduced oxygen concentrations. Therefore to “clean” the fibres, a second higher temperature stage is needed with an oxygen concentration of about that of air (~21%), temperatures around 550^{o}C-600^{o}C and residence times of one to ten minutes.

So far the DOE under consideration is a single stage with a set dwell time, temperature, and oxygen concentration. As can be seen from Figure 32 and Table 11, twenty-one recycling test runs have been conducted using thin composite samples ~20 mm x 70 mm in size. Based on the analysis from these test runs, a proposed parameter space can be constructed. The parameter space must compromise between operating under similar conditions to a real recycling process and producing enough variation in fibre properties. If very little variation in fibre properties is measured, the DOE may not be able to resolve why the properties have changed.

Table 11. Fibre weight fraction and observations for trial recycling runs. Letter in brackets [] refers to the image in Figure 33.

Resin	Recycling Condition	Measured X_f	Observations	Pass/Fail
MTM 57	21% O_2 550°C 30 min	0.64	clean, small spots/smudges of char	Pass
MTM 57	15.5%O_2 650°C 10 min	0.61	fully separated, very loose	Pass
MTM 57	21% O_2 550°C 10 min	0.67	can pull the sample apart but the resistance is easily felt. Fibres in top ply are less bound together	Fail
MTM 57	100% N_2 550°C 15 min	Not measured	matrix is degraded but fibres are still surrounded	Fail
MTM 57	100% N_2 550°C 30 min	Not measured	some loose fibres	Fail
MTM 57	21% O_2 600°C 10 min	0.64	loose fibres	Pass
MTM 57	21% O_2 600°C 30 min	0.60	soft; well separated	Pass [D]
MTM 57	5% O_2 550°C 15 min	0.68	burnt/ stiff	Fail
MTM 57	5% O_2 550°C 30 min	0.70	soft to the touch but still bound together within each layer	Fail
MTM 57	15.5% O_2 650°C 35 min	0.48	many of the fibres are pitted. Pitting may be location dependent	Pass [C]
MTM 57	10% O_2 600°C 20 min	0.64	well separated easy to pull apart. Some sections stiffer than others	Pass
MTM 57	10% O_2 600°C 33 min	0.62	well separated, soft	Pass
MTM 44	21% O_2 650°C 15 min	N/A	fibres were quite stiff, the plys had started to separate but were still bound together.	Fail
MTM 44	21% O_2 650°C 30 min	0.63	fibres were loose although somewhat difficult to pull apart. fibres seem to charge under SEM but otherwise look clean. Very small bits of char.	Pass
MTM 44	21% O_2 650°C 38 min	0.70	very easy to pull part. Fibres feel light. Small bits of char on every fibre. Not as much char between fibres	Pass

Figure 33 shows SEM micrographs of fibres recycled as part of the effort to define the parameter space for the DOE. Figure 33 reveals varying amounts and formations of char on the fibres. The fibres in Figure 33C are clean; however the pitting was found to reduce the tensile strength and elastic modulus by 36% and 27%, respectively (Figure 34). Obviously running a recycling process so that it produces pitted fibres is unacceptable, but including this condition in the DOE will hopefully show what conditions cause pitting and what tests can detect pitting. Additionally, there have been fibre samples from ELG-RCF and eMIT-RCF that have poor tensile strength but no visual indicators. Using a DOE to establish the relationship between a fast test, such as Raman Spectroscopy, and tensile performance could be a valuable tool for carbon fibre recyclers.

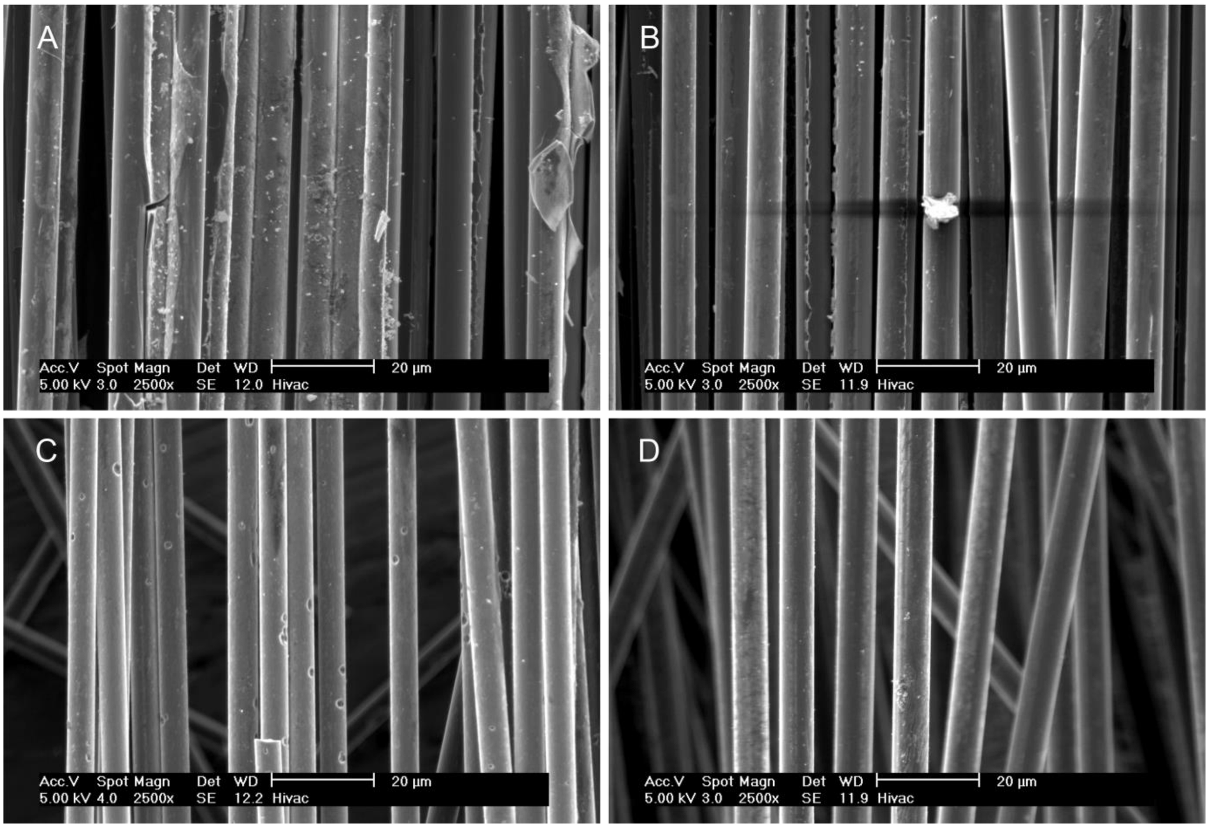

Figure 33 SEM Micrographs of recycled carbon fibres. A) 10% O_2 550^{o}C 30 min MTM 44. B) 10% O_2 600^{o}C 20 min MTM 44. C) 15.5% O_2 650^{o}C 35 min MTM 57. D) 21% O_2 600^{o}C 30 min MTM 57

Fibres in Figure 33A easily charged in the SEM most likely because of being covered with so much char. Large chunks of char can be seen throughout this fibre sample. Char on fibre edges has a gooey appearance. The fibres in Figure 33D, are generally cleaner than those in Figure 33A, having much less area of the fibre covered by char. Small sized bits of char are well distributed throughout the fibre sample shown in Figure 33D, while larger chunks of resin are sporadic and localized.

Initially the surfaces of fibres in Figure 33B look similar to the fibres in Figure 33D. Upon further inspection the fibre diameter is 0.2 µm-0.5 µm larger than expected, suggesting resin has not been fully removed from around each filament. In addition to the streaky appearance of the char, there are what appear to be holes in the surface of the fibre that is actually a small portion of resin or char that has been fully removed. The cleaner appearance of Figure 33D over Figure 33A suggests an increase of temperature from 550^{o}C to 600^{o}C is useful for more fully removing the resin matrix. The fibre sample with pitting (Figure 33C) was recovered from a composite using MTM 57 as the matrix, which is not as thermally stable as epoxy resins commonly used in aerospace such as the MTM 44 resin.

Two recycled fibres were characterized using single filament tensile testing. The first fibre sample was chosen since the SEM revealed pitting on the fibre’s surface (Figure 33C). This fibre sample was expected to be severely damaged as measured by its tensile strength. The second fibre sample was chosen since it was recycled under similar conditions found in The University of Nottingham’s Fludised Bed Recycling process [4]. Figure 34 shows the tensile strength of these recycled fibres as determined by the normal, two parameter Weibull, and three parameter Weibull distributions. In this case Minitab was used to calculate the Weibull distribution. The data labels over the virgin fibre are its tensile strength, while the data labels over the recycled fibres are their percent retention in tensile strength. The fibre recycled using 15.5% oxygen at 650^{o}C for 35 minutes from a matrix of MTM 57 epoxy resin has a severely degraded tensile strength. A similar loss in tensile strength is seen in the second fibre sample recycled in air at 600^{o}C for 10 minutes.

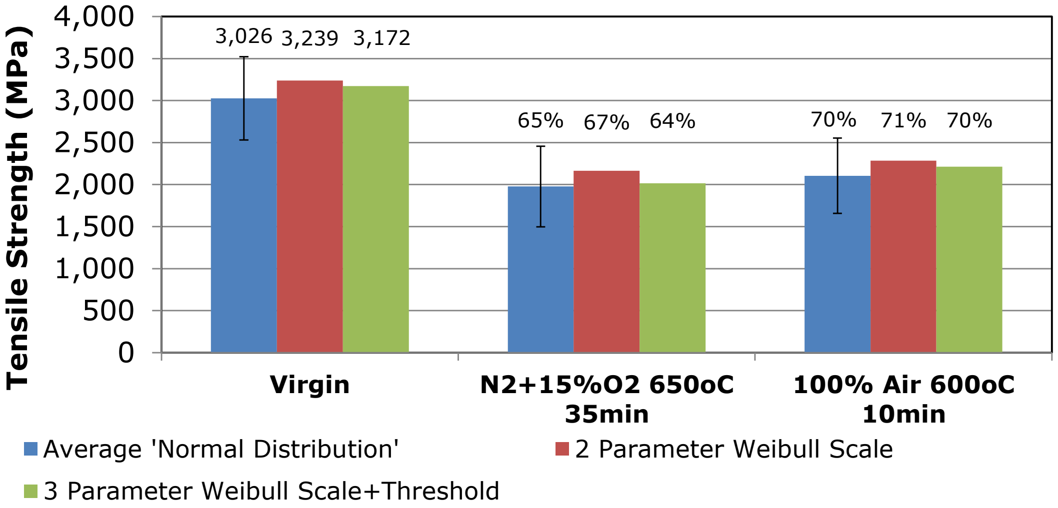

Figure 34 Tensile strength of recycled fibres determined through multiple data analysis procedures. Error bars are standard deviation. Data labels are percent property retention

Compared to conditions used in the Fluidised Bed, 650°C is hot and 35 minutes is a long time. However, in this experiment the oxygen concentration was lower (15.5% vs. ~21%) suggesting that the higher temperature may have aided the oxidation of the carbon fibre. From a mechanical strength point of view, less oxygen and cooler temperatures should be used for the recycling process. On the other hand SEM imaging shows the epoxy resin being difficult to remove under gentler conditions such as Figure 33B vs. Figure 33C. Clearly a design of experiments will be helpful in determining the trade-offs between fibre cleanliness and mechanical strength.

Figure 35 shows the elastic modulus of the two recycled fibres as well as virgin T700 for comparison with data labels showing percent retention in elastic modulus. Under the more aggressive recycling conditions a drop in the fibre's elastic modulus of 27% was measured. It is tempting to assume that since the strength of the fibre dropped so much that its stiffness might also decrease. However, structurally what gives a carbon fibre its strength is not completely the same as what determines its stiffness. The maximum tensile strength is based on the

C-C bond strength of graphite like sheets and the orientation of these bonds to the fibre axis. Commercially available carbon fibres only achieve 3.5% of their maximum theoretical tensile strength [23] and this is because strength is more strongly limited by defects than the C-C bond strength and alignment.

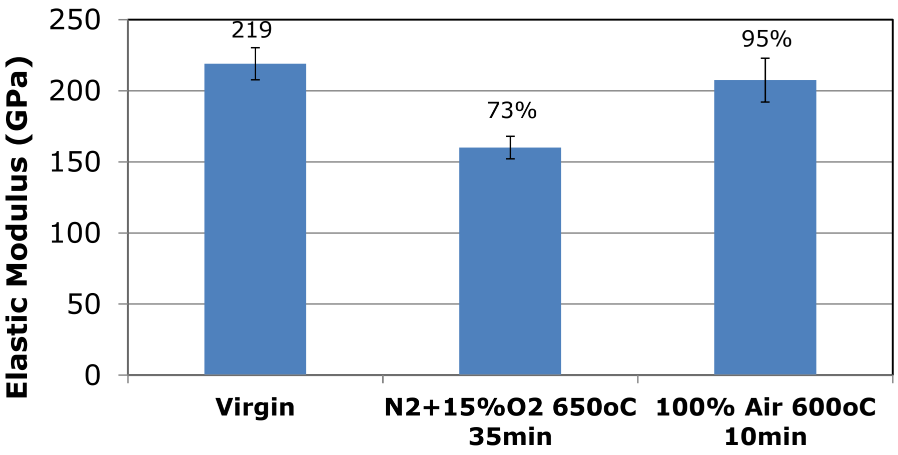

Figure 35 Elastic modulus of recycled fibres

Unlike the tensile strength results, the fibre recycled in air did not show an appreciable decrease in its elastic modulus. Testing done at NCSU has shown behaviour consistent with the above tensile strength and elastic modulus results. That is: it is possible to see both a large drop in tensile strength and elastic modulus (this was seen in fibres recycled by ELG-RCF in 2009) [41], but it is also possible to see a large drop in tensile strength without a corresponding decrease in elastic modulus (this was seen in fibres recycled by ELG-RCF in 2010) [42].

5.3 Design of Experiments (DOE)

Initially a screening DOE was going to be used to find which recycling parameters and over what range should be considered more closely. Testing of the T700 fibres was started as a half-fraction screening DOE; however the results seemed erratic, so a full factorial DOE on the T700 fibres was carried out.

As discussed in section 6, Raman, XRD, and single fibre tensile test results from all of the T700 fibre samples were reviewed and it was decided that the testing planned for the three additional fibre samples should also be run as a full factorial DOE. Three factors at two levels each is eight treatment conditions, plus a centre point of 30 minutes at 600°C under 15.5% oxygen. A replicate of each condition was also run resulting in eighteen recycling runs for each of the four fibre types meaning seventy-two recycling runs overall. The recycling runs were setup as a DOE so a mathematical model relating the recycling condition along with fibre type and fibre producer to Raman, XRD, and single filament tensile testing measurements could be built. Minitab was selected as a software package to set up the DOE model and perform subsequent statistical analysis [85]. Two powerful analysis tools used were interaction plots and Analysis of Variance (ANOVA).

Table 12. Fibres Only DOE

	Levels		
Factors	**Low**	**Centre**	**High**
Time (minutes)	20	30	40
Temperature (°C)	550	600	650
Oxygen Content (%)	10	15.5	21
Fibre Type	Standard Modulus		Intermediate Modulus
Fibre Producer	Hexcel		Toray

Interaction plots show the influence on a response when changing factor levels; each factor is plotted as its own line. As seen in Figure 36 the actual value of the factor is plotted on the X-axis with the value for the response plotted on the Y-axis. If the factor lines are not parallel, this suggests an interaction between the two factors. Factor lines that intersect, such as time and temperature in Figure 36, indicate a very strong interaction between the factors. The strength of the interaction can be quantified by fitting the data to a factorial model. An example of the information Minitab gives for this analysis is shown in Figure 37. The effect column is the relative strength of the factor or of the interaction. Each factor and interaction are treated as variables in a linear equation relating the factors to the response; the coefficient column shows the coefficient on each factor or interaction in the factorial model equation. P-values are used to decide if a factor or interaction has a statistically significant impact on the response. A p-value of <0.05 (corresponding to 95% confidence intervals) was chosen as the level of significance for this analysis. Factors and interactions with a larger magnitude number in the effect column have correspondingly smaller (more significant) p-values. The p-values calculated by fitting the data to a factorial model are the same p-values calculated using ANOVA.

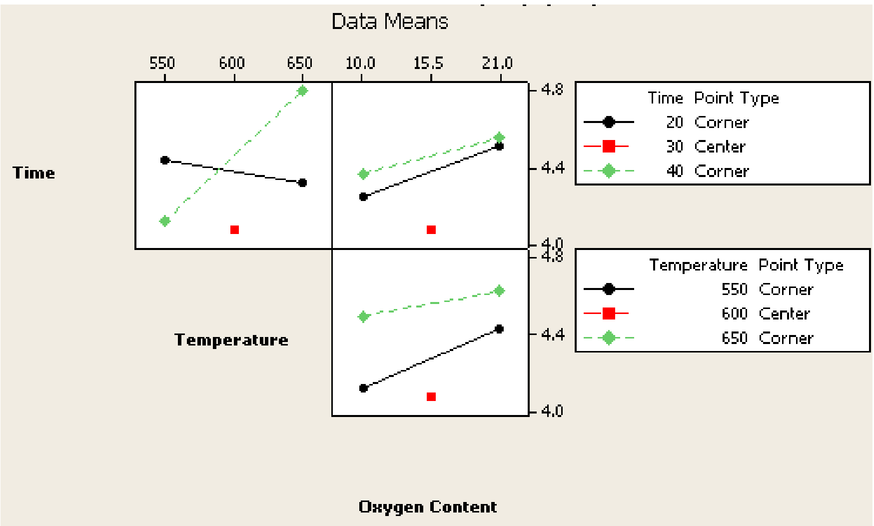

Figure 36. Interaction Plot for La(10)

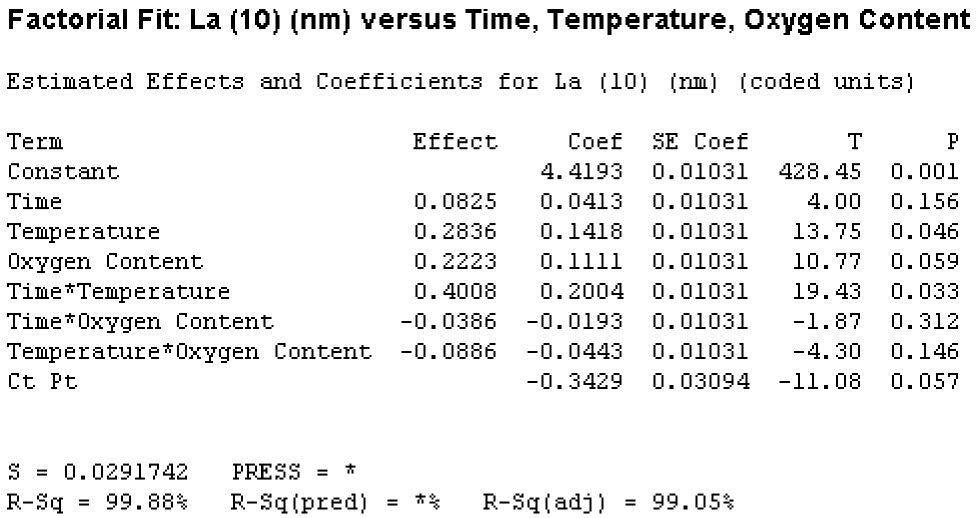

```
Factorial Fit: La (10) (nm) versus Time, Temperature, Oxygen Content

Estimated Effects and Coefficients for La (10) (nm) (coded units)

Term                            Effect     Coef  SE Coef       T      P
Constant                                 4.4193  0.01031  428.45  0.001
Time                            0.0825   0.0413  0.01031    4.00  0.156
Temperature                     0.2836   0.1418  0.01031   13.75  0.046
Oxygen Content                  0.2223   0.1111  0.01031   10.77  0.059
Time*Temperature                0.4008   0.2004  0.01031   19.43  0.033
Time*Oxygen Content            -0.0386  -0.0193  0.01031   -1.87  0.312
Temperature*Oxygen Content     -0.0886  -0.0443  0.01031   -4.30  0.146
Ct Pt                                   -0.3429  0.03094  -11.08  0.057


S = 0.0291742    PRESS = *
R-Sq = 99.88%    R-Sq(pred) = *%    R-Sq(adj) = 99.05%
```

Figure 37. Minitab output for analysing La$_{(10)}$ according to a factorial model

5.4 Thermal Modelling

To compliment the physical testing a computer model to study carbon fibre recycling was also developed. Two different methodologies for modelling a recycling process were considered. One approach would be a modelling of the physical process which would give the temperature of the composite over time and would examine how different resin chemistries might affect the local temperature distributions or how well the uniformity of intended process conditions would be preserved. The second approach, chosen for this work, was to model the processes taking place in the composite as it is recycled. This has the advantage of being much more process independent so long as the process provides thermal energy and decomposes the resin by oxidation. Previous work at the University of Nottingham did provide an existing model for thermal-kinetic degradation of composites [7]. This work uses the same principals but expands on the utility and flexibility of that model. The previous model was built in COMSOL where complex computations where handled by MATLAB and the result then brought back into COMSOL.

Initial model development was conducted in ANSYS Fluent to take advantage of the Computational Fluid Dynamics (CFD) which would incorporate in the model some elements of the physical recycling equipment such as geometry and air flow as well as work using the same platform as a concurrent project to model fluidised bed behaviour. The fluidised bed model covers the behaviour and characteristics of a fluidised bed such as fluidisation velocity, bed density, and heat transfer as well as adds the ability to track particles moving through the bed. In this framework the composite being recycled can be the particles tracked by the fluidised bed model, and the thermal kinetic model can be given temperature and heat transfer information from the fluidised bed model and then provide back information such as the temperature, size, density, and mass off the composite as it undergoes recycling. Unfortunately the chemical reaction capabilities of Fluent were too limited to allow oxidation reactions where the products included a partially oxidised solid. Next, COMSOL was considered. The existing model using COMSOL did not use COMSOL to keep track of the oxidation reaction because of software limitation at the time. Since the original model was developed, COMSOL has produced new versions with the ability to handle chemical reactions.

Rather than be reliant on a specialised software package, the entire thermal kinetic oxidation reaction modelling was written originally in Microsoft Excel. Writing the model in Excel provides easy access to all processes taking place as part of the recycling operation as well as information on the physical state of the composite. The downside to working in Excel is the large data set and complex calculations needed do not run efficiently, resulting in very slow calculations. While running the model uses all of Excel's resources, Excel does not make full use of the RAM or processing power available of the computer it runs on. Another advantage of Excel was it was supposed to be easy to integrate with other models used to determine the cost, process time, and general behaviour of the fluidised bed. However, late in the development process Excel crashed and corrupted the model file. Backup copies would similarly become corrupt when opened. The program file was ‘recovered’ but all named ranges and formulas were lost. Instead of rebuilding the model in Excel, the model was written from scratch using the Java programming language. Material properties are hardcoded as constants but in the future could be edited with a user dialogue. Each calculation step is not stored in run time, making the application much more stable compared to Excel. Intermediate calculations as well as final results of temperature and mass of each layer over time are stored in a comma separated value text file. Java would enable the modelling code to be compiled into an executable and used as a standalone program, or the code and program flow can simply be adapted to a different programming language, maintaining the ability to integrate it with other fluidised bed models.

6 Lab Scale Recycling

Recycling and subsequent testing of fibres took place in two phases. The fibres were not recycled from a composite, but instead conditioned in the 9 different time, temperature and oxygen concentrations as explained in section 5.3. The first phase focused on T700 fibres and using these fibres to assess the utility of the Raman, BET, TEM, and XRD characterization techniques. Additional virgin carbon fibres were also characterized by XRD and Raman to verify how well these techniques work on carbon fibres and to see the differences between different types of virgin fibres versus different recycled carbon fibre samples. T700 fibres are high strength PAN fibres made by Toray Carbon Fibre and were available from the start of this work while T800S, AS4, and IM7 had to be purchased and shipped to the UK. During the second phase the remaining fibre types (T800S, AS4 and IM7) were recycled and all fibres were characterised using single filament tensile testing, and XPS.

6.1 T700 DOE and Microstructural Analysis

The T700 subset of testing was conducted using a full factorial design of experiments with two replicates and one centre point. Figure 38 shows the nine conditions of the T700 DOE and the corresponding sample names are listed in Table 13. Fibres recycled in air are labelled as recycled in 21% O_2 in their naming convention. Analysis from Raman, XRD, and single filament tensile testing were used as the response values. From Raman: A_D/A_G, from XRD: interplanar spacing, crystal size, and orientation factor, and from tensile testing tensile strength and elastic modulus are considered. Minitab® was used to conduct ANOVA and to generate interaction plots.

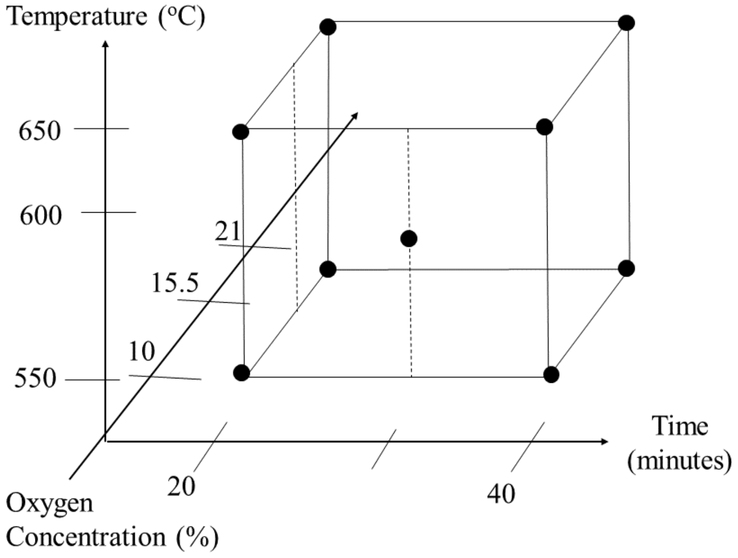

Figure 38. Fibre recycling DOE conditions

Table 13. T700 DOE sample names

1.	T7_20min_550C_10%O_2
2.	T7_40min_550C_10%O_2
3.	T7_20min_550C_21%O_2
4.	T7_40min_550C_21%O_2
5.	T7_30min_600C_15.5%O_2
6.	T7_20min_650C_10%O_2
7.	T7_40min_650C_10%O_2
8.	T7_20min_650C_21%O_2
9.	T7_40min_650C_21%O_2

Table 14 presents a summary of the microstructural analysis by listing which interactions of factors are significant for each microstructural feature/ response, while more detailed analysis of the results is presented in sections 6.3 and 6.4. Factor lines which intersected in an interaction plot were considered important. Factor interactions with a p-value of <0.05 were considered significant. Interaction plots give a visual indication of the strength of interaction, whereas the factorial model provides a quantifiable metric for the strength of the interaction and runs a standard test that can be used to say whether or not an interaction is significant. Oxygen content is abbreviated as [O_2], since in chemistry [] indicates concentration. If no significant interactions were found then ‘none’ is listed in the Table 14. Considering all the interaction plots, the interaction of time and oxygen concentration appears to be significant in only one case whereas the interaction of time and temperature as well as the interaction of oxygen content and temperature are each significant in four cases. The factorial model indicates only $La_{(10)}$ and $d_{(10)}$ having significant factors or interactions. The interaction of time and temperature are significant in both cases.

Table 14. Significant factors and interactions in T700 DOE

Response/ Microstructural Feature	**Interaction Plot**	**Factorial Model**
$Lc_{(002)}$	Time X Temperature	none
$La_{(10)}$	Time X Temperature	Temperature and [O_2] Time X Temperature
$La_{(11)}$	Time X Temperature Temperature X [O_2] Time X [O_2]	N/A
$d_{(002)}$	none	none
$d_{(10)}$	Time X Temperature Time X [O_2]	Temperature and [O_2] Time X Temperature Temperature X [O_2]
$d_{(11)}$	Temperature X [O_2]	N/A
A_d/A_g	Temperature X [O_2]	none
Orientation Factor	none	none

6.2 Tensile Data

No simple relationships between recycling conditions and tensile strength or elastic modulus were discovered from testing the T700 fibres. Hypothesis testing using Tukey's Method [86] revealed significant differences between sample tensile strengths and elastic moduli. However, ANOVA of the DOE data does not suggest any significant factors or interaction of factors that indicate the change in tensile strength and elastic modulus is based on the recycling treatments. A high-level review of tensile strength and elastic modulus results reveal a few interesting and otherwise unpredicted results: Firstly, sample T7_40min_650°C_21% O_2 has the highest tensile strength despite being recycled under the condition with the most oxidising power. Further investigation reveals a slightly reduced breaking load and an extreme reduction in fibre diameter with respect to V-T700. The breaking load decreases from 11.3 cN to 10.3 cN and the diameter from 6.5 µm to 5.6 µm

Table 15. Fibre diameter of T700 fibres

Sample	Diameter (μm)
V-T700	6.54 ± 0.91
T7_20min_550C_10%O_2	6.93 ± 0.69
T7_40min_550C_10%O_2	6.91 ± 0.83
T7_20min_550C_21% O2	6.81 ± 0.85
T7_40min_550C_21% O2	6.77 ± 0.75
T7_30min_600C_15_5%O_2	6.63 ± 0.77
T7_20min_650C_10%O_2	6.21 ± 0.71
T7_40min_650C_10%O_2	6.17 ± 0.71
T7_20min_650C_21% O2	6.22 ± 0.93
T7_40min_650C_21% O2	5.60 ± 0.50

Table 15 shows the average fibre diameter of the T700 samples as measured by the LDS0200. The small diameter of the T7_40min_650°C_21% O_2 contributes to its high tensile strength, but does not explain why the breaking load is lower than less aggressive recycling conditions. SEM micrographs such as Figure 39 show clean, relatively smooth looking fibres with a few round features in addition to localised areas of lighter discoloration. Given the uniformity of the fibre surface after undergoing a significant diameter reduction, it makes sense for the round features to be deposits of material that had previously been removed. The areas of discolouration make it look as though the fibre is slightly indented in those regions but SEM alone was unable to determine this definitively. These discolouration patches are more prevalent on fibres recycled under very hotter conditions and could be very thin deposits of carbonaceous material or a local weakening of the structure which has made the fibre less conductive. A high tensile strength might mean the surface damage was smoothed out or oxidised away to avoid failure from surface defects or it could suggest that the strength of carbon fibres is more core than surface driven (in the absence of defects).

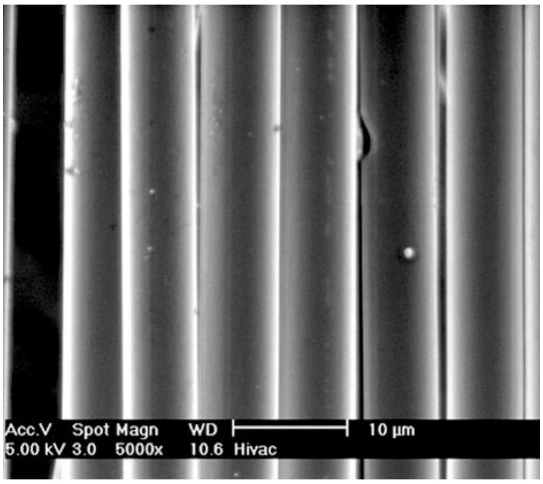

Figure 39. T7_40min_650C_21% O_2

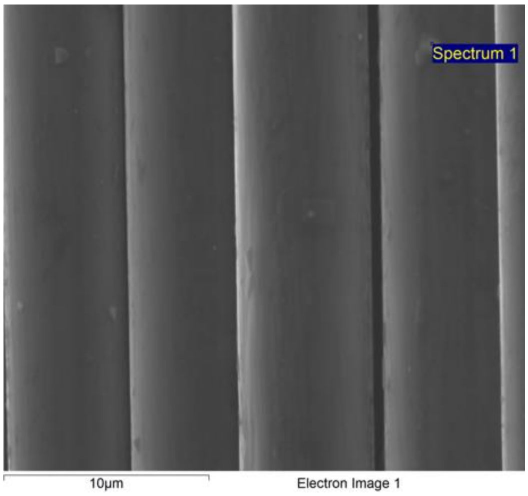

Figure 40. MTM 44 – T700 CRP 40min_650C_21% O_2

Using the same recycling conditions as above, the fibres recovered from composite show a large drop in tensile strength and elastic modulus. SEM of this fibre showed a clean surface without pitting (Figure 40). In the absence of visible defects, any defects must be very small (which would then also suggest the loss in strength should not be as severe) or there are structural or chemical changes to the fibre resulting in the change in fibre mechanical properties. EDS of a raised feature on this fibre sample indicated the presence of silicon, sodium, and chlorine in addition to the usual carbon, oxygen, and nitrogen. Silicon could be from a releasing agent on the tool surface, resin film backing paper from when the composite panel was made, from the worktube of the furnace, resin chemistry, or more simply a component in the fibre precursor. Since the silicon is in low concentrations and the deposits have a low small area of coverage, any potential release properties of the silicon is not expected to impede resin to fibre adhesion. The sodium and chlorine are probably from a salt compound in the resin chemistry, part of the resin precursor or from the fibre's electrolytic surface treatment. The oxygen and nitrogen content is slightly higher compared to that of a virgin fibre which would be consistent with residual epoxy char being on the fibre surface.

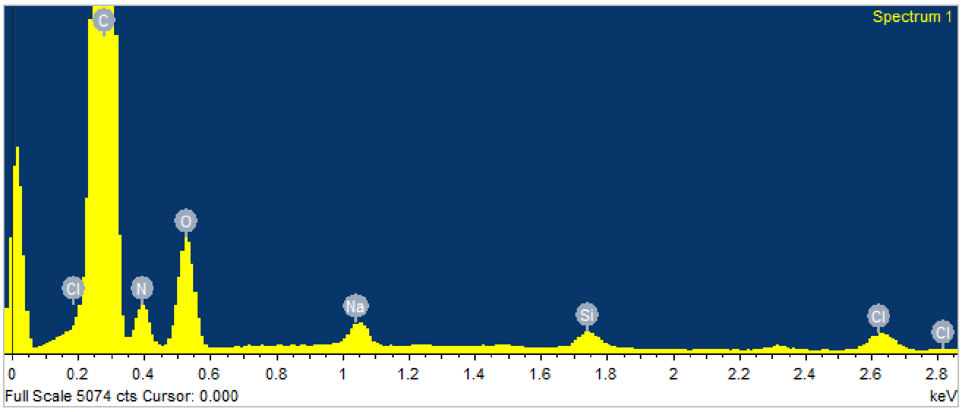

Figure 41. EDS Spectra of area indicated in Figure 39

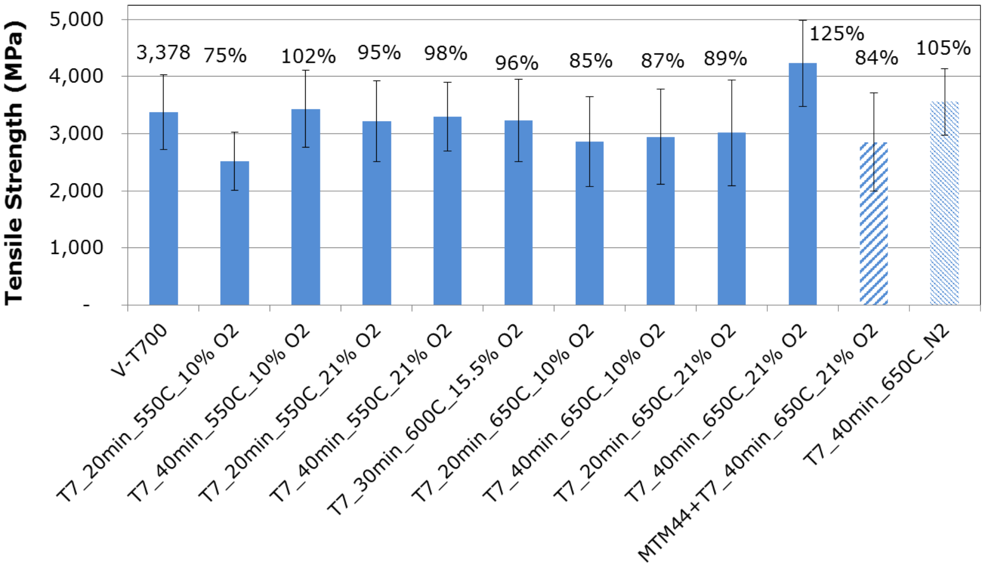

Figure 42. Tensile Strength of recycled T700 fibres. Data labels are percent retention w.r.t virgin fibre. Error bars show standard deviation.

T7_40min_550°C_10%O_2 has a tensile strength at least as high as the virgin fibre despite fibres with similar recycling conditions showing a 13% - 25% decrease in tensile strength. A larger cross-sectional area than measured could explain the exceptionally high tensile strength. While 0.1 - 0.2 μm of error may be expected in the LDS measurement on a single filament, the diameter measurement is not consistently on the low side of average, but rather well distributed around the average as demonstrated by the residuals plot of a normal distribution of fibre diameter measurements. Additionally, the measured diameter is actually greater than that for the V-T700 fibre sample. Considering crystal size and interplanar spacing are not significantly different for T7_40min_550C_10% O_2 than for V-T700 either the XRD measurement is not sensitive enough or other physical or chemical changes to the fibre structure are responsible for its increase in diameter (the same being true for all fibres that exhibit an increase in fibre diameter). 40min_550C_10% O_2 is a potentially favourable recycling condition since tensile strength and elastic modulus remain unchanged with respect to the virgin fibre. Unexpectedly, T7_40min_550C_10% O_2 fared better than the fibre sample treated under the same temperature and oxygen concentration conditions but for half the time (20 minutes). SEM of T7_20min_550C_10% O_2 reveals a smooth but patchy appearance with occasional debris on the surface of the fibre providing little evidence to suggest this fibre should have the lowest tensile strength of the T700 fibres.

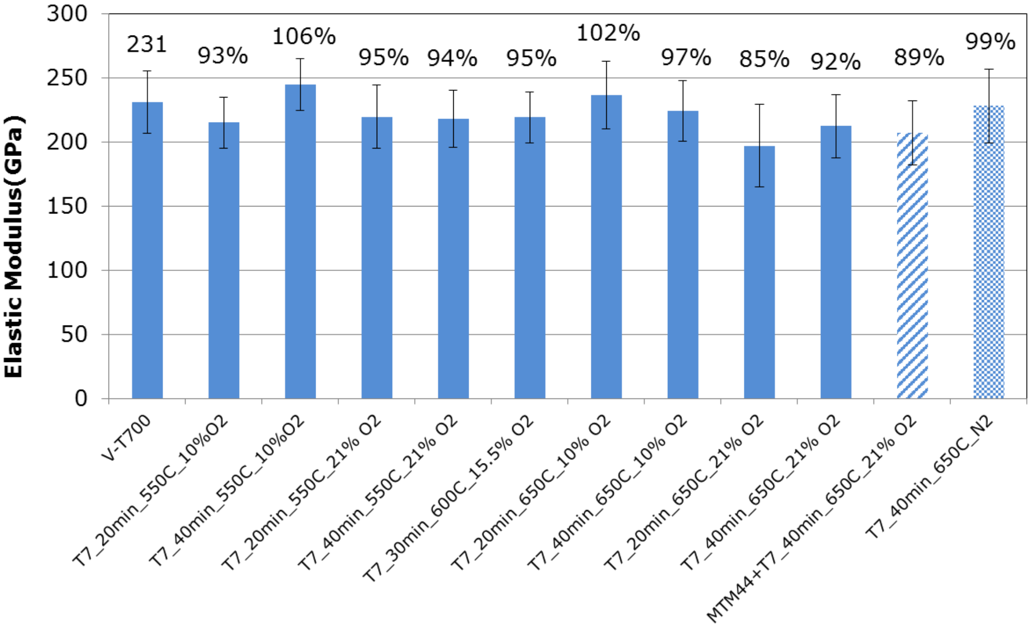

Figure 43. Elastic Modulus of recycled T700 fibres. Data labels are percent retention w.r.t V-T700. Error bars show standard deviation.

Fibre sample T7_20min_650C_21% O_2 has the lowest elastic modulus and perhaps behaves somewhat more traditionally given that its tensile strength is also reduced. SEM shows pits on the fibre surface. Pits form under extreme oxidative conditions. Related carbon fibre recycling work gives an example of fibres being exposed to 600°C in 21% O_2 and developing severe pitting on their surface which was attributed to lowering the tensile strength of the fibre by as much as 60% [41]. From these three examples it is clear the structural elements contributing to fibre strength and fibre stiffness have an even more complex behaviour when a fibre is damaged compared to how the structure informs the strength and stiffness during manufacture of virgin fibre. An additional example is T7_20min_550C_10% O_2 where its tensile strength is reduced by 25% but it elastic modulus remains unchanged compared to virgin T700 fibre. Why the mildest recycling conditions resulted in the most damaged fibre sample is not yet clear. The T800S, IM7, and AS4 fibre types did not have the same oddity, but at the same time no clear trends are evident to suggest the T700 result is false.

Table 16. Weibull Parameters

Sample	Scale Parameter (MPa)	Shape Parameter
V-T700	3652	5.09
T7_20min_550C_10%O_2	2815	5.19
T7_40min_550C_10%O_2	3718	5.43
T7_20min_650C_10%O_2	3192	4.06
T7_40min_650C_10%O_2	3283	3.89
T7_30min_600C_15.5%O_2	3628	5.09
T7_20min_550C_21% O_2	3443	5.40
T7_40min_550C_21% O_2	3551	5.96
T7_20min_650C_21% O_2	3379	3.62
T7_40min_650C_21% O_2	4540	6.27
MT44 T7-40min_650C_10% O_2	3977	6.41
MT44+T7_40min_650C_21% O_2	3131	3.30

Weibull scale and shape parameters for each fibre sample are shown in Table 16. The Weibull shape parameter is a measure of the sharpness of the Weibull distribution. Large shape parameters mean a very sharp distribution where most of the samples fail within a very narrow range of applied stress. The Weibull scale parameter is used here as a measure of tensile strength. Fibre samples T7_40min_650C_10% O_2 and T7_20min_650C_21% O_2 have the two smallest Weibull shape parameters yet have very obvious damage to the fibre in the form of pits. Conventional thought is the pits would be stress concentrators and once enough stress was applied to the fibre these pits would cause the rapid failure of the filaments which would then produce a large Weibull shape parameter. Possibly a by-product of pitting is the release of residual stress such that a larger increase in applied stress is needed to propagate a crack from a defect to another than in a fibre without pits. Three of the four fibres recycled at 650°C have the smallest shape parameter, followed by the sample treated at 600°C, followed by all the samples recycled at 550°C followed by the virgin fibre. As originally anticipated the fibre sample with the most aggressive recycling conditions, 40 minutes at 650°C in 21% O_2, has the largest Weibull shape parameter. No universal trends are evident from the tensile data.

Most often recycling has a minimal effect on the modulus and when it does it is usually limited, percentage wise, to within half the loss in tensile strength [40, 41]. Unlike the T800, AS4, and IM7 fibres analysed, the T700 fibres do not show a trend based on temperature. Average elastic moduli of recycled T700 carbon fibres were within 10% of the value for virgin T700, except for 20min_650C_21% O_2. The recycled T700 fibre with the highest tensile strength is 40min_650C_21% O_2, although this sample actually has an increase in strength which is suspicious and did not happen with any of the other fibre types tested. Since this test result was so unexpected, the tensile tests were repeated in triplicate. Table 17 shows the tensile properties for the three times T700 fibre was treated at 650°C for 40 minutes in 21% O_2 and also a baseline repeatability check which used T700 fibre at 550°C for 20 minutes under 10% O_2. The T7_20min_550C_10% O_2 samples showed good agreement on both tensile strength and elastic modulus. The second set of tests indicated a 74% strength retention and 82% stiffness retention but the third set of test were much like the first set which would suggest a non-uniform treatment or some unknown variability with the fibres themselves. The poorest tensile strength and elastic modulus were from two different recycling conditions as were the best tensile strength and elastic modulus. T700 is the only fibre type to need four different recycling conditions to produce the fibre with the highest tensile, the highest elastic modulus, the lowest tensile strength and the lowest elastic modulus.

Table 17. Repeatability testing on select T700 fibre samples

Sample	**Tensile Strength (MPa)**		**Elastic Modulus (GPa)**	
		COV		COV
T7_40min_650C_21% O_2	4,230	18%	212	11.3%
T7_40min_650C_21% O_2_2	2,509	35%	190	20.4%
T7_40min_650C_21% O_2_3	4,221	17%	240	14.1%
T7_20min_550C_10% O_2	2,521	20%	215	9.2%
T7_20min_550C_10% O_2_2	2,593	23%	195	17.6%

Since recycled carbon fibres can have their tensile strength decrease while the elastic modulus actually increases or remains the same and vice-a-versa (with respect to the virgin fibre), it suggests attributes that make a fibre strong don’t also make the fibre stiff. Previous work [41] in carbon fibre recycling has reported small losses in tensile strength with no significant decrease in elastic modulus, but tensile strength loses greater than 20% were usually accompanied by a large reduction in elastic modulus. The differences in results between this work and prior carbon fibre recycling studies highlights the need to understand how and why recycling changes fibre properties (beyond the simple oxidation damage explanation). By considering how a fibre fails and relating that to defects and fibre microstructure, a stronger understanding of the effects of recycling conditions on fibre properties may be achieved.

6.3 Fibre Surface Characterisation

XPS and BET were used to study the surface of T700 fibres in an effort to use surface chemistry and or surface area to examine the severity of the recycling conditions and its impact on the tensile strength of the treated fibres. For XPS the atomic percentages of carbon, oxygen, and nitrogen were determined. The ratio of oxygen to the sum of the remaining major species (carbon, and nitrogen in this case) was used as a measure of oxidation extent that would be comparable from sample to sample. Figure 44 shows the oxygen concentration on the surface of T700 fibres. The virgin T700 has a surprisingly high oxygen concentration for an unsized fibre. The oxygen concentration does not increase with temperature, duration, or oxygen concentration of the recycling process. T7_40min_550C_10% O_2 clearly has the lowest oxygen concentration while T7_20min_550C_10% O_2 and V-T700 have the highest.

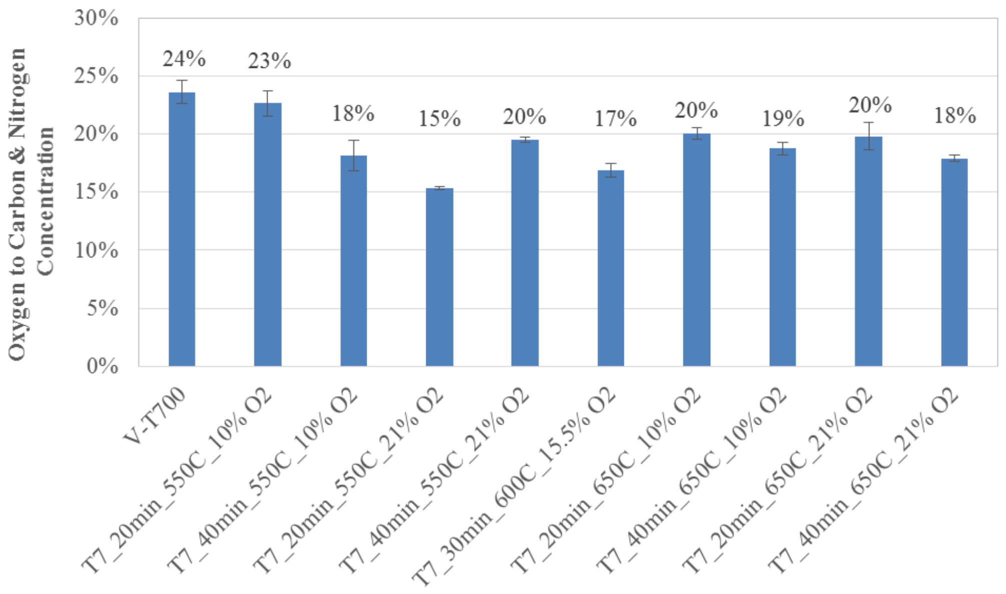

Figure 44. XPS oxygen concentration data for T700 fibres. Data labels are percent oxygen concentration. Error bars are standard deviation

The oxygen concentration does not seem to reliably change in response to the recycling conditions. Figure 45 shows oxygen concentration and tensile strength side by side. From the 20min_550C_10% O_2 to 40min_550C_10% O_2, from 20min_650C_10% O_2 to 40min_650C_10% O_2, and from 20min_650C_21% O_2 to 40min_650C_21% O_2 recycling conditions, there is a decrease in the oxygen concentration accompanied by an increase in tensile strength. However, the scale of the changes is not consistent. Additionally, from 20min_550C_21% O_2 to 40min_550C_21% O_2, there is both an increase in tensile strength and oxygen concentration. From Figure 44 and Figure 45 it is clear there is no relation between the recycling conditions and oxygen concentration or between the tensile strength and oxygen concentration.

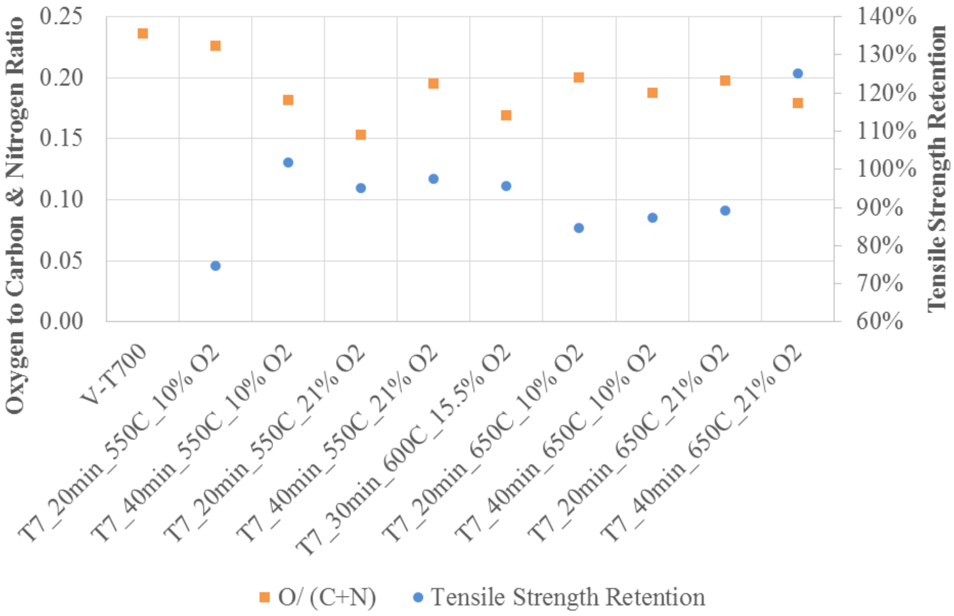

Figure 45. Comparison of XPS and tensile strength results

BET experiments were conducted across three different machines before determining the BET facilities immediately available were not suitable for this work. The first machine used was the Quantachrome Autosorb1 and krypton as an adsorbate gas. Table 18 shows results from the Quantachrome instrument. V-T700a1 and V-T700a2 are the same sample but just running the BET analysis back to back without exposing the sample to atmosphere. In-between BET analysis runs the sample was pumped down to vacuum to allow it to return to a dry state with no adsorbed gas. For the same sample to register 0.57 m^2/g and 0.78 m^2/g was an unacceptable amount of variation. To further assess the abilities of the Quantachrome machine, a second V-T700 fibre sample was run. This fibre sample had an even lower surface area of 0.42 m^2/g which indicated the BET technique on this instrument was not reliable. Further exploration of BET on the Quantachrome was abandoned when the turbomolecular pump broke and was not replaced.

Table 18. Quantachrome BET data

Fibre Sample	Surface Area (m^2/g)
V-T700a1	0.57
V-T700a2	0.78
V-T700b	0.42

The next piece of BET equipment used was the Micrometrics ASAP 2020 using nitrogen as an adsorption gas. Krypton gas lines were not yet run for this machine. Again virgin T700 fibre was used to test the repeatability of the BET test procedure and the test results are shown in Table 19. V-T700_1a and V-T700_1b are the same fibre sample just with BET analysis run back to back with a conditioning phase in-between. The sample was not exposed to atmosphere in-between BET analysis runs. V-T700_2 was a second V-T700 fibre sample. Similar surface area results for all three V-T700 fibre samples were obtained as on the Micrometrics BET which was both encouraging and disappointing. Encouraging in that there was consistency between both machines and that nitrogen might work as an adsorbate gas, but disappointment in the variability of results. A forth fibre sample, also shown in Table 19, was tried. This fibre had been exposed to the 30min_600C_15.5% O_2 recycling condition. The surface area reported for this fibre was 4.29 m^2/g which was a unusually large increase compared to the virgin T700 fibre estimates. A recycled fibre having a higher surface area than the virgin fibre made sense. However on closer inspection, the BET ‘C’ constant was negative meaning the test results could not be used with the BET theory. The ASAP 2020 had recently been recommissioned after an extended period of disuse and its calibration for low surface area materials was somewhat in question. Additionally, the BET surface area results just using nitrogen were still quite variable.

Table 19. Micrometrics ASAP 2020 BET data

Fibre Sample	Surface Area (m^2/g)
V-T700_1a	0.576
V-T700_1b	0.742
V-T700_2	0.421
T7-30min_600C_15.5% O_2	4.29

The last BET machine to be used was a Micrometrics ASAP 2420 run by the department of Chemical and Environmental Engineering. This machine was frequently used by researchers doing materials development in the energy field and was managed by a member of the faculty, so more expertise about the BET technique and the piece of equipment itself was available. Five samples were prepared for an initial trial in nitrogen. If these samples worked well than nitrogen could be used in further BET analysis instead of costly krypton. A single blind study was done where the technician operating the BET machine did not know which samples were which nor how they were treated. Three of these samples were actually the same and were virgin T700 fibres. The surface area results for these fibres are shown below Table 20. Again the results were quite variable and did not give much confidence in the repeatability of the BET technique.

Table 20. Micrometrics ASAP 2420 BET surface area

Fibre Sample	Surface Area (m^2/g)
V-T700_A	0.210
V-T700_C	0.445
V-T700_E	0.398

Discussions with the faculty member managing the ASAP 2420 resulted in the suggestion that the fibres were registering below the reliable surface area detection limit for nitrogen and that instead krypton should be used. An additional recommendation was to go back to using the ASAP 2020 as it now had the krypton gas lines plumbed in. Due to the limited technician or faculty support on the ASAP

2020 and the extended period of time needed to run samples one at a time (compared to 6 at a time plus 12 conditioning stations on the ASAP 2420), BET was not reinvestigated on the ASAP 2020.

6.4 Structure Property Exploration

The relation between the recycling conditions and microstructure or tensile properties is examined above and efforts to relate microstructure to tensile properties is discussed below. From Raman spectroscopy the A_D/A_G ratio gives an indication of the likeness of the structure to graphite where the smaller the A_D/A_G ratio, the more perfect the structure. Similarly, a smaller FWHM of the G peak the more refined the structure is and thus would be expected to have fewer defects and a higher tensile strength. Figure 46 shows an overlay of tensile strength and the A_D/A_G ratio from Raman. The samples are arranged in order of increasing severity of the recycling process. From Figure 46 there is some evidence that a larger A_D/A_G ratio corresponds to a higher tensile strength. The most clear examples of this are comparing: the virgin fibre to the first recycling condition (20 minutes, 550^{o}C, and 10% O_2), the 2nd recycling condition (40 minutes, 550^{o}C, and 10% O_2) to the 3rd recycling condition (20 minutes, 550^{o}C, and 21% O_2 and from the 2nd most severe (20 minutes, 650^{o}C in 21% O_2) to the most severe condition (40 minutes, 650^{o}C in 21% O_2). However the rest of the samples show very little change in strength or A_D/A_G or even show the opposite linear trend where a drop in tensile strength corresponds to an increase in the A_D/A_G ratio. The high degree of disorder in carbon fibre compared to graphene-like materials mean small changes in disorder were difficult to see as a significant change rather than just variation in the measurement. Additionally, as shown in Figure 47, the size of the change in the A_D/A_G ratio for one sample to the next is inconsistent with the size of the change in tensile strength.

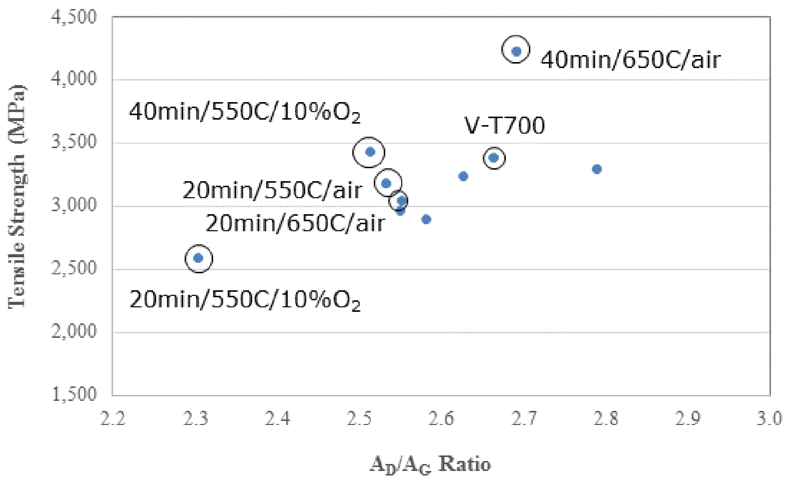

Figure 46. Comparison of tensile strength and A_D/ A_G peak area ratio

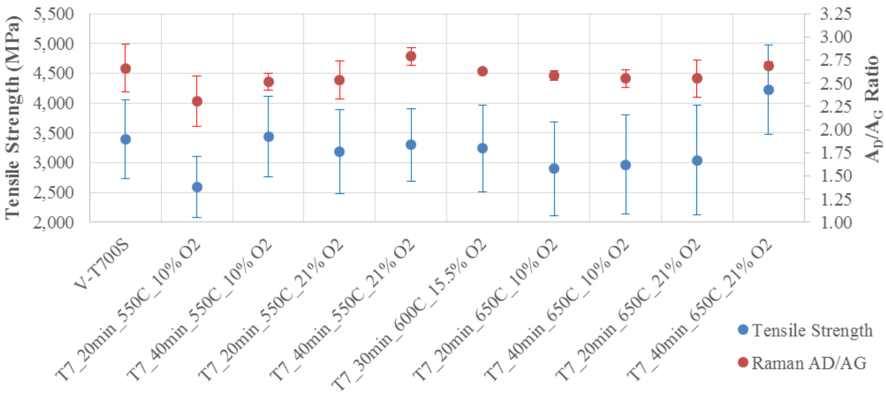

Figure 47. Tensile strength and Raman A_D/A_G results. Error bars are standard deviation.

Figure 47 shows the tensile strength and A_D/A_G ratios for T700 fibres. The standard deviation of the Raman measurement is 12% or less while the COV on the tensile strength is usually in the range of 20-30%. The A_D/A_G ratio is about 2.6 with the exception of T7_20min_550C_10% O_2. The tensile strength measurement for T7_20min_550C_10% O_2 is below average, but the below average Raman measurement would suggest less damage and a higher tensile strength. A_D/A_G is the highest for T7_40min_550C_21% O_2, but the matching tensile strength measurement is not below average as the Raman measurement would suggest. Overall Raman spectroscopy was determined not to be a useful tool for predicting the tensile strength of recycled carbon fibres.

X-ray Diffraction was used to make measurements of crystal size in both in-plane and thickness directions. Figure 48 shows the physical representation of crystal properties determined from XRD measurements. As shown by Figure 49 fibres can have about the same tensile strength for a very wide range of crystal sizes. The (10) and (11) reflections of carbon are much weaker than the (002) reflection and as a result not every recycled carbon fibre sample had resolvable (10) and (11) peaks. Comparing the crystal thickness measurements to the tensile strength measurements also shows no discernible correlation between the two. XRD measurements of crystal size and thickness were determined not to be a useful indicator of tensile strength. This could be the limitations of the method and or simply that there is no relation between crystal size or thickness and tensile strength. Using fibre bundles as opposed to single filaments contributed to peak broadening, however measurements on a single filament were not possible with the XRD equipment available. XRD is also a bulk measurement so any heterogeneity or distribution of crystal size in the fibre simply appears as a large variation in the crystal size measurement.

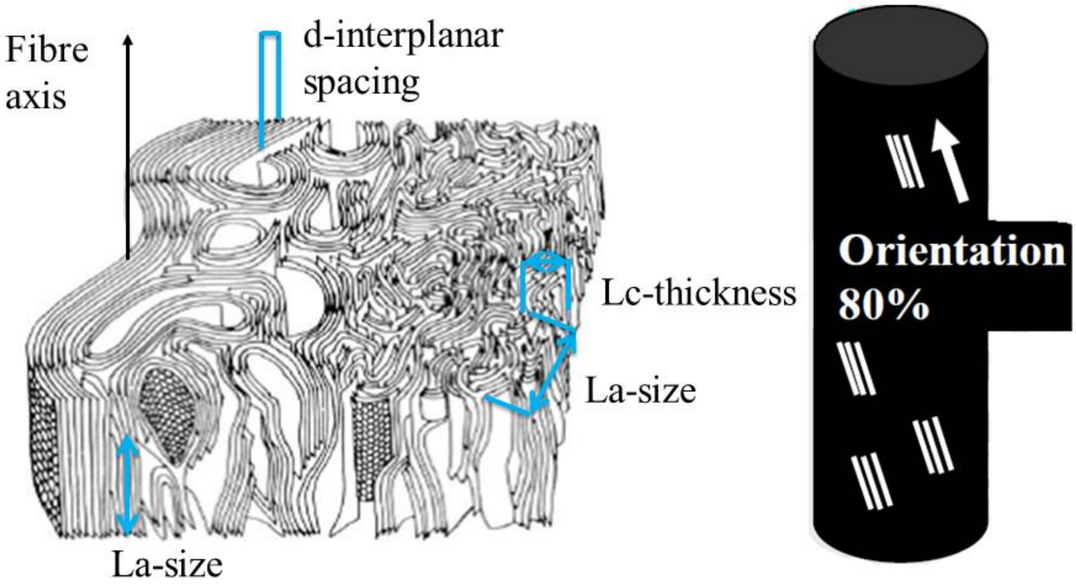

Figure 48. Fibre structure parameters measured by XRD

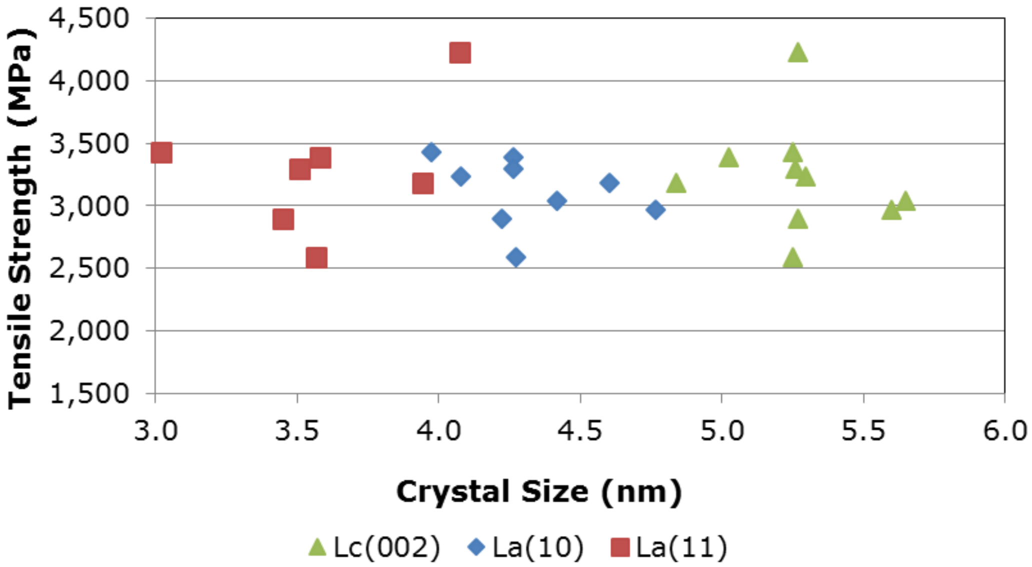

Figure 49. Crystal size and tensile strength

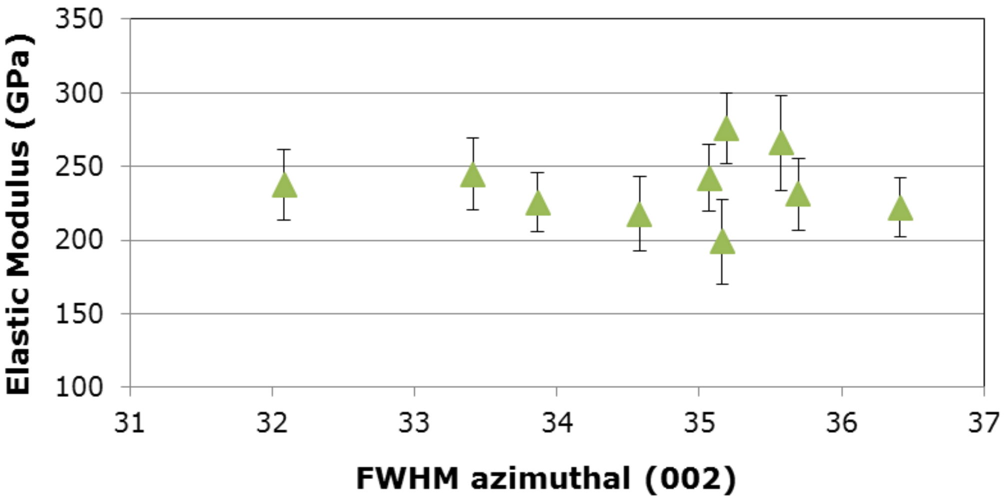

Figure 50. Relation between elastic modulus and crystallite orientation

XRD was also used to measure crystal orientation with respect to the fibre axis to see if changes in the crystal orientation could be the reason for a change in the elastic modulus of a recycled fibre compared to its virgin fibre. Figure 50 uses the FWHM of the azimuthal scan of the (002) planes as a measure of crystal orientation. A smaller FWHM would be an indication of better aligned crystals which in turn would be expected to result in a higher elastic modulus. Like the crystal size measurements, the orientation measurements shown in Figure 50 can vary over a wide range with little to no change in the elastic modulus of the fibre.

Transmission Electron Microscopy (TEM) was tried as a tool to look at crystal structure on a more local basis than XRD. The primary focus was general arrangements of the graphite planes and the d-spacing of these planes. Diffraction patterns from TEM were not perused. Examples from the literature of what is possible using TEM is seen in Figure 51 and Figure 52. Figure 51 shows misorientation (with respect to the fibre axis) of crystallites in the vicinity of a fracture. The misorientation of the crystallites introduced a localized high stress area that induced a crack while the fibre was under load. Attempts at cross sections in this study were not able to achieve such a large continuous section as in Figure 51. In Figure 52 the difference in the packing of the graphite planes between **a** and **b** is visible. The authors suggest that in **a** the graphite planes are straighter and more well aligned with the fibres axis than in **b.** Further **a** is taken from the outer perimeter of the fibre while **b,** showing wavy graphite planes,is taken from an inner central region, suggesting a difference in crystal orientation between the core and sheath of the fibre. Micrographs in this work were not sufficiently clear enough to see continuous structure nor were sections mechanically robust enough to be able to cut a section containing both the inner and outer cross section of the fibre.

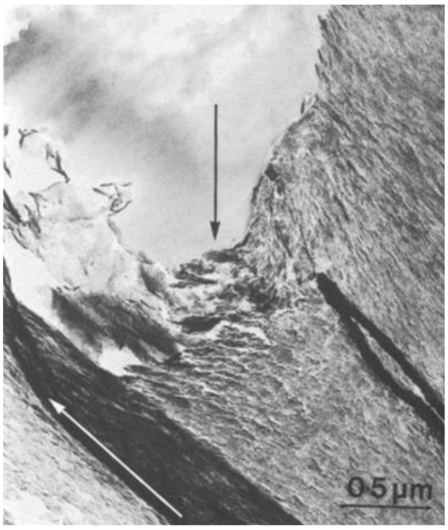

Figure 51. TEM micrograph showing misorientation of crystallites at fracture surface [29]

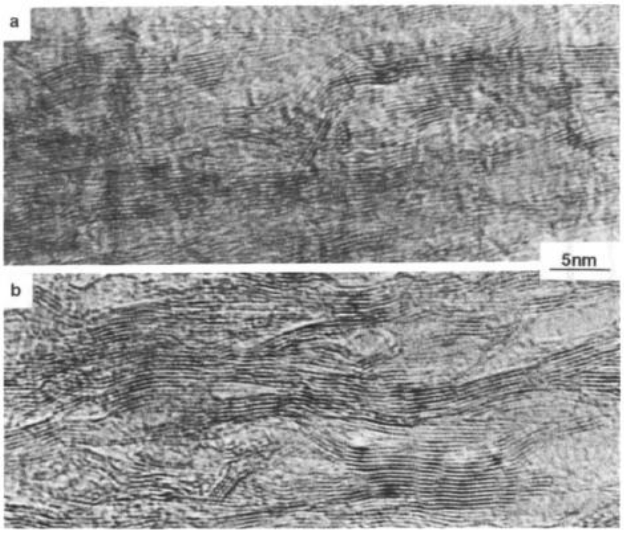

Figure 52. Core-Sheath heterogeneity: a. core-planes have larger radius of curvature (straighter) b. small radius of curvature—waviness of graphite planes [87]

Figure 53 through Figure 56 are representative of the TEM micrographs produced during this study. Figure 53 shows a cross-section on a TEM grid, but in the cross section there are holes where a fibre or a few fibres bunched together have pulled out of the embedding resin during sectioning.

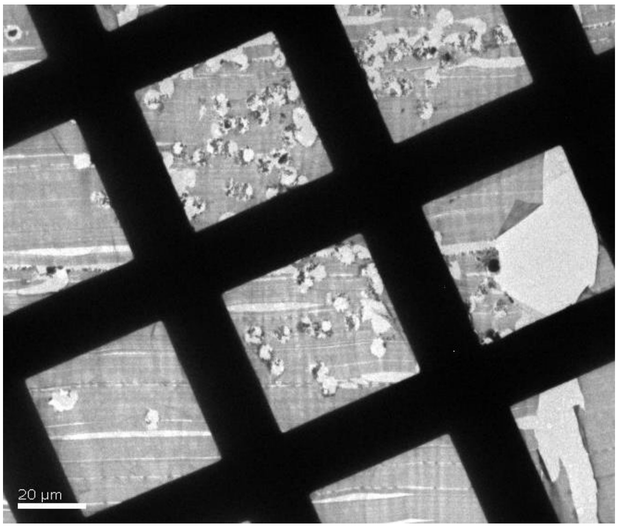

Figure 53. Fibre/embedding resin cross section on TEM grid. Holes in cross section from pulled out fibres

Figure 54 shows a sheet structure, but overall the structural elements are not very distinct. Around the outer edge of the cross section the graphite planes are most clearly seen, but the resolution is not high enough to make meaningful measurements.

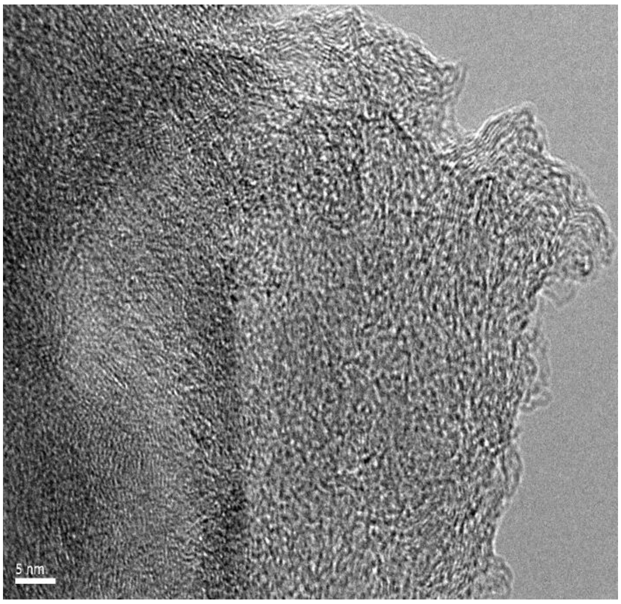

Figure 54. Fragment of virgin T700 fibre. The resemblance of graphitic structure is seen, but with insufficient detail for measurements.

In Figure 55 the magnification is higher than in Figure 54 which allows for the sheet-like structure to be more clearly seen. Sheets on the outermost edge towards the embedding resin are faintly seen but are clearly separated. The different shades of grey and black suggest a multi-layered structure which, due to the superposition of planes from each layer, makes structural features more difficult to see.

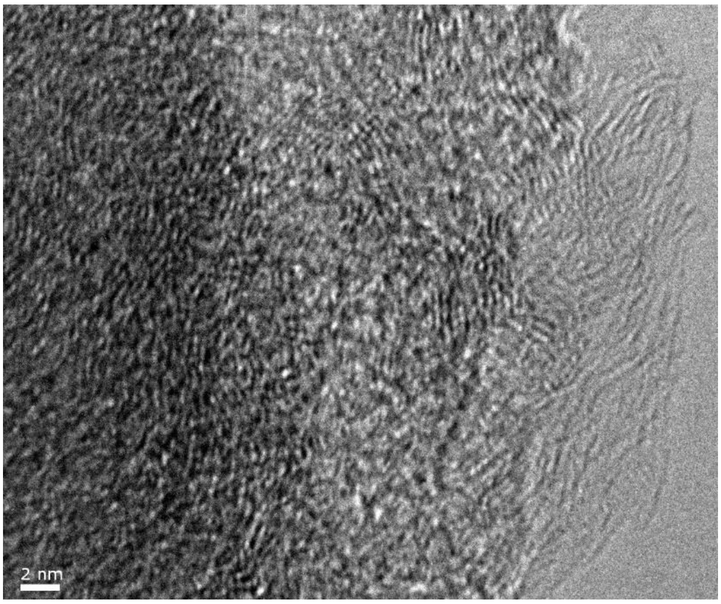

Figure 55. Micrograph showing multiple layers of graphite contributing to the image.

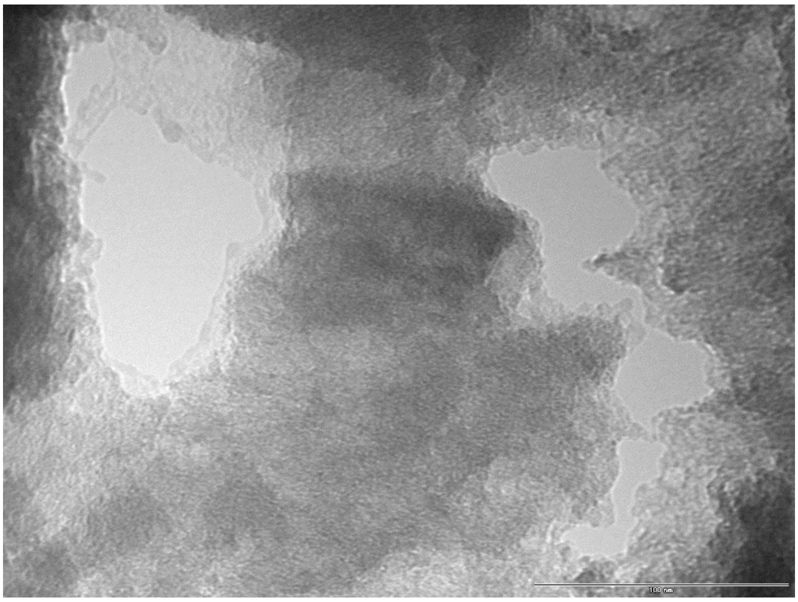

Figure 56. Nominal 300,000X TEM micrograph of virgin T700 fibre. Scale bar is 100nm.

Figure 56 again shows evidence of multiple layers of graphite being captured by TEM. Short dashes give the indication of sheets of graphite. There are also two holes in the cross section that are much smaller than the fibre diameter so it would suggest that the cross section was perhaps damaged during collection.

6.5 Conclusions From Work On T700 Fibres and on Microstructural Characterization Methods

There is no clear relationship between the tensile data and the microstructure data provided by Raman and XRD. ANOVA was used to identify the relative importance of the effect of recycling conditions on fibre microstructure. Temperature was the most dominant factor. Variations in crystal thickness, crystallite orientation, and the ratio of the disorder peak to the graphite peak in Raman could not be accounted for by any of the recycling condition factors or interaction of factors. Most of the recycling conditions tested produced fibres that retained 85%-95% of their original strength and stiffness. However, the recycling conditions which did result in a significant loss of tensile properties are not simply more severe than the conditions which maintained the fibre properties. One notable exception is sample T7_40min_650C_21% O_2. The diameter of this fibre sample is on average ~1 µm smaller than the virgin fibre which may suggest the outer ~500 nm of the fibre was oxidised away. Alternatively, this could have been due to the shrinking of the d-spacing, but XRD data shows this was most likely not the case. The removal of the outermost material may have left a pristine surface with fewer defects which would explain the increase of tensile strength over the virgin fibre. Figure 42 shows the fibre sample recycled at 650^{o}C for 40 minutes in only nitrogen showed no change in tensile properties, which strongly implies oxygen concentration or the interaction of oxygen concentration and another factor are responsible for the changes to the fibres' mechanical properties. Perhaps the most significant challenge in the data analysis has been the large range of changes in averages, but most of these differences are of little statistical interest after taking into account standard deviation.

Well known relationships such as $A_D/A_G\ \alpha^{-1}$ La (and elastic modulus α 1/azimuthal $(002)_{FWHM}$) were derived by surveying over a wide range of carbon materials. However, these relationships did not hold true for the fibres in this work. Figure 57 shows the expected decrease in crystal size with an increase in the A_D/A_G ratio between the Dialead K139 fibre and V-T700, but the difference in crystal size between the virgin and recycled samples is quite small whereas Raman would suggest a much larger difference.

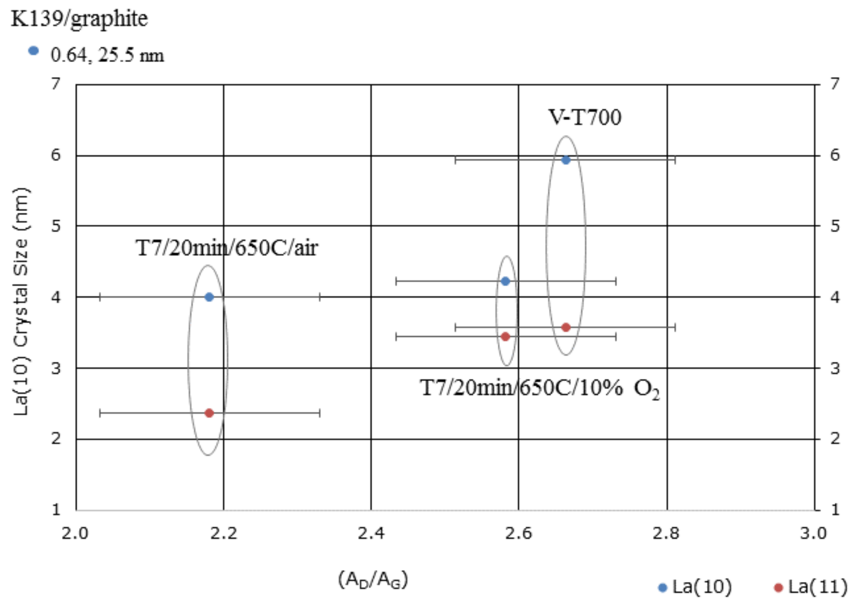

Figure 57. Relation between Raman A_D/A_G and XRD crystal size

In Figure 58 the expected linear relation between elastic modulus and crystal orientation is seen when comparing the K139 pitch fibre to M46J a HM PAN fibre to the HS and IM fibres such as V-T700 and V-T800S. However the differences between two different IM or HS fibres like the difference between V-T800 and V-

IM7 or between V-T700 and V-AS4 are small enough to be within the error bounds on the both the XRD and the tensile modulus measurements.

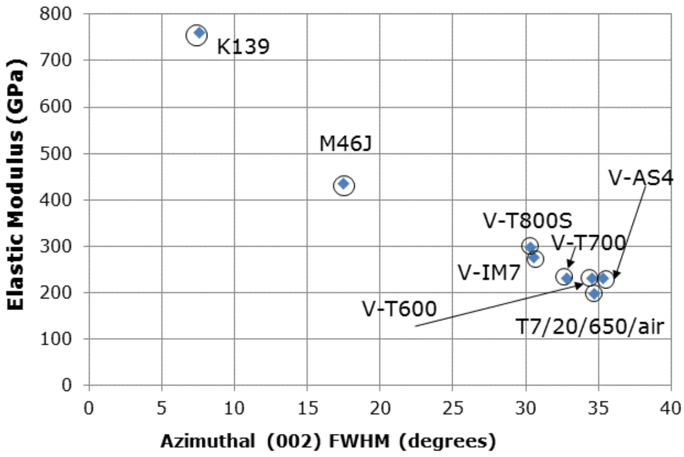

Figure 58. Relationship between elastic modulus and crystal orientation

In the literature, in order to study the structure-property relationships like those above, carbon fibre precursor was heat treated to varying final heat treatment temperatures. It is not clear if the structural changes caused by recycling will affect the properties of recycled carbon fibre in the same way that structural differences in different types of virgin fibre correspond to dramatically different mechanical, thermal, and electrical properties. The results of this microstructural investigation are well within the range presented in the literature, suggesting characterisation and data reduction procedures are appropriate for the materials under study.

SEM and EDS analysis revealed several questions that need to be answered to more fully understand the recycling process. SEM and fibre diameter measurements were not enough to reconcile the visual observation of fibre quality with the measured tensile strength and elastic modulus, introducing the need to understand defect limiting behaviour and how that is related to crystal structure. In future work, TEM would be very helpful in identifying any changes to the crystal structure that occur as a result of carbon fibre recycling. Of particular interest is any structural heterogeneity in the virgin fibre and then how it changes (or not) as a result of recycling such as highly oriented crystallites in the skin region being oxidised away. The area around pits should also be studied further to understand why pits form under some recycling conditions but not others, if the pits are catalysed by local surface chemistry or debris at a specific point on the fibre, and how pits affect the local structure’s contribution to elastic modulus and tensile strength.

TEM showed some promise in visualising the graphitic structure of carbon fibres. At present the cross sections collected had many missing and incomplete fibre cross sections. Further work in optimising the dispersion of the fibres in the embedding resin or the resin to hardener ratio to make a stiffer Embed 812 might help to keep fibres from pulling out of the resin during cutting. Thicker cross-sections may help the fibres from fragmenting during the cutting. From the TEM work so far, it would seem improving sample preparation will lead to better images faster than just optimising imaging conditions.

BET is another characterization technique that would vastly improve the understanding of the recycling conditions on the fibre. The BET work presented from the Quantachrome Autosorb-1 and Micrometrics ASAP 2020 probably suffered from the equipment not being well maintained and possibly being limited by the mass of fibre that could be fit in a sample bulb. More mass in the sample bulb would increase accuracy and repeatability since errors due to free volume would be decreased. The Micrometrics ASAP 2420 was a promising piece of equipment and the technical staff were familiar with its capabilities, however it turned out not to be suitable for this work since it was not set up to run BET analysis with krypton gas. A well maintained multisample BET machine using krypton gas would be a sensible choice for future BET work. Reliable surface area and pore size distribution data would be an excellent physical data complement to the chemical data obtained from XPS to gauge the degree on oxidation of a fibre.

7 Tensile Testing: Mechanical Properties

7.1 Tensile Strength and Elastic Modulus

The remaining three fibre sample sets (T800S, IM7, and AS4) also had their tensile properties evaluated with the same procedure and equipment used for the T700 fibre sample set. Tensile strength of T800S fibres is shown below in Figure 59.

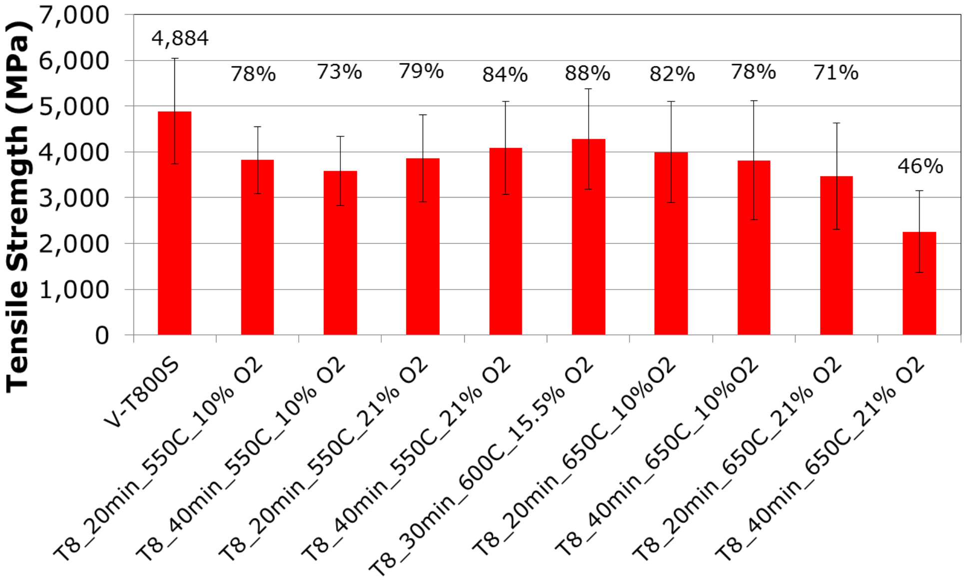

Figure 59. Tensile strength of T800S type recycled fibre samples. Data labels show percent retention. Error bars show standard deviation.

In all cases the loss in tensile strength is accompanied by a drop in the breaking load. The percent loss in breaking load is slightly higher than the loss in tensile strength. The loss in breaking load comes from a weakening of the material (loss in tensile strength) and then a small additional loss in cross-sectional area. For example consider sample T8_20min_650C_10% O_2 which has an 18% loss in tensile strength and a 2% loss in cross sectional area (which can be worked out from Table

21); therefore the expected loss in breaking load would be around 20%. The actual measured reduction in breaking load was very close, coming in at 21%. The sample that underwent the most severe recycling conditions, T8_40min_650C_21% O_2 has the lowest tensile strength and the highest coefficient of variation in tensile strength. This sample is also the only sample that is less strong than virgin T700 or AS4 fibres. IM fibres come from superior precursors compared to HS fibres [88] thus recycled IM fibres even after losing tensile strength due to recycling are stronger than a virgin HS fibre.

Table 21. Fibre Diameter of T800S fibres

Fibre Sample	Diameter			COV
V-T800S	5.06	±	0.54	11%
T8_20min_550C_10% O_2	4.93	±	0.29	6%
T8_40min_550C_10% O_2	5.09	±	0.41	8%
T8_20min_550C_21% O_2	4.87	±	0.16	3%
T8_40min_550C_21% O_2	5.01	±	0.65	13%
T8_30min_600C_15.5% O_2	5.05	±	0.52	10%
T8_20min_650C_10% O_2	5.01	±	0.35	7%
T8_40min_650C_10% O_2	4.89	±	0.26	5%
T8_20min_650C_21% O_2	4.87	±	0.28	6%
T8_40min_650C_21% O_2	4.85	±	0.25	5%

Table 22. Weibull shape and scale parameters and tensile strength coefficient of variation for T800S recycled fibre samples

Sample	Scale Parameter (MPa)	Shape Parameter	Tensile Strength COV
V-T800S	5331	4.80	24%
T8_20min_550C_10%O_2	4115	5.97	19%
T8_40min_550C_10%O_2	3883	5.39	21%
T8_20min_550C_21% O_2	4217	4.67	25%
T8_40min_550C_21% O_2	4461	4.69	25%
T8_30min_600C_15.5%O_2	4687	4.43	26%
T8_20min_650C_10%O_2	4391	4.14	28%
T8_40min_650C_10%O_2	4300	2.95	34%
T8_20min_650C_21% O_2	3878	3.36	33%
T8_40min_650C_21% O_2	2527	2.91	40%

Another measure of variability is the Weibull shape parameter which is inversely proportional to the standard deviation of a set of data. For the T800S fibres the highest and lowest coefficient of variation are matched by the smallest and largest Weibull shape parameter. As can be seen in Table 22 the largest Weibull shape parameter is 5.97 belonging to T8_20min_550C_10% O_2 and the smallest Weibull shape parameter is 2.91 belonging to T8_40min_650C_21% O_2. The three most severe recycling conditions show a small upwards jump in the COV of tensile strength (mid to high 20%s to mid 30%s) and then the most severe treatment has a COV of 40%. The jump in COV is also evident in the Weibull shape parameters. The more severe the recycling condition the more variability in tensile strength there is.

Figure 60, below, shows the elastic modulus for T800S fibres. As in Figure 59,, Figure 60 also shows a gradual rise in elastic modulus up until the 30min_600C_15.5% O_2 sample and then gradual decline such that the 40min_650C_21% O_2 sample is of similar strength/stiffness as the 20min_550C_10% O_2 sample. This seems to indicate that at low severity and high severity, recycling does the most damage to fibres; whereas with a medium intensity of recycling, although the fibre is damaged, the recycling process seemed to have removed the weakest and least stiff portions of the fibre in order to recover some of its initial strength and stiffness.

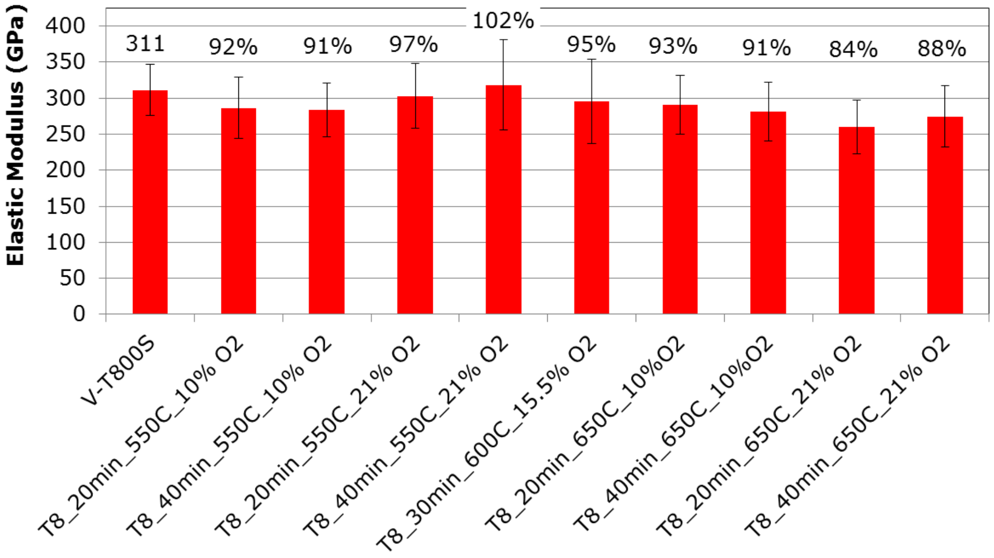

Figure 60. Elastic modulus of T800S type recycled fibre samples. Data labels show percent retention. Error bars show standard deviation.

Figure 60 shows the elastic modulus of recycled T800S fibres is generally at least 90% and never falls below 80% of the virgin fibre's stiffness. The sample with the lowest elastic modulus is T8_20min_650C_21% O_2 while T8_40min_550C_21% O_2 is the most stiff having the same, if not a slightly higher elastic modulus, than the virgin fibre. The elastic modulus is less affected by recycling than the tensile strength. It is not until the two most severe recycling conditions that the elastic modulus is reduced by more than 10%. Unlike in the tensile strength analysis, the COV for elastic modulus does not increase with increasing recycling severity. T8_40min_550C_21% O_2 and T8_30min_600C_15.5% O_2 have the highest COV and one of the highest elastic moduli, but samples with a similar elastic moduli have a much lower COV. All recycled T800S fibre samples are still stiffer than virgin T700 and AS4 fibres.

Hexcel IM7 was selected as a comparison to the T800S fibre. Both fibres are used in high performance applications; but are made from different precursors. The missing IM7 samples in both graphs of tensile strength (Figure 61) and elastic modulus (Figure 62) are strikingly different compared to the T800S and T700 data previously reviewed. For the IM7_20min_650C_21% O_2 recycling condition, the recovered fibres were all so short that they couldn't even be tested with a 4mm gauge length. Any fibres longer than 4mm would immediately break upon handling. No fibres survived the IM7_40min_650C_21% O_2 recycling condition. The inability to last under the extreme oxidation conditions of 650°C in 21% O_2 was also observed with Hexcel AS4 fibre samples.

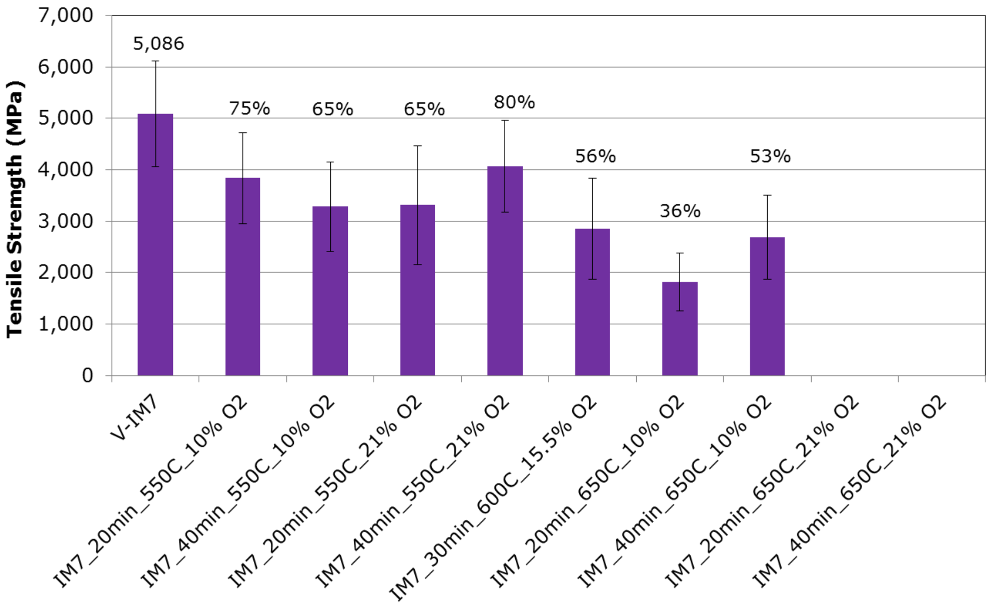

Figure 61. Tensile strength of IM7 type recycled fibre samples. Data labels show percent retention. Error bars show standard deviation.

As can be seen in Figure 61 IM7 fibres are easily damaged by thermal recycling. Even under mild conditions the loss in tensile strength is significant such as the IM7_20min_550C_10% O_2 sample with a 25% loss. In contrast to the T800S results, the recycled IM7 fibres are weaker than virgin AS4 HS fibres except for the 20min_550C_10% O_2 and 40min_550C_21% O_2 samples. Also easily noticeable is the much larger loss in tensile strength associated with 600°C and 650°C temperatures compared to 550°C. Like the T800S fibres, the breaking load for IM7 fibres followed the same trend as the tensile strength with increasing oxidation severity. The fibre diameter of recycled IM7 fibres as shown in Table 23 roughly decreases with increasing recycling severity although the most convincing decreases in diameter do not occur until the 650ºC treatment conditions.

Table 23. Fibre diameter and weight loss of IM7 Fibres

Fibre Sample	**Diameter (µm)**	**COV**	**Weight Loss**
V-IM7	4.80 ± 0.07	1.5%	
IM7_20min_550C_10% O_2	4.81 ± 0.12	2.6%	1.6%
IM7_40min_550C_10% O_2	4.79 ± 0.07	1.5%	1.5%
IM7_20min_550C_21% O_2	4.78 ± 0.07	1.4%	1.4%
IM7_40min_550C_21% O_2	4.77 ± 0.06	1.2%	1.8%
IM7_30min_600C_15.5% O_2	4.72 ± 0.22	4.8%	2.0%
IM7_20min_650C_10% O_2	4.65 ± 0.06	1.3%	5.0%
IM7_40min_650C_10% O_2	4.70 ± 0.08	1.7%	11.2%
IM7_20min_650C_21% O_2	N/A		8.8%
IM7_40min_650C_21% O_2	N/A		100%

The weakest measurable fibre sample is IM7_20min_650C_10% O_2 which is also the sample with the lowest elastic modulus. Sample IM7_40min_550C_21% O_2 has the highest tensile strength and elastic modulus. The IM7 fibre type is the only one where the same recycling conditions result in a fibre with the best tensile strength and elastic modulus. The opposite is also true where the same set of recycling conditions produced a fibre with the lowest tensile strength and elastic modulus. IM7_40min_550C_21% O_2 also has the lowest COV (other than virgin IM7) for both tensile strength and elastic modulus. The fibre with the highest COV of tensile strength was not the most damaged as in the case of the T800S fibres nor did COV generally increase with increasing recycling intensity. However, good agreement was found between the Weibull shape parameters and the COV of tensile strength. Good agreement between these two measures of variation suggests that there is only one failure mechanism.

Table 24. Weibull shape and scale parameters for IM7 recycled fibre samples

Sample	Scale Parameter (MPa)	Shape Parameter
V-IM7	5,484	5.91
IM7_20min_550C_10% O_2	4,180	4.99
IM7_40min_550C_10% O_2	3,621	4.10
IM7_20min_550C_21% O_2	3,681	3.42
IM7_40min_550C_21% O_2	4,454	4.70
IM7_30min_600C_15.5%O_2	3,182	3.29
IM7_20min_650C_10%O_2	2,019	3.82
IM7_40min_650C_10%O_2	2,988	3.54
IM7_20min_650C_21% O_2	N/A	N/A
IM7_40min_650C_21% O_2	N/A	N/A
IM7_30min_600C_15.5% O_2	3,182	3.29

The loss in elastic moduli of IM7 fibre samples is greater than that for the T800S fibres. Like tensile strength, the loss in elastic modulus becomes more significant at temperatures greater than 550^{o}C. Examining Figure 62 the results can roughly be grouped by temperature: moderate but significant loss in the 550^{o}C range, at 600^{o}C the loss in elastic modulus is close to IM7_40min_550C_10% O_2 but clearly in its own category with only a 70% strength retention, and at 650^{o}C the stiffness of these fibres is only half of what they were originally. The combination of 650^{o}C and 21% O_2 is clearly detrimental to fibre properties but it doesn’t seem that 21% O_2 on its own is a more significant factor for IM7 fibres than it is for T800 fibres. For IM7 and T800S fibre types, the elastic modulus and tensile strength of fibre samples recycled at 550^{o}C in 21% O_2 performed just as well or better than the fibre samples recycled at 550^{o}C with only 10% oxygen.

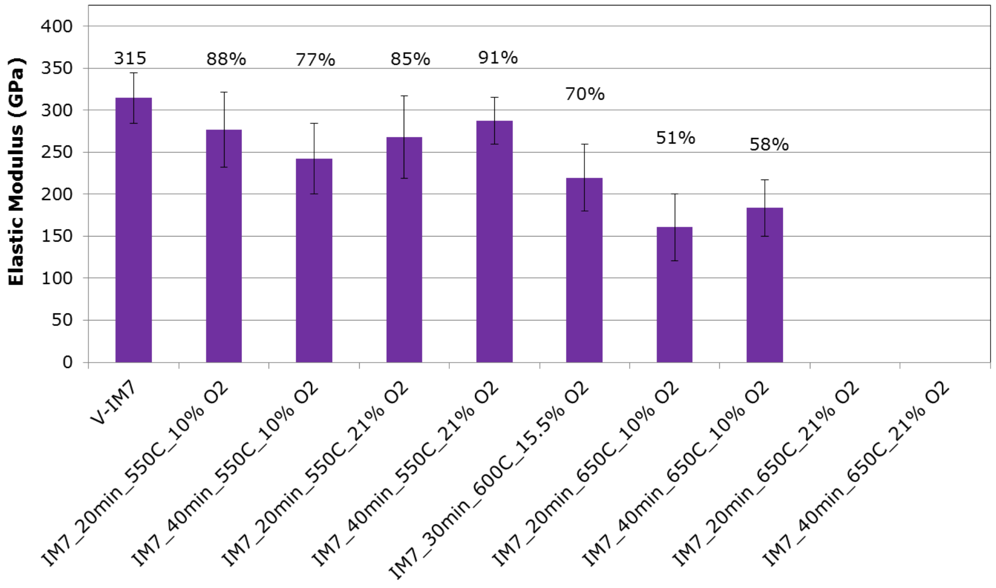

Figure 62. Elastic modulus of IM7 type recycled fibre samples. Data labels show percent retention. Error bars show standard deviation.

Hexcel AS4 was selected as the HS complement to Hexcel IM7. Like the IM7 fibre samples the most severe recycling conditions using 650°C and 21% O_2 resulted in fibre samples that were too degraded for testing. The AS4_20min_650C_21% O_2 sample had over 93% weight loss. Weight loss was determined by measuring the mass of the fibre sample before and after treatment and the data is shown in Table 25. The effects of temperature and oxygen concentration are seen in the AS4 weight loss data. Weight loss where the recycling conditions are 550°C results in less than 10% weight loss, 600°C and 15.5% oxygen results in 30% weight loss, and in the 650°C range there is a marked different between 10% oxygen (30-44% weight loss) and 21% O_2 where the weight loss is ~90wt%.

Table 25. Weight loss of AS4 fibres

Fibre Sample	Weight Loss
AS4_20min_550C_10% O_2	2%
AS4_40min_550C_10% O_2	6%
AS4_20min_550C_21% O_2	10%
AS4_40min_550C_21% O_2	7%
AS4_30min_600C_15.5% O_2	30%
AS4_20min_650C_10% O_2	44%
AS4_40min_650C_10% O_2	51%
AS4_20min_650C_21% O_2	93%

Comparing Figure 61 and Figure 63 shows that AS4 fibres behave similarly to IM7 fibres both in terms of the percent tensile strength retention and how they react at each recycling condition. The AS4 fibres generally have a slightly higher strength retention than the IM7 fibres but their overall strength is much less than the IM7 fibres. Compared to T700 fibres AS4 fibres are not as resistant to damage during the recycling process. The influence of temperature that is seen in the weight loss data is also seen in the tensile data; when recycling conditions use 550^{o}C, the tensile strength retention is 76-80%, but then at 600^{o}C and 650^{o}C the tensile strength retention is in the 50% range, up until combining 650^{o}C and 21% O_2 where the fibre is far too disintegrated to test. Similarly, the cross-sectional area of the fibres recycled at 600^{o}C or 650^{o}C is 20-30% less than the virgin fibre, putting the diameter in the size range expected for IM fibres.

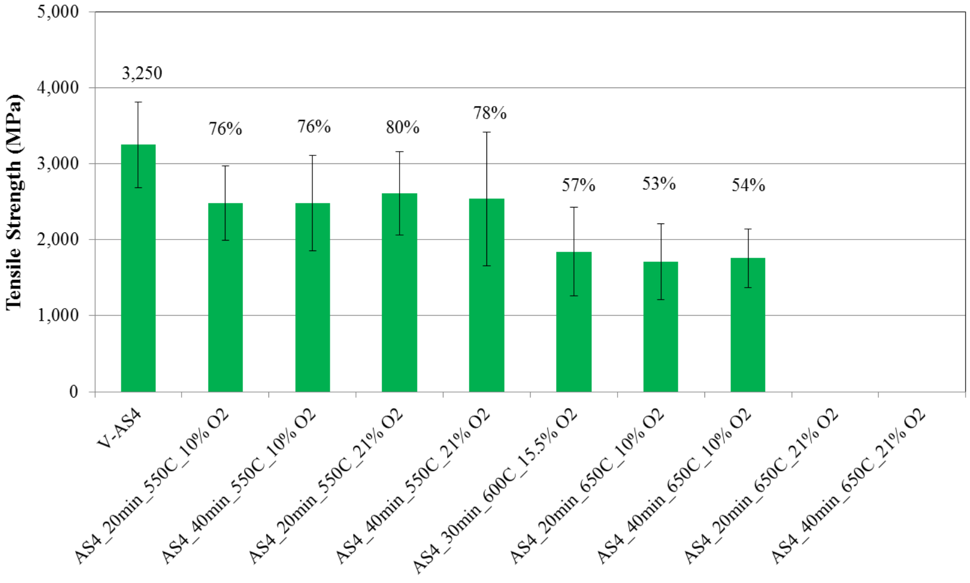

Figure 63. Tensile strength of AS4 type recycled fibre samples. Data labels show percent retention. Error bars show standard deviation.

Samples AS4_20min_650C_10% O_2 and AS4_40min_650C_10% O_2 were extremely fragile and difficult to test. The corresponding IM7 fibres were also troublesome, but not to the same extent as the AS4 fibres. The recycled AS4 fibre sample with the highest tensile strength was AS4_20min_550C_21% O_2 and the weakest sample tested was AS4_20min_650C_10% O_2. These are the same conditions that produced the strongest and weakest testable IM7 fibres. For the T700 and T800S fibre samples, no single recycling condition produced the strongest or weakest fibre in both sample sets.

Table 26. Weibull shape and scale parameters for AS4 recycled fibre samples

Sample	Scale Parameter (MPa)	Shape Parameter
V-AS4	3,476	6.88
AS4_20min_550C_10%O_2	2,671	5.93
AS4_40min_550C_10%O_2	2,721	4.55
AS4_20min_550C_21% O_2	2,823	5.57
AS4_40min_550C_21% O_2	2,840	3.17
AS4_30min_600C_15.5% O_2	2,061	3.29
AS4_20min_650C_10% O_2	1,913	3.58
AS4_40min_650C_10% O_2	1,927	4.45
AS4_20min_650C_21% O_2	N/A	N/A
AS4_40min_650C_21% O_2	N/A	N/A

Figure 64 indicates that the elastic modulus for recycled AS4 fibres is generally within 10% of the original virgin fibre and that up until the most aggressive recycling conditions the modulus is approximately the same for each sample. The exception to this observation is either 30min_600C_15.5% O_2 or 20min_650C_10% O_2. These were also the samples with the highest COV for elastic modulus and had the least number of tests contributing to the results. 30min_600C_15.5% O_2 could be the exception since it retained only 78% of the original stiffness.

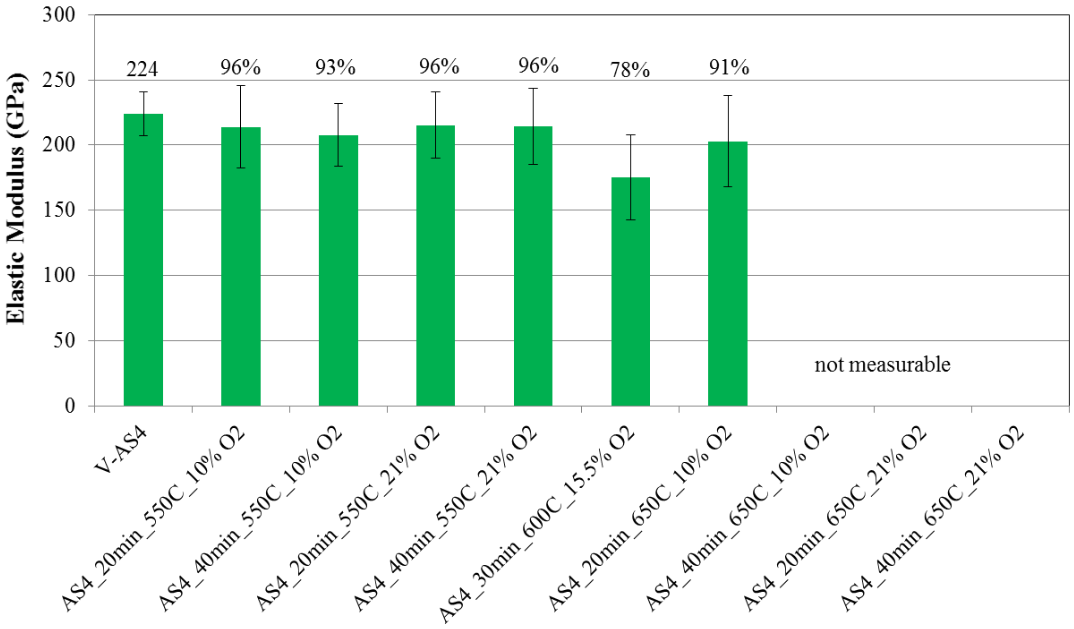

Figure 64. Elastic modulus of AS4 type recycled fibre samples. Data labels show percent retention. Error bars show standard deviation.

On the other hand, as seen in AS4 tensile strength and with IM7 fibres, the 600°C threshold usually results in more severe property loss. So in this case 20min_650C_10% O_2 has an unexpectedly high elastic modulus. This sample could be biased in that only the stiffer fibres survived the handling of the sample preparation. The number of filaments tested for this data point was far below optimal. Testing reached a point where it would take several days of poor yields of successful tests in order to get to the level of 60-80 filaments tested, but the obvious indication was poor tensile strength and very low resilience to handling. Tensile data was obtained for sample AS4_40min_650C_10% O_2, but the very low number of filaments tested and the very high variability in stiffness calculations across all three gauge lengths meant there was very little confidence in determining the elastic modulus for this fibre; therefore, as indicated by Figure 64, no result was reported.

7.2 Correlation Between Tensile Strength and Surface Oxidation

XPS measurements on the remaining T800S, AS4 and IM7 fibre sample are presented here. Measurement and sample preparation procedures were the same as for the T700 fibres. Oxygen concentration results are shown in Figure 65 for T800S fibres. Overall the oxygen concentration is lower than for T700 fibres. The sample with the highest oxygen concentration is 20min_550C_21% O_2 and the sample with the lowest oxygen concentration is 20min_650C_10% O_2. 20min_550C_21% O_2 for T700 fibres is actually the sample with the lowest oxygen concentration. 21% O_2 recycling conditions do not result in fibres with a higher oxygen concentration. There is some indication that the 550°C recycling condition results in higher oxygen concentrations than 600°C and 650°C. Like the T700 fibres the comparison of oxygen concentration to tensile strength, shown in Figure 66, does not show a trend of increasing oxygen concentration with decreasing tensile strength nor are the scale of the changes consistent such that a large change in oxygen concentration results in a large change in tensile strength.

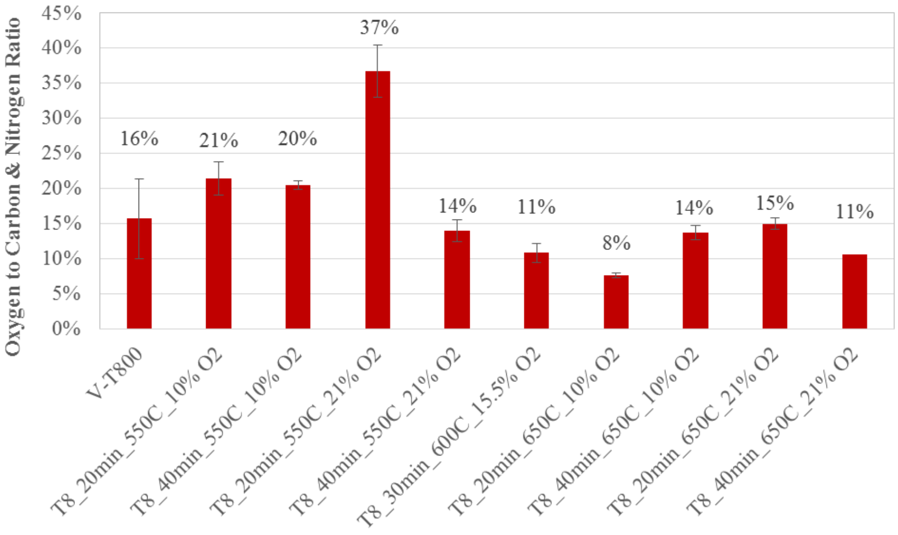

Figure 65. Oxygen concentration data for T800S fibres. Data labels are percent oxygen concentration. Error bars are standard deviation.

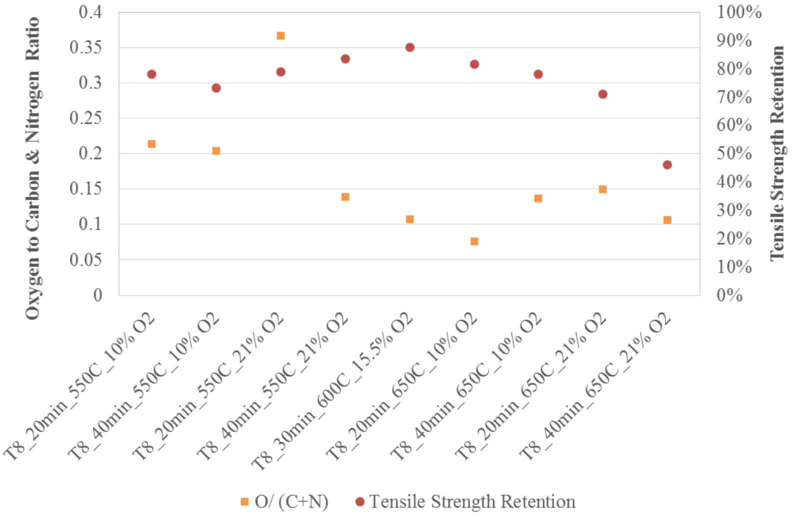

Figure 66. Comparison of T800S XPS and tensile strength results

AS4 oxygen concentration results are presented in Figure 65. The sample with the highest oxygen concentration is AS4_30min_600C_15.5% O_2. Again this does not match T700 or T800S results nor does it result in the fibre with the lowest tensile strength. Like the T800S results the 20 minutes and 40 minutes at 550^{o}C in 10% O_2 result in higher than average oxygen concentrations. The AS4 samples recycled at 650^{o}C in 21% O_2 were too degraded for testing.

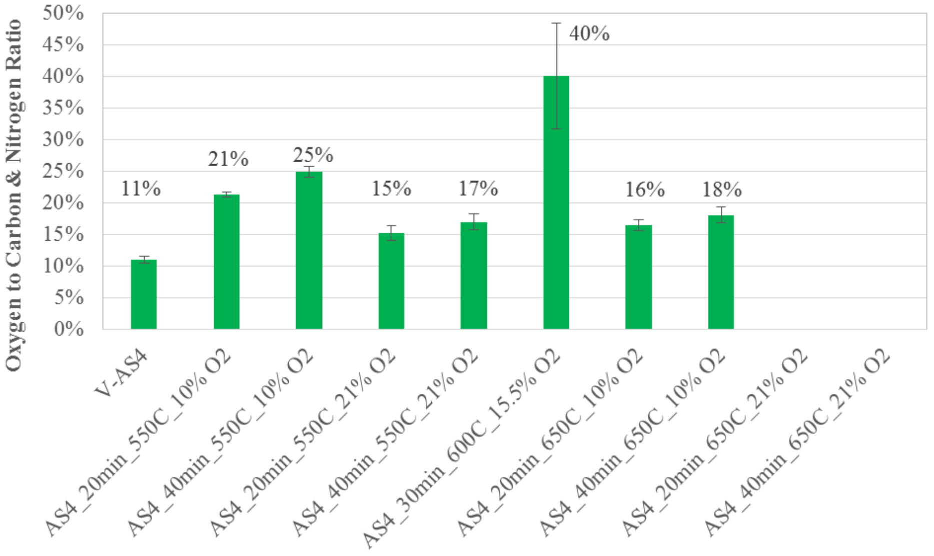

Figure 67. Oxygen concentration data for AS4 fibres. Data labels are percent oxygen concentration. Error bars are standard deviation.

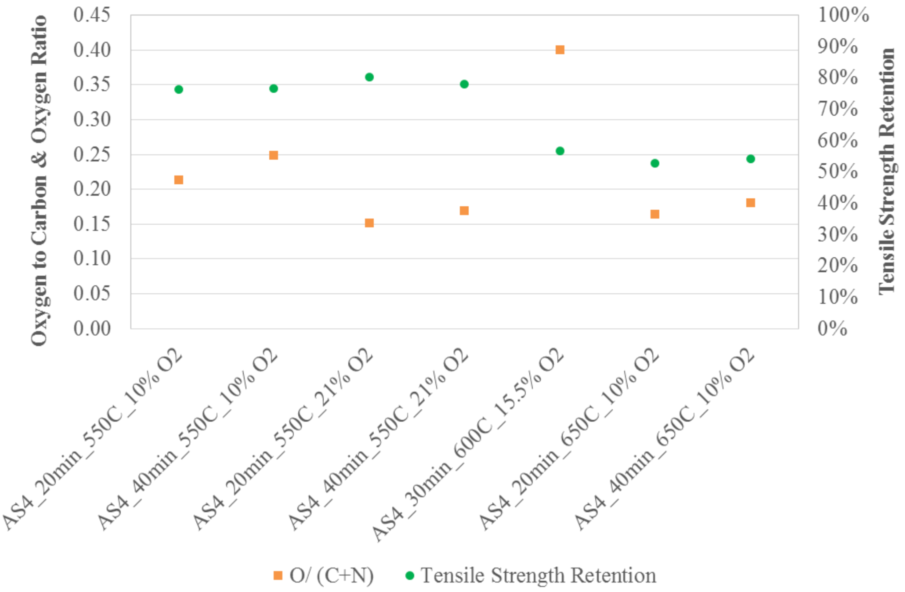

Figure 68. Comparison of AS4 XPS and tensile strength results

Figure 71 presents the tensile strength to oxygen concentration comparison for AS4 fibres. The tensile strength is fairly constant for the samples treated at 550°C but the oxygen concentration on the fibres drops for fibres treated at 550°C in 21% O_2. Similar levels of oxygen concentration are found for samples treated at 10% O_2 at 650°C which may suggest some equivalence of oxidation severity. The high oxygen concentration for the 30min_600°C_15.5% O_2 condition is accompanied by a drop in tensile strength, but this behaviour was not seen in the Toray fibres.

7.4 Summary of Tensile Results

Looking across all the single fibre testing results two factors dominate: 650°C recycling temperatures, and the easy oxidation of Hexcel fibres under the most severe recycling conditions. All four fibre types tested have a significant drop in tensile strength when recycled at 650°C compared to 550°C with the exception of T7_20min_650C_21% O_2. Fibre samples can be subdivided into a grouping of fibres recycled at 550°C and another grouping for those recycled at 650°C. At 550°C there is minimal loss in tensile strength and minimal weight loss; whereas at 650°C significant losses in tensile strength are seen and the combination of temperature and oxygen concentration becomes important. For the Toray T700 and T800S fibres the loss in cross-sectional area is minor at 550°C (up to 7% for T800S and none for T700 fibres), and at the 650°C range the loss is steady at around 7% for T800S fibres and ~10% for T700 with the exception of T7_40min_650C_21% O_2 which shows ~30% loss in cross-sectional area. The weight loss behaviour of the Hexcel fibres is quite different. IM7 has 2% weight loss at 550°C and around 10% at 650°C except for 40min_650°C_21% O_2 where all the fibre is oxidised away. AS4 has higher and more gradual weight loss. At 550°C AS4 has weight losses of ~7%, 30% at 600°C, and then at 650°C it escalates from 40wt% (20 minutes at 10% O_2) to 50wt% (40 minutes at 10% O_2) and then 90wt% for the two conditions in 21% O_2. The recycling condition of forty minutes at 550°C in 21% O_2 yields the most favourable elastic modulus for T800S, IM7, and AS4 fibre samples. 40min_550C_21% O_2 is not the best, but still very favourable, for the tensile strength of the four fibre types considered.

7.3 Tensile Properties Analysis

To determine which factors of the recycling process affect fibre mechanical properties the most, Analysis of Variance (ANOVA) can be used. Before using ANOVA an initial analysis of the difference in fibre properties between the 20 minute and 40 minute treatment at the same temperature and oxygen concentration was conducted. An example result of this analysis for T800S fibres is shown in Table 27. The symbols used are: > for an increase, < for a decrease, and ≅ for about the same.

Table 27. Example comparison of property change when treatment time is increased from 20 minutes to 40 minutes but time and oxygen concentration remain unchanged

T800s	550°C		650°C	
	10% O_2	21% O2	10% O_2	21% O2
Tensile Strength	>	<	>	>
Elastic Modulus	≅	≅	≅	≅

The modulus for T800S fibres is not appreciably different between the twenty minute and forty minute treatments. Tensile strength was generally higher for the forty minute treatments except for at 550°C in 21% O_2. For AS4 fibres the only meaningful difference was the elastic modulus results where twenty minutes at 650°C in 21% O_2 left a testable fibre whereas a forty minute treatment did not. For IM7, fibres from the twenty minute at 550°C in 10% oxygen treatment are stronger and stiffer than at forty minutes. The opposite is true for IM7 fibres recycled at 550°C in 21% O_2 and at 650°C in 10% oxygen. For T700 fibres the forty minute treatments at 10% oxygen and 550°C and 650°C in 21% O_2 were stronger and stiffer than their corresponding twenty minute treatments. From these comparisons we see that when the tensile strength is substantially different; then most of the time the modulus increases when tensile strength goes up and decreases when the tensile strength goes down. Across all four fibre sample sets, in eight of these fourteen comparisons the elastic modulus did not change appreciably. Tensile strength does not change in only five cases suggesting tensile strength is more strongly affected by recycling than the elastic modulus. Additionally there does not seem to be a repeatable change in fibre properties as a result of increasing the treatment time from twenty minutes to forty minutes. Additionally, milder conditions such as 10% oxygen at 550°C for twenty minutes results in a change of tensile strength (compared to virgin fibres) just as many times as forty minutes in 20 minutes at 650°C in 21% O_2.

The same format of analysis was also used to examine the effect of increasing oxygen concentration from 10% to 21% O_2 while maintaining the same temperature and treatment time. For the T800S fibres the trend of the changes is similar for tensile strength and elastic modulus whereas for T700 fibres the elastic modulus and tensile strength usually change in opposite ways. Not much change in strength or stiffness was seen for the AS4 fibres when the oxygen content was increased from 10% to 21%. On the other hand, there are changes for the IM7 fibre, and like the other IM fibre sample (T800S) there is the suggestion that tensile strength and elastic modulus follow similar change trends. As a result of increasing the oxygen concentration the tensile strength was found to be different eight out of twelve times and the elastic modulus was found to be different seven out of twelve times. The tensile strength decreased five out of eight times and the elastic modulus decreased three out of seven times.

Increasing treatment time and holding all other factors constant resulted in a change in tensile strength 64% of the time and a change in elastic modulus 42% of the time. Increasing the oxygen concentration and holding all other factors constant resulted in a change in tensile strength 66% of the time and a change in elastic modulus 58% of time. The time factor affects tensile strength just as much as the oxygen concentration factor. Elastic modulus is more often affected by changing the oxygen concentration than the treatment time. Tensile strength decreases 55% of the time when changing treatment time from twenty minutes to forty minutes and 62% of the time when changing oxygen concentration from 10% to 21% O_2. Elastic modulus decreases 66% of the time when changing treatment time from twenty minutes to forty minutes and 43% of the time when changing oxygen concentration from 10% to 21% O_2.

8 Tensile Properties: Factorial Model

ANOVA was used to examine the tensile data in a more rigorous way then the previous comparisons. As has been described earlier, a design of experiments was set up to conduct the recycling trials and collect the tensile data. Five two-level factors were used: Type, Manufacturer, Time, Temperature, and Oxygen Concentration ($[O_2]$). Minitab was used to perform the ANOVA by selecting a set of factors and interactions to use in the DOE model and also picking a response (tensile strength or elastic modulus).

A common mistake with factorial models in DOEs is to over parameterise the model by including interactions that are not truly affecting the outcome. The difficulty is knowing which interactions actually are affecting the response. One measure of this is the p-value in the ANOVA, but a bit of forethought using knowledge of the process can help rule out interactions before needing to rely on the statistics. Sometimes the statistics will indicate a strong interaction when there is no scientific or engineering principal to support that interaction. For example there is no logical reason to expect time and manufacturer to be a significant interaction; the way the recycling process works just doesn't support this reasoning. On the other hand oxidation rate is expressed with as an Arrhenius equation so an interaction between oxygen concentration and temperature would make sense. Similarly, an interaction between manufacturer and temperature or a three way interaction between manufacturer, temperature, and oxygen concentration is supported by observations of the process itself; in that neither the IM7 nor AS4 fibres (made by Hexcel) survived recycling conditions of 650^{o}C in 21% O_2. The damage to the IM7 fibres under both 10% O_2 and in 21% O_2 at 650°C was also apparent before making the tensile strength measurements which would support a proposed interaction between manufacturer and temperature. However the damage to the AS4 fibres at 10% oxygen and 650°C was not as obvious as with the IM7 fibres, so the interaction may not be significant. This is an example where the p-values in ANOVA can be used as an objective way of deciding whether or not an interaction should be included in the model. Another rule for interactions is an interaction between two factors may not be used in a model unless those two factors are also included in the model. The factors do not need to have a p-value suggesting they are significant.

An over parameterised model will fit the data it was derived from very well, but is likely to poorly predict the value for additional measurements. If a model is under parameterised it will also have deficiencies in how well it fits a set of measurements but the risk of falsely asserting an interaction between two or more terms is greatly reduced.

8.1 Models for tensile strength & elastic modulus of all fibres

Firstly a model considering all factors and all two way and three way interactions was used to try to fit the tensile strength data. This model showed no significant factors. Minitab uses a Pareto plot (such as the one shown in Figure 69) to show how influential each term (factor or interaction of factors) is. Longer bars mean more influence and the dotted line running up and down is the level at which a term is significant based on a p-value in ANOVA of 0.05 or less. To increase the effectiveness of the model; terms that do not have the 0.05 significance level are removed from the model.

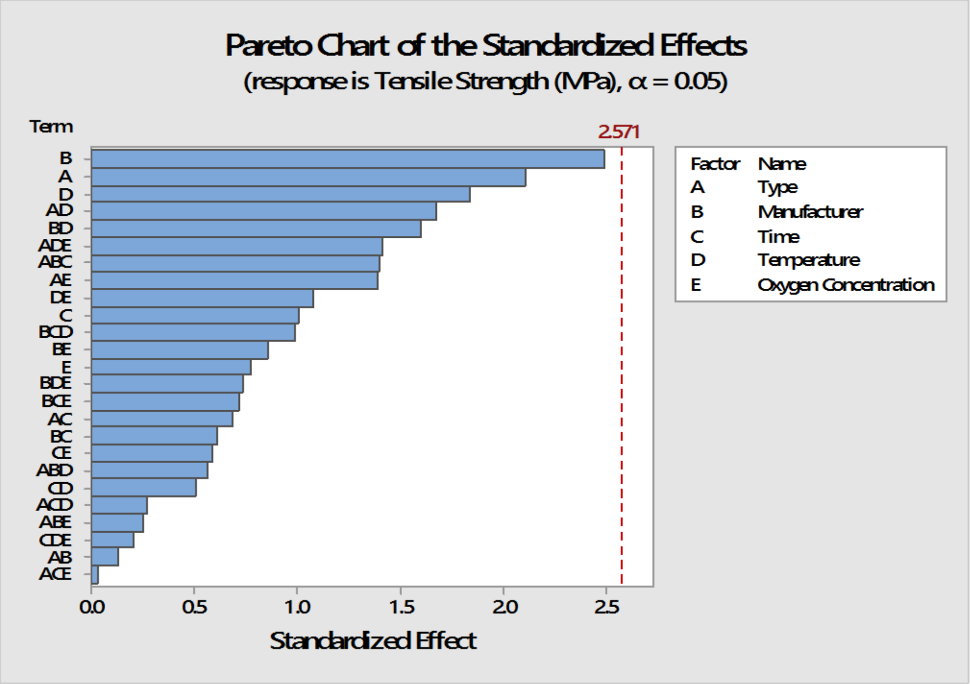

Figure 69. Pareto plot for tensile strength showing up through 3rd order interactions

The interactions TypeXTimeX[O_2] and TypeXManufacturer had to be removed in order to make any model terms significant. At this stage the factor Manufacturer became significant. Further refinement removed the interaction TypeXManufacturer. Three terms were then significant: Manufacturer (as before), Type, and TypeXTemperature. At this stage in the refinement of the model the least significant interaction was, TimeXTemperaturex[O_2], followed by TimeXTemperature. Therefore the 2nd order interaction of TimeXTemperature and any 3rd order interaction terms containing TimeXTemperature were removed from the model. As a result, the factor Temperature became an additional significant term. Further model refinement eliminated all 3rd order interactions expect for TypeXTemperatureX[O_2]. The pareto plot for the final tensile strength model containing 3rd order interactions are shown in Figure 70. ANOVA expresses the quality of a model through ‘R’ values. R^2 is an indicator of how well the model fits the data, R^2(adj) scales R^2 taking into account how many terms are used in the model. A model with many terms could have a very good R^2 value but with so many terms the model is actually a bit weaker and so it gets a lower R^2(adj) than R^2. R^2(pred) is a measure of how well the model will predict additional observations. For this model the R^2(adj) is 70.3 and the R^2(pred) is 42.4. Having the R^2(pred) so much less than the R^2(adj) suggests the model is over parametrised. While the term TypeXTimeX[O_2] is shown to be significant, component terms like TimeX[O_2] or just [O_2] are not which may mean the higher order interaction is modelling noise rather than an actual response. In contrast to other significant 2nd order interactions TypeX[O_2] is the only one that does not have both its factors showing as significant.

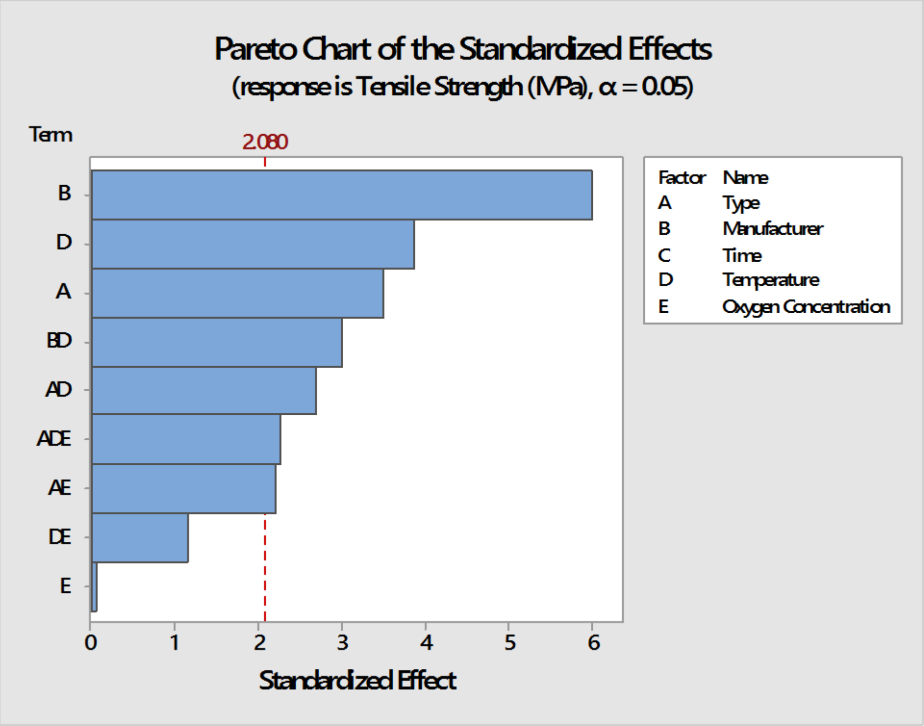

Figure 70. Pareto plot for final tensile strength model with 3rd order interactions

Since the model for tensile strength using up through 3rd order interactions may be over parametrised a model only using up through 2nd order interactions was also investigated. A model utilizing all factors and all 2nd order interactions immediately showed Type, Manufacturer, Temperature, and

ManufacturerXTemperature as significant terms. TimexTemperature, ManufacturerXTime, and TimeX[O_2] were removed as weak model terms. The resulting model had an R^2(adj) of 62.4%. The most significant terms were: Type, Manufacturer, Temperature, and Manufacturer X Temperature. The least significant interactions of this model were ManufacturerX[O_2] and TypeXManufacturer. Removing [O_2] and any interactions using [O_2] no further terms became significant. Next the term Time (and any of its interactions) was removed from the model. The Pareto plot for this model is shown in Figure 71. Type, Temperature, manufacturer, and ManufacturerXTemperature are still the only significant terms in the model. Further simplification of the model was not possible. The finalised model achieved an R^2(adj) of 63.5% and and R^2(pred) of 50.8%. While still a low predictive power overall the 2nd order interaction model is preferable to the 3rd order interaction model since it has a higher predictive power.

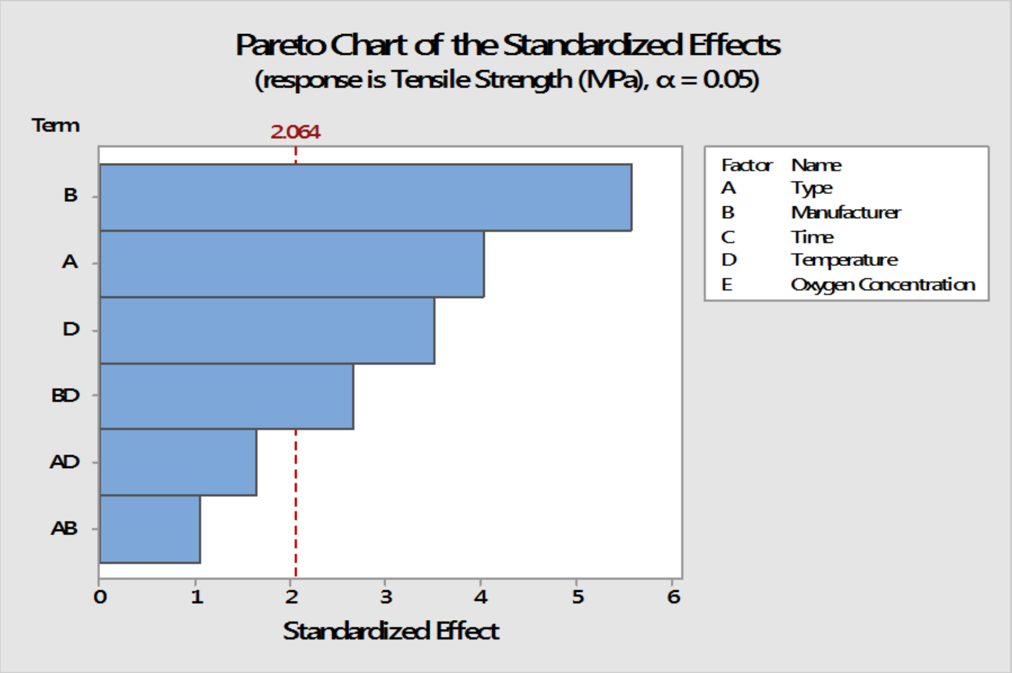

Figure 71. Pareto plot for final tensile strength model with 2nd order interactions

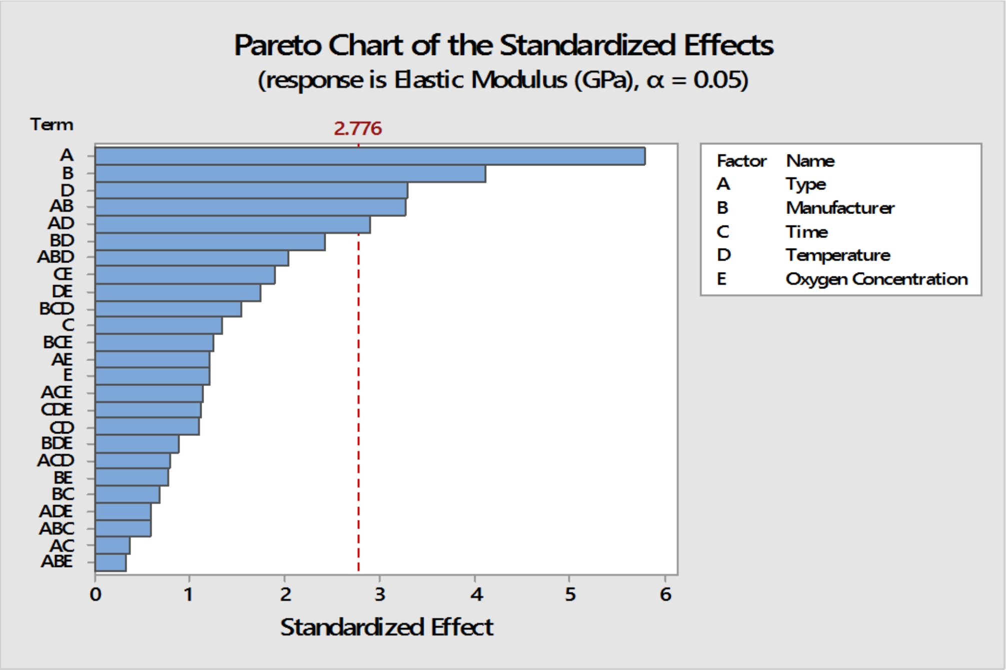

Figure 72. Initial factorial model for elastic modulus using up through 3rd order interactions

A similar strategy for analysing the tensile strength results for the fibre recycling DOE was used to analyse the accompanying elastic modulus data. To begin with a full factorial model including all factors and up to third order interactions was used. The significant factors and interactions are shown in Figure 72, and were Type, Manufacture, Temperature, TypeXManufacturer, and TypeXTemperature. Right away the elastic modulus results seem to be more easily described by a factorial model than the tensile strength results. This initial model had an R^2(adj) of 87.54% and the R^2(pred) was not able to be determined. The least significant interaction was: TypeXManufacturerX[O_2]. This interaction was removed and the model re-evaluated. As seen in Figure 73, Temperature becomes more significant than the TypeXManufacturer interaction, and the interaction ManufacturerXTemperature becomes significant. The R^2(adj) value increases to 89.75% but R^2(pred) is still not able to be calculated.

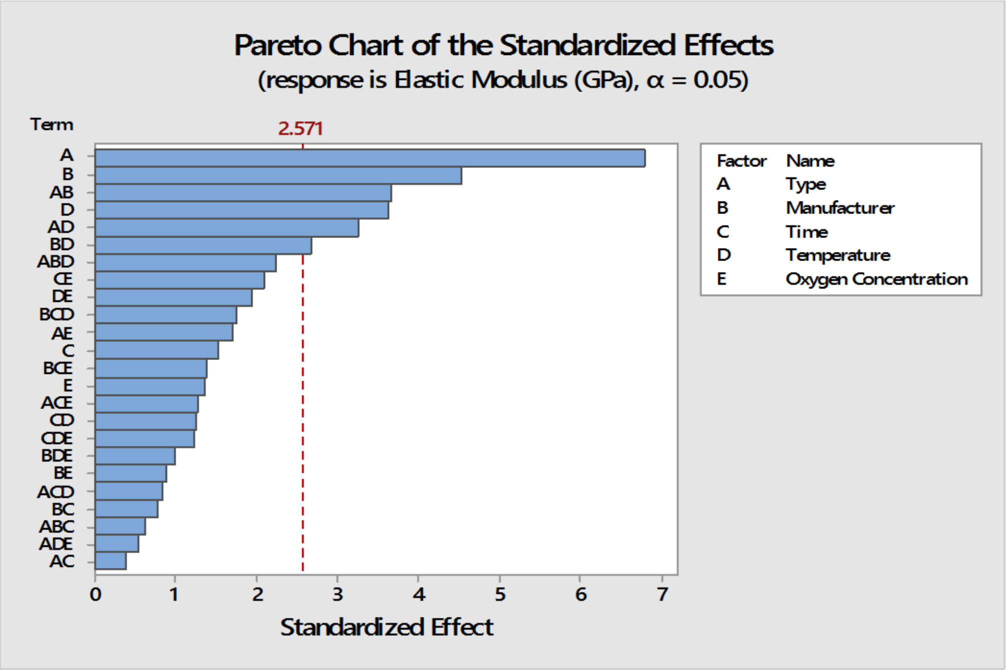

Figure 73. 2nd model/1st revision for elastic modulus

Further iterations of the model removed the interactions TypeXTime, TypeXTemperatureX[O_2], and TypeXManufacturerXTime at which point the R^2(pred) was able to be determined and was calculated as 62% while R^2(adj) also increased to 92%. The corresponding Pareto chart is shown in Figure 74. TypeX[O_2] was the weakest of the significant factors. Time is a common factor in all of the remaining terms. Oxygen concentration is not a significant factor, however it is part of second order interactions that are significant therefore the term was not removed when considering the final model. Figure 75, shows which terms are included in the most simplified version of a factorial model to describe elastic modulus behaviour with up to 3rd order interactions. The only term included in the model that is not significant is oxygen concentration. The R^2(adj) for the model is 92% and the R^2(pred) is 80%.

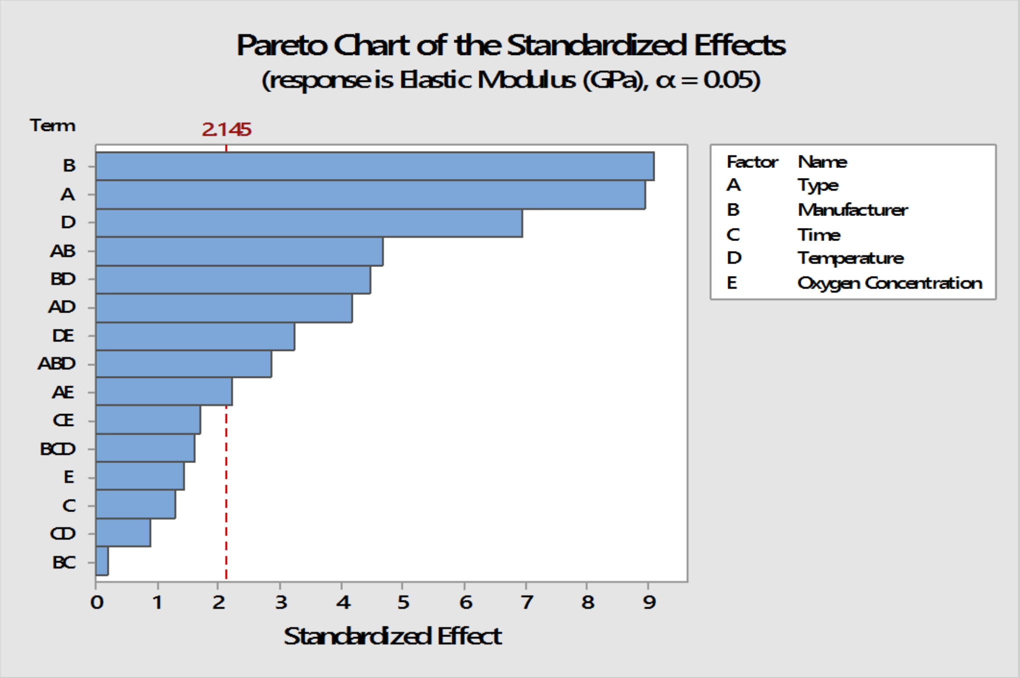

Figure 74. Revised factorial model of elastic modulus using up through 3rd order interactions

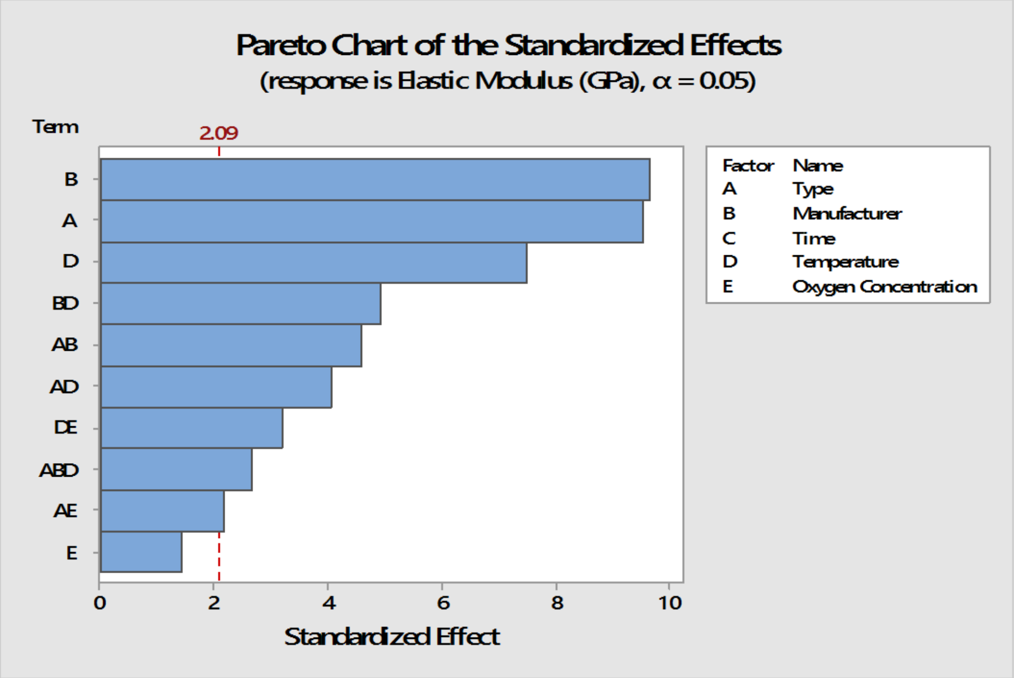

Figure 75. Pareto plot showing terms used in final elastic modulus model

The interaction of Type and Manufacturer was not an assumed result of the ANOVA. Perhaps it actually means there is a 3rd order interaction that is important but only TypeXManufacturer was found to be statistically significant.

TypeXTemperature was also a significant interaction in the 3rd order model. The observation that seems to lead to this interaction being significant is either that IM fibres are more easily damaged at 650°C or they are more easily damaged in air, but only when also at 650°C. IM7 fibres are heavily damaged at 650°C which could bias this result so much that it also suggest T800S fibres are more susceptible to damage at 650°C than HS fibres. XPS results are inconclusive as to if 650°C and 21% O_2 result in a higher degree of surface oxidation.

8.2 Models by Fibre Type and by Fibre Manufacturer

Four different subsets of the data were also analysed to see if a model could be built that has more predictive power than what is discussed above but that only applies to a narrower data set of interest. The four subsets of data considered were restricted down to only: Hexcel, Toray, intermediate modulus, or high strength fibres. ANOVA was based on a factorial model that included up through all second order interactions. The first subset considered was the Hexcel fibres. With regard to Tensile Strength; Type, and Temperature were significant factors with [O_2] and TemperatureX[O_2] being the least significant terms (Figure 76). Type being significant was obvious since AS4 and IM7 fibres have very different tensile strengths to begin with. Temperature also makes sense since the tube furnace experiments show that both AS4 and IM7 can be completely oxidized at 650°C. The model was simplified to Type, Temperature, Time, TypeXTemperature, and TimeXTemperature as terms. Type and Temperature were still the only significant terms. The R^2(adj) was 84% and the R^2(pred) was 53%. Next, elastic modulus was considered, and the original full factorial model yielded no significant terms. The model was reduced to the terms shown in Figure 77 and the terms Temperature and TypeXTemperature were found to be significant. The R^2(adj) was 85% and the

R^2(pred) was 47%. ANOVA for just the Hexcel fibres didn't reveal any new results and the model fits were poor. A slightly redeeming result is the tensile strength model for Hexcel fibres has higher R^2 values than for the model for all fibres.

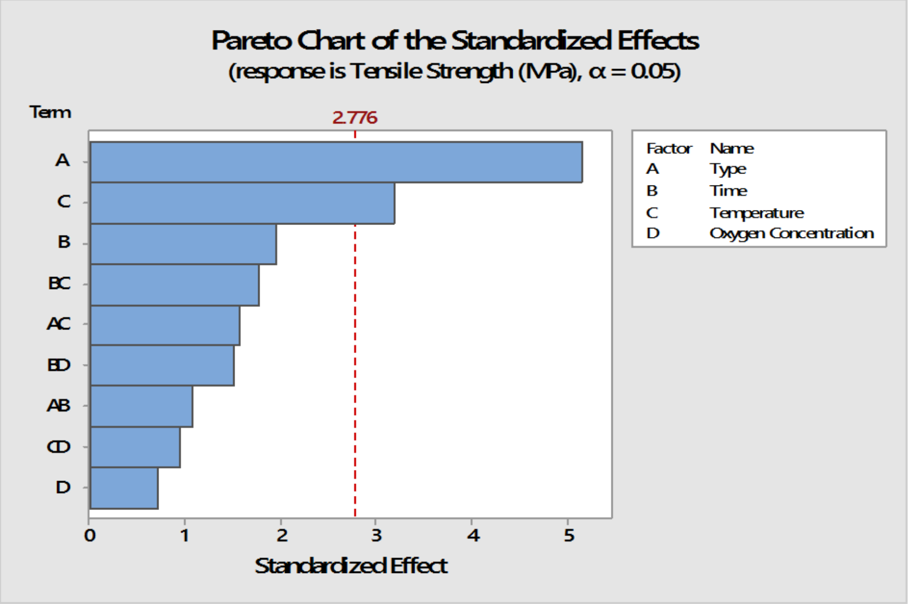

Figure 76. Model for tensile strength of Hexcel fibres using 2nd order interactions

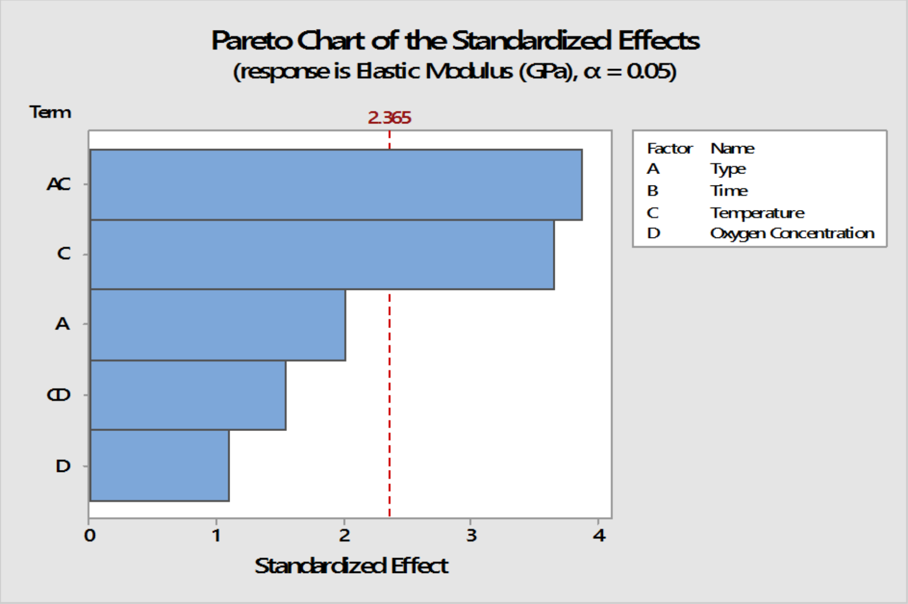

Figure 77. Final model for elastic modulus of Hexcel fibres

Complementary to the analysis of the Hexcel fibres was an analysis of the Toray fibres. Again a factorial model including all 2nd order interactions for tensile strength was the starting point. No significant terms were found for this model. By eliminating terms with low significance the model was reduced to the five terms seen in Figure 78. In the revised model still no significant terms are present. The lack of Temperature as a significant factor is suspicious and the R^2(pred) was 0% therefore this model was not useful either. Further simplification of the model was attempted by removing Type and TypeX[O_2] however the residuals became larger with increasing recycling severity instead of being random. Therefore the model was not simplified further.

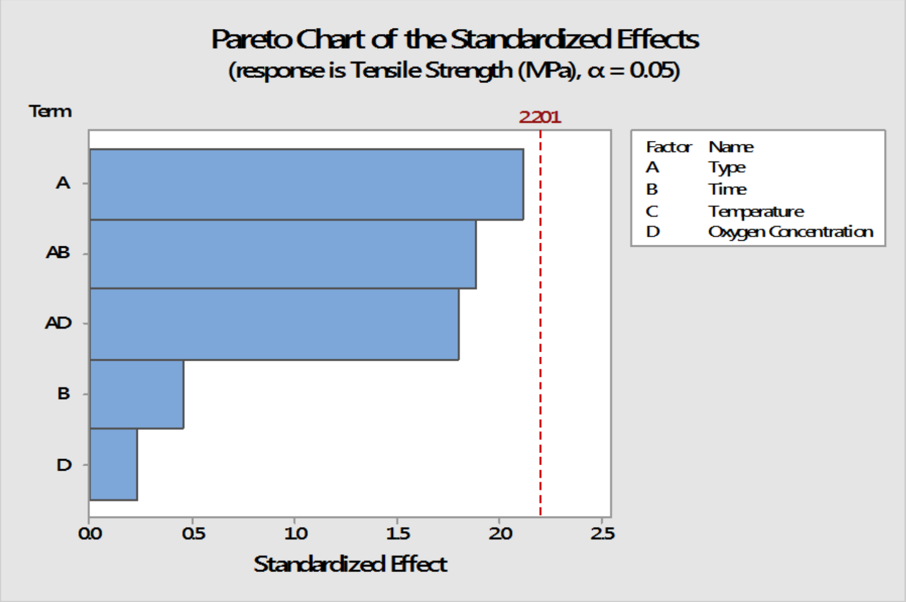

Figure 78. Final model for tensile strength of Toray fibres

Unlike the model to describe tensile strength, the model for describing elastic modulus did have significant factors. The unsimplified model had type and TemperatureX[O_2] as significant terms. Temperature was almost significant having a p-value of 0.055. Removing TypeXTime which was the least significant term made temperature a significant factor. Removing Time and all terms that were an interaction with time did not make any more terms significant, but the R^2 values for the model did increase. Figure 79 shows the relative significance of the terms remaining in the final model which had an R^2(adj) value of 91% and an R^2(pred) value of 85%.

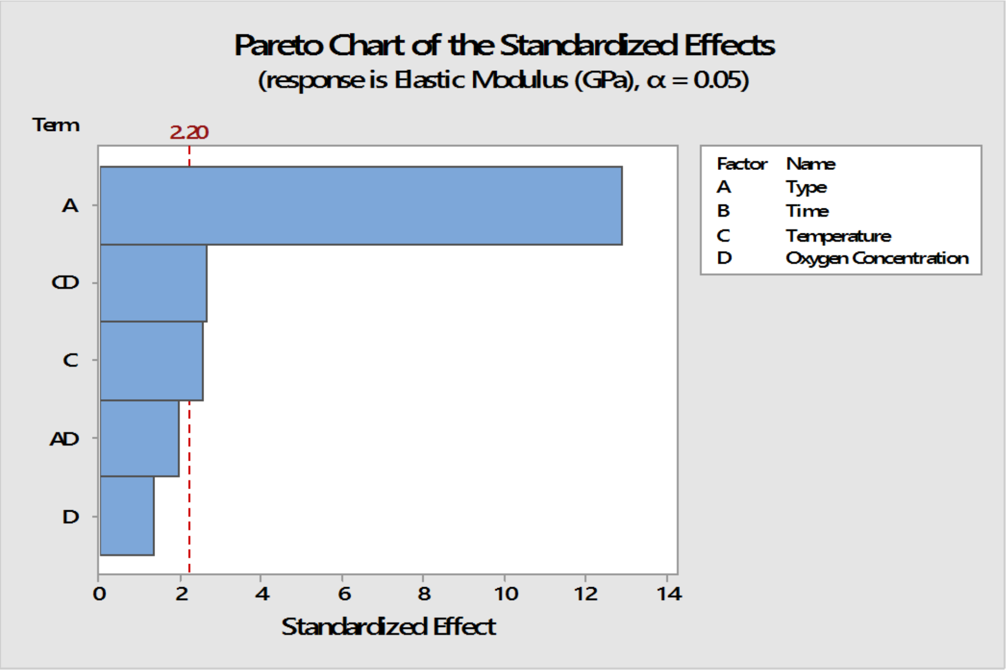

Figure 79. Final model for elastic modulus of Toray fibres

A third round of analysis was conducted on the intermediate modulus fibres (T800S and IM7). The first step in the ANOVA analysis was a full factorial model using up through 2nd order interactions. Tensile strength of the fibres is principally affected by Manufacturer and Temperature as shown in Figure 80. Again, Manufacturer being significant is not a surprise given the difference in strength between virgin T800S (Toray) and IM7 (Hexcel) fibres. The weakest terms were Time and TimeX[O_2]. Given that Time wasn't part of the top four most significant terms it was eliminated as a factor and as well as terms having an interaction with Time. The revised model has Temperature, Manufacturer, and ManufacturerXTemperature as significant terms with TemperatureX[O_2] almost being significant. Next, ManufacturerX[O_2] was eliminated as a factor. The revised model then also included TemperatureX[O_2] as a significant term. Further simplification was not possible and the model's R^2 values were: 61% for R^2(adj) and 17% for R^2(pred). Although the ANOVA revealed several significant factors the predictive strength of the model was still quite poor.

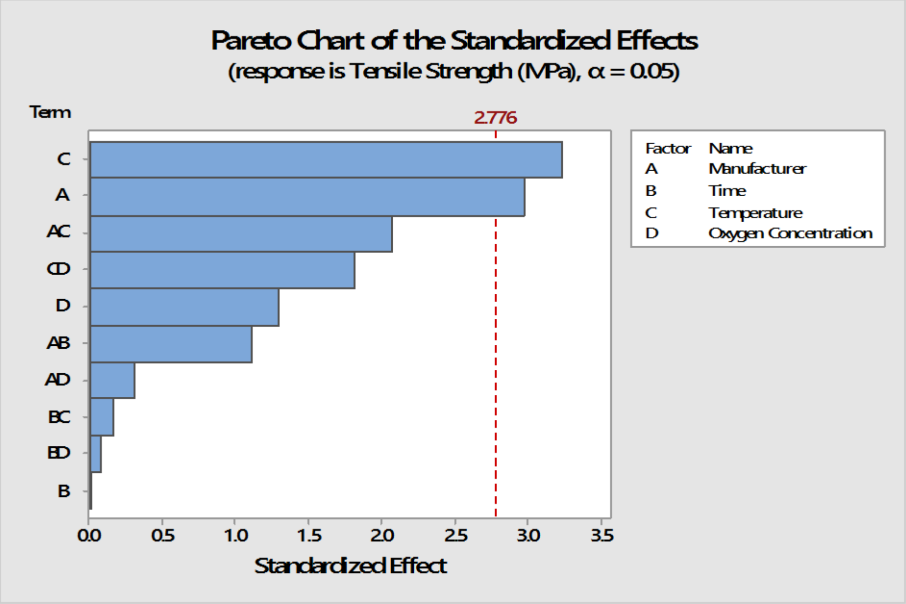

Figure 80. Factorial model for the tensile strength of IM fibres

For the elastic modulus analysis the initial model had several significant terms including: Manufacturer, Temperature, and ManufacturerXTemperature. The Pareto plot of this initial analysis is shown below in Figure 81. The interaction ManufacturerXTime was removed from the model and the TemperatureX[O_2] term became significant. The Pareto plot showing the final model for the elastic modulus of IM fibres has manufacturer, Temperature, and the interaction of Manufacturer and Temperature as significant terms and is shown in Figure 82. Only manufacturer is also a significant term in the elastic modulus model for all fibres.

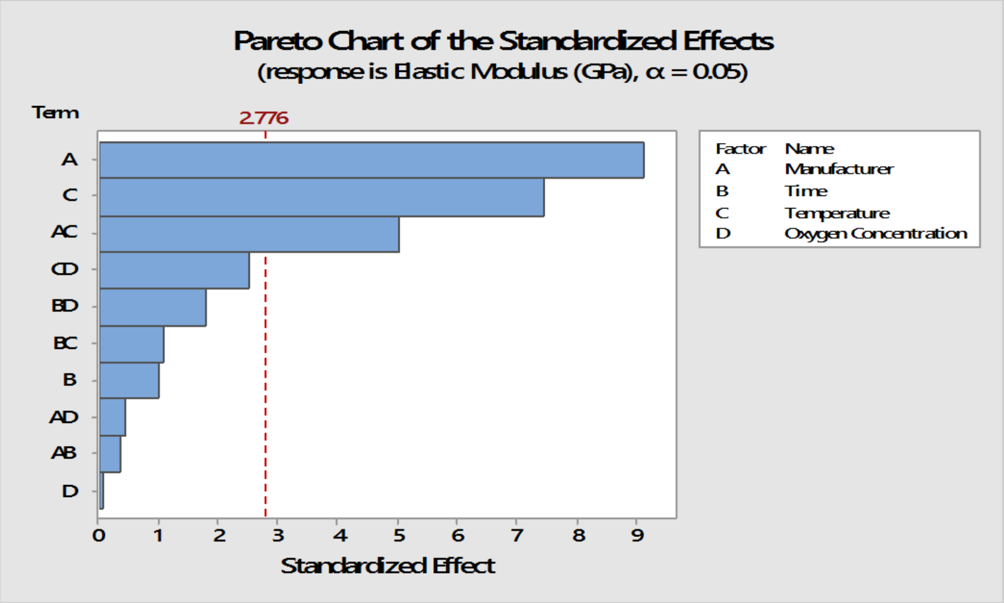

Figure 81. Initial factorial model for the elastic modulus of IM fibres

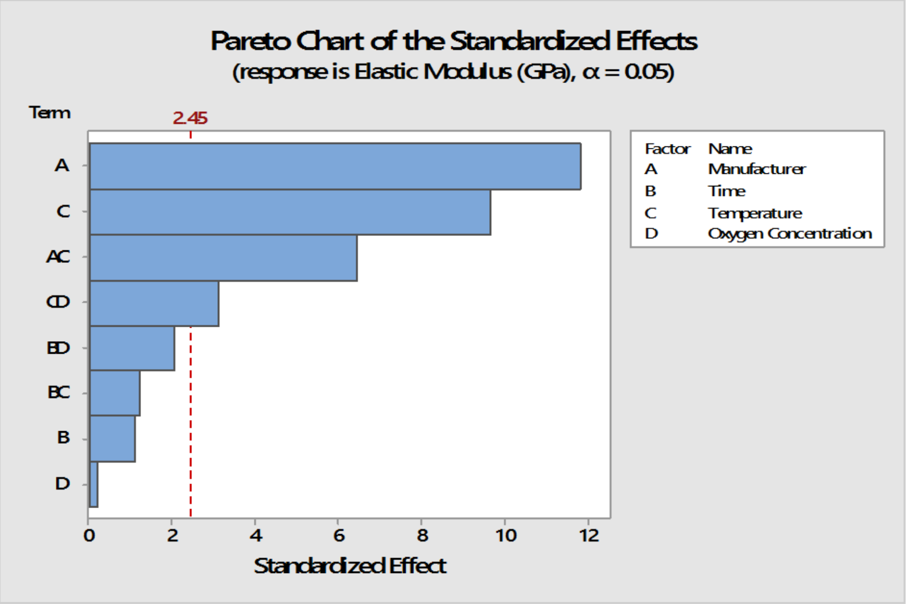

Figure 82. Final factorial model for the elastic modulus of IM fibres

AS4 and T700 were the high strength fibres studied in the fourth and final subset of data. Like the tensile strength analysis for IM fibres, Manufacturer was right away a significant factor using a full 2nd order factorial model. The weakest three interactions (TimeX[O_2], TimeXTemperature, and ManufacturerX[O_2]) were removed to produce the model shown in Figure 83 which had an R^2(adj) of 80%, and an R^2(pred) of 45%. Manufacturer was the only significant term closely followed by oxygen concentration with a p-value of 0.053. Further simplification of the model such as by removing the ManufacturerXTemperature or TemperatureX[O_2] interaction resulted in other terms becoming significant however the R^2 values for the model dropped. It is surprising to find that Temperature is not a significant factor in this model.

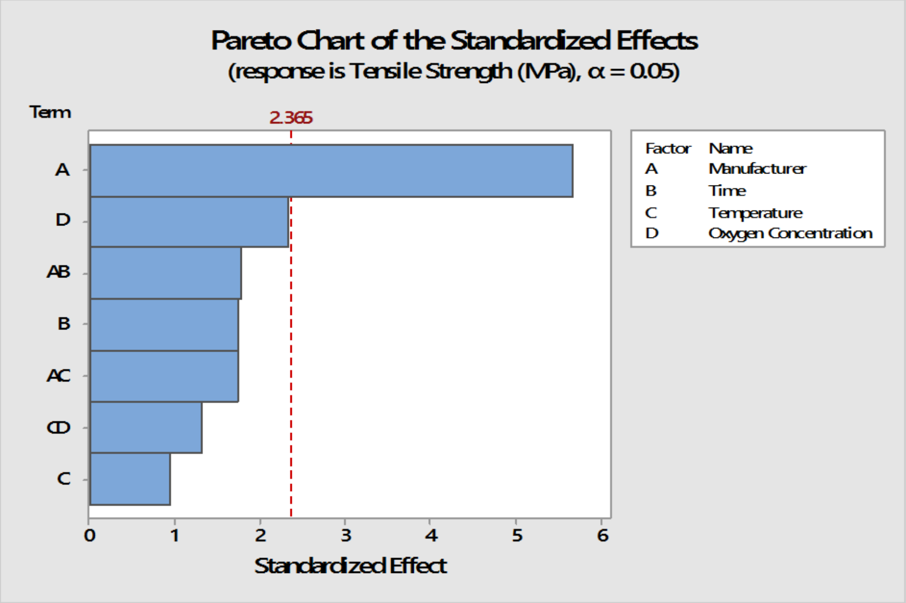

Figure 83. Final model for tensile strength of HS fibres

Data for the elastic moduli of the HS fibres was analysed as before. The factorial model with all 2nd order interactions yielded no significant terms. Removing the least significant term, TimeX[O_2] made Manufacturer a significant factor. This model had an R^2 of 80%, R^2(adj) of 45%, and R^2 (pred) could not be determined. Further simplification of the model down to five terms (Figure 84) brought R^2(adj) up to 51% although R^2 goes down to 72% and R^2 (pred) still can't be calculated.

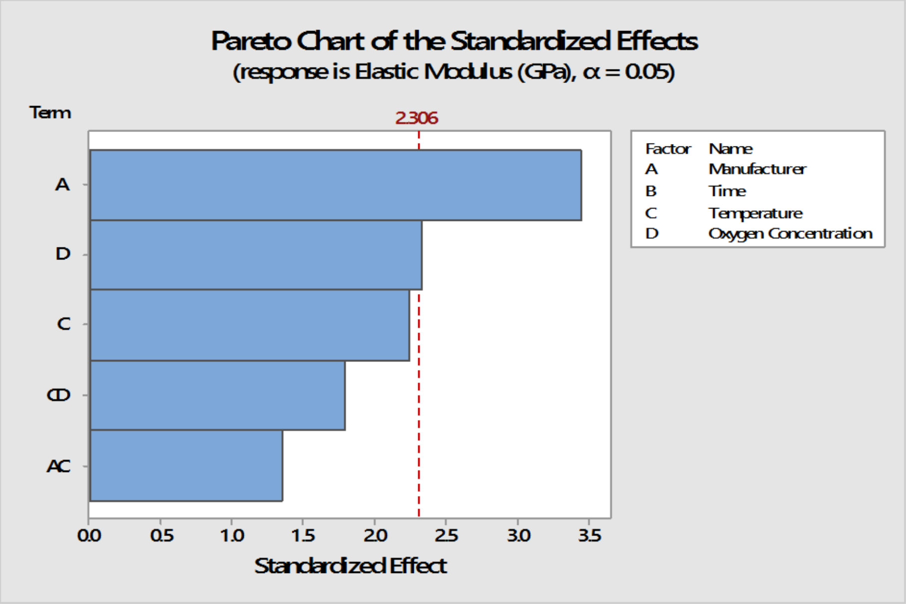

Figure 84. Final model for elastic modulus of HS fibres

8.3 Factorial Model Summary

For IM and HS fibres the factor that is always significant is Manufacturer and similarly Type is the strongest factor when considering Hexcel and Toray fibres which suggests that for recycling composites should be grouped into batches based on fibres of common type and manufacturer. For HS fibres temperature is less of an important factor than oxygen concentration. Also the strength and modulus of HS fibres are more affected by the factors of the recycling process rather than the interaction of any factors. On the other hand for IM fibres the most significant factor of the recycling conditions is Temperature. The most significant terms for the IM fibre models are: Manufacturer, Temperature, TemperatureXManufacturer, and TemperatureX[O_2]. Temperature and Manufacturer are significant factors for both tensile strength and elastic modulus models whereas TemperatureXManufacturer, and TemperatureX[O_2] are only significant in the elastic modulus model. Compared to the overall model for elastic modulus the elastic modulus model for Hexcel fibres is about as strong, while the Toray model is slightly stronger, and the models for IM and HS fibres reveal the different sensitivities between the two fibre types to recycling conditions. The strongest terms in the Toray fibre models are not among the strongest terms in the overall tensile strength and elastic modulus models except for Type. For the models of Hexcel fibres the terms that were significant were also significant in the overall models for Tensile Strength and Elastic Modulus. Temperature is a significant factor in the models for Hexcel but not in the tensile strength model for Toray fibres.

9 Thermal Modelling

9.1 Objectives

Carbon fibre composite recycling is a complex task with many variables which are difficult and or time consuming to change on a physical process. Throughout this chapter the development and implementation of a reaction kinetics model for carbon fibre recycling, including heat flow, is discussed. The model allows for process as well as material form and composition variables to be changed. Combinations of factors could also be changed such as resin type, fibre type, thickness, process temperature etc., to see how the recycling process behaves with each different set of parameters. For example, a design of experiments could be set up to determine the optimal process time and temperature needed to recycle a composite with a given thickness, fibre, and resin. Optimality could be based on the cost of running the process, cleanliness of the resulting fibre, and/or fibre quality. All of this experimentation could be done offline and with comparatively little time as opposed to doing this on a physical recycling process. The utility of the model is that a Recycler can determine what materials are best to recycle and also predict fibre quality for a given set of process conditions.

9.2 Scope

The process of recycling a composite is broken down into three reactions: pyrolysis, char oxidation, and fibre oxidation. Further details explaining how the model works during each reaction phase is found in section 9.3. The framework of the model has been designed so that it may be applied to any thermal type recycling method and also any composite system. To achieve this flexibility an extensive thermal-kinetic characterisation of the resin, fibre, and composite must be conducted. A 1D model was justified on the basis that the in-plane directions are expected to behave nearly identically, and based on previous experience with composite recycling, that the thickness of the composite significantly altered the behaviour of the recycling process and fibre quality [40]. The model can be used to predict how long it will take for the matrix of a composite to be removed, leaving usable carbon fibres. For a static process where fibres are not removed from the process as they become freed from the resin matrix, the model can be used to optimize process time so that as many clean fibres as possible are produced with an acceptable level of thermal-oxidative damage. In the case of the fluidised bed, since the model tracks how much char remains on the fibre during the char oxidation phase, the elutriation time may be predicted.

9.3 Implementation

The model uses a one dimensional finite difference framework with a constant time step and is written in Java. A piece of composite of a given thickness is considered. The composite is then subdivided through its thickness into fourteen layers that are sufficiently thin to assume homogeneity within each layer. Mirror symmetry is assumed to reduce the computational complexity so only seven layers are considered in the code of the model. Boundary conditions are used at layer one (boundary between composite and recycling atmosphere) and at layer seven (at the symmetry line). Figure 85 shows these boundary conditions as well as heat and mass flow between each layer. Additionally, the temperature, mass, composition, and extent of reaction of each layer are tracked as a function of time. Each layer undergoes only one reaction (pyrolysis, char oxidation, or fibre oxidation) at any given time. This is a limitation of the modelling strategy. However, to make this modelling more realistic the volume of the layers can be made smaller by using an increasing number of layers.

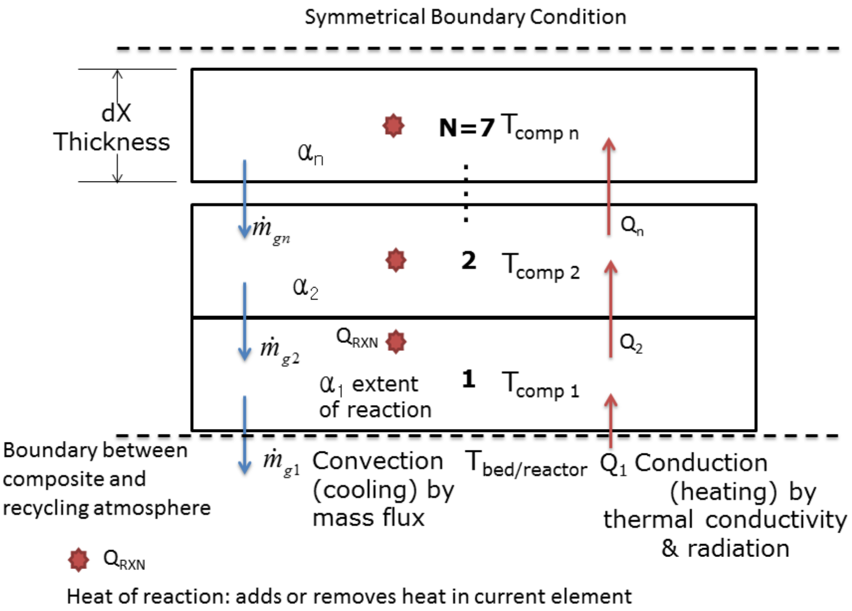

Figure 85. Model schematic showing directions of heat and mass flow as well as sources of heat

The Transient Heat Conduction Equation (equation 11) provides the core functionality of the model. This equation is used to determine the change in temperature of a layer in the model. This change in temperature drives the pyrolysis, char oxidation, and fibre oxidation reactions that generate or consume heat, and evolve volatile mass. The term on the left hand side (LHS) of the Transient Heat Conduction Equation relates to the temperature of a layer. The first term on the right hand side (RHS) is heat delivered from the gaseous atmosphere and its conduction through the composite, the second is the convection of gases evolved from the decomposition of the composite, and the third is an energy balance. In the energy balance term there is heat evolved from the pyrolysis or oxidation reaction, a change in enthalpy of the layer based on the change in temperature of the gas in that layer, and a change in internal energy based on the change in temperature of the layer. The LHS represents the change in temperature of the layer with respect to time. The terms in Equation 11 are tabulated below. The convention for exothermic reaction to have a negative enthalpy is maintained.

Table 28. Terms in Equation 11 and their definition

Term	**Definition**	**Term**	**Definition**
m	Mass of composite	$c_{p,g}$	Heat capacity of volatiles
c_p	Heat capacity of composite	$\frac{\partial T}{\partial x}$	Temperature difference between layers
$\frac{\partial T}{\partial t}$	Change in temperature of layer w.r.t. time	$\frac{\partial \alpha}{\partial t}$	Change in extent of reaction
k	Thermal conductivity	H	Internal energy
$k\frac{\partial^2 T}{\partial x^2}$	Heat flow through boundary layer and through composite	H_g	Enthalpy of volatiles
$\dot{m}_g$	Volatile release rate (1/s)	H_{Rxn}	Enthalpy of reaction

$$mc_p\frac{\partial T}{\partial t} = k\frac{\partial^2 T}{\partial x^2} - \dot{m}_g c_{p,g}\frac{\partial T}{\partial x} + \frac{\partial \alpha}{\partial t}(-H + H_g - H_{Rxn}) \qquad 11$$

$$\frac{d\alpha_x}{dt} = Ae^{-E_a/RT}(1-\alpha)^n \text{ and } 1-\alpha = m/m_o \qquad 12$$

Three sets of inputs must be provided to the model, one for each set of thermal, kinetic, and physical parameters. Within the thermal category: conduction, convection, heats of reaction, heat capacity, and thermal conductivity are considered.

All of the kinetic parameters relate to α, the extent of reaction. α is defined by equation 12. In equation 12 A is the pre-exponential factor, E_a is the activation energy, n is the reaction order, m is the current mass of the layer, and m_o is the original mass of the layer. However, there is an α for each reaction: pyrolysis, char oxidation, and fibre oxidation as well as for the overall recycling process. TGA curves are analysed to determine the α range for which each reaction is operative. Additionally, Friedman's method (discussed in Section 3.5.1) is used to determine the pre-exponential, activation energy, and reaction order for each reaction. Physical parameters, such as weight fractions, thickness, and density are used to define the construction of the composite.

9.3.1 Composition Tracking

To determine the starting composition of the composite a TGA experiment must be run for a long enough time to see the transitions from pyrolysis to char oxidation and char oxidation to fibre oxidation. The original composition of the composite is just fibre and resin in the amounts determined by the TGA experiment. During pyrolysis the composite is comprised of virgin composite not yet reacted, fibre in char, and char. At the end of the pyrolysis reaction all the resin has been converted into char and volatiles and the mass fibre in char is the same as the mass of fibre in the virgin composite (no fibre mass has been converted into volatiles). During char oxidation the char is oxidised, turning it into volatiles, and fibres are liberated from char as loose bundles. The mass of fibre does not change during char oxidation. During fibre oxidation the fibres are oxidised and converted into volatiles. The heat capacity and thermal conductivity of fibre does not change during fibre oxidation. When alpha for the overall composites recycling reaction reaches 0.995, that particular layer is considered fully recycled (fibres are considered fully oxidized) and the heat transfer boundary moves one layer towards centre. Equations 13 -18 are used to change the composition of the composite. Equations 13-15 are valid during pyrolysis, equation 16 is valid during char oxidation, equation 17 is used during fibre oxidation, and equation 18 is always valid. The thermal conductivity and heat capacity of the composite is determined by the rule of mixtures for weight using thermal conductivity and heat capacity values of char, fibre, and virgin composite.

$$m_{char} = m_{o,pyr}\alpha_{pyr} \tag{13}$$

$$m_{fibre} = m_o X_f \tag{14}$$

$$m_{virgin} = m_o - (m_o - m_{pyrToCharOx})\alpha_{pyr} \tag{15}$$

In equation 13, $M_{o,pyr}$ is the initial mass available for pyrolysis, and α_{pyr} is the extent of the pyrolysis reaction. In equation 14, m_o is the initial mass of the composite and X_f is the fibre weight fraction. In equation 15, $m_{pyrToCharOx}$ is the mass of the composite at the point in time when the reaction switches from pyrolysis to char oxidation.

$$m_{char} = m_{o,CharOxidation}(1-\alpha_{CharOxidation}) \tag{16}$$

In equation 16, $m_{o,CharOxidation}$ is the original mass of char available to be oxidised and $\alpha_{CharOxidation}$ is the extent of the char oxidation reaction. In equation 17, $\alpha_{fibreOxidation}$ is the extent of the fibre oxidation reaction.

$$m_{fibre} = m_o X_f (1-\alpha_{fibreOxidation}) \tag{17}$$

$$m_{virgin} = m_o(1-\alpha) \tag{18}$$

9.3.2 Heat Flow

Thermal parameters are used to describe the recycling atmosphere, the thermal conductivity, and heat capacity of the virgin composite and its constituent components. The parameterisation for the composite is broken down to the constituent level so that as the composition of the composite changes during the recycling process the thermal behaviour can be recalculated accordingly. The thermal conductivity of resin and char were taken from references listed in Table 29. The thermal conductivity of the composite was measured to be 0.491W/m·K according to the procedures described in Section 10.2. Heat transfer at the boundary between the composite and the recycling environment was calculated using the net contribution from both forced convection and radiation. Sections 10.1 and 10.2 provide further detail on this measurement.

Table 29. Conduction Parameters

Thermal Conductivity	Value (W/m·K)	Heat Transfer Coefficient	Value ($W/m^2 \cdot K$)
Fibre (k_f)	2	**Natural Convection**	10
Resin, (k_r)	0.169	**Forced Convection**	45.5
Char, (k_{ch})	0.955 [89]	**Fluidised Bed**	100
Composite, (k_c)	0.4901		

Mass flux of volatiles is responsible for convective heat transfer. Values for mass flux and heat capacity of volatiles are needed to determine the convective heat transfer. Mass flux is dependent on the reaction rate and will be discussed later. To simplify the model, the heat capacity of CO_2, as a function of temperature, was used for the heat capacity of volatiles term in the model. Equation 19 gives this function in the units of J/mol·K. Section 9.3.3 shows an example of the convective heat transfer equations.

$$c_{p,g} = (24.99735 + 55.18696 * T - 33.69137 * T^2 + 7.948387 * T^3 - 0.136638 / T^2)^{[90]} \qquad 19$$

Three heats of reaction are considered: pyrolysis, char oxidation, and fibre oxidation. Simultaneous TGA and DSC measurements were used to measure the heats of pyrolysis and char oxidation. The energy evolved for the oxidation of graphite, 393 kJ/mol, is used as the heat of reaction for fibre oxidation [71]. On the LHS of the transient heat conduction equation c_p is the heat capacity of the composite. The heat capacity of the composite is determined by the rule of mixtures using the weight fractions of virgin composite, char, and carbon fibre. Table 30 lists the heat capacities used to calculate the overall heat capacity of the composite.

Table 30. Heat capacity of constituent components of composite

Material	**Heat Capacity (J/g·K)**
Carbon Fibre	0.753 [91]
Char	0.987 [89]
Virgin Composite	1.1

9.3.3 Extent of Reaction

Simultaneous TGA/DSC curves were analysed to determine the range over which each sub-reaction (pyrolysis, char oxidation, and fibre oxidation) is active. The range over which each sub-reaction is active is unique to each composite system. The composite system chosen for the reaction range analysis is a Boeing specified material “BMS8-276”. This material is extensively used in the composite structure of the Boeing 787. Figure 86 gives an example of this analysis. First, tangent lines are drawn on each side of the inflection point in the weight (%) curve. Then the intersection of these tangent lines is taken as the changeover from one reaction to another. For the case shown in Figure 86 the changeover from pyrolysis to char oxidation is 79.7 wt% corresponding to an α of 0.203 (1-0.797). The first indication of mass loss in the 2-3 minute range is attributed to the removal of water and any adsorbed species. From the 6 minute to 8 minute mark the weight loss is attributed to the volatilisation of low molecular weight polymers and is distinct from pyrolysis [7]. To make the inflection point in the weight (%) curve easier to identify, the exothermic peak in the heat flow curve can be used as a guide to find the transition range in the weight (%) curve. The time lag of the mass loss curve behind the heat flow curve will be influenced by the heating rate of the experiment with faster ramp rates resulting in a larger lag.

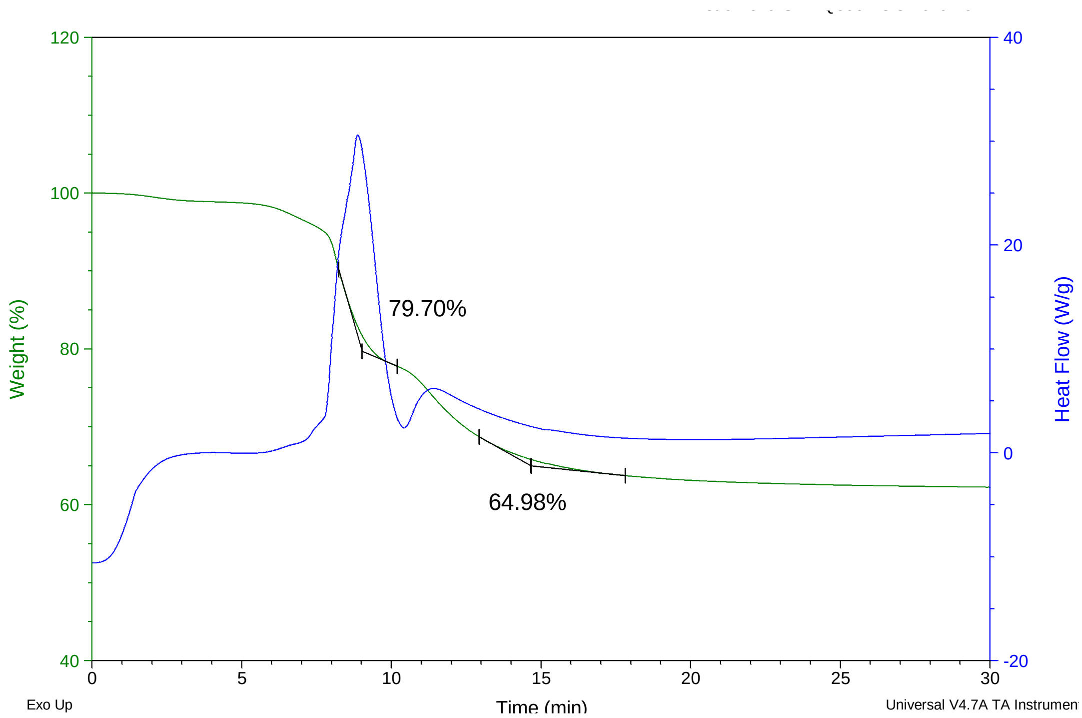

Figure 86. DSC-TGA curves with analysis points. Experiment performed in air on BMS8-276 composite. A ramp rate of 50°C/min to 550°C followed by a two hour isothermal hold was the thermal cycle used.

9.3.4 Calculation Procedure

In this section the calculations used to determine the change in temperature of a layer will be demonstrated step by step. The calculations will cover the 10th time step of the outermost layer and pyrolysis will be the reaction under consideration.

The boundary conditions used are: at the outer surface of the composite there is a boundary layer where heat transfer occurs as described by equation 20 and there is no mass flux into the composite, and at the centre of the composite a symmetrical boundary condition is used such that there is no heat or mass transfer further into the composite. Assumptions used throughout the model are: volatiles are in thermal equilibrium with the layer they are leaving, and the recycling atmosphere stays at a constant temperature and gas composition [7, 89, 92]. Assumptions for the initial conditions are that each layer in the composite is at equilibrium at the same given temperature, there is no mass flux in the system, and all extent of reaction variables are zero. The first of these assumptions has been verified experimentally. If the third assumption is true then it follows that the second assumption of no mass flux is also true.

Referring back to Figure 85, the outermost layer is exposed to the recycling atmosphere and boundary conditions for heat transfer are applied accordingly as demonstrated in equation 20. In equation 20 X_a is the cross-sectional area (length x width) of the layer, H_{trans} is the heat transfer coefficient, T_{oven} is the temperature of the recycling process, and dt is the time step.

The pyrolysis reaction during composite recycling turns resin into char, and mass loss, in the form of volatiles, occurs. An example calculation for the change in temperature at the 10th time step is show next. The 10th time step was chosen so that it was close to the initial conditions but there is a non-zero temperature difference between layers and a non-zero reaction progress. The change in temperature is solved for according to the Transient Heat Conduction Equation (equation 11). From equation 11 the first term can interpreted as equation 20, where the subscript t is for time and N is for layer. Using the initial conditions T_{oven} is 550^{o}C (823.15K),

$T_{10,1}$ is 24.03°C (297.18K), $K_{0,2}$ is 0.4909W/m-K (as the composition of the composite at this time is predominantly virgin material), $T_{10,2}$ is 297.15K, dx is 4.28x10^{-4} m (6 mm thick laminate divided into 14 layers), and X_a is 0.0375m^2 (laminate 150 mm in width x 250 mm in length). Equation 21 is simply equation 20 worked out.

$$\begin{aligned}
&k\frac{d^2T}{dx^2} = Q1 = \\
&layer1: \left(H(T_{oven} - T_{\mathrm{t}-1,1}) - K_{t-1,2}(T_{\mathrm{t}-1,1} - T_{t-1,2})/dx\right)Xa \\
&layer2-6: \left(k_{t-1,N}(T_{t,N-1} - T_{t-1,N}) - k_{t-1,N+1}(T_{t-1,N} - T_{t-1,N+1})\right)Xa/dx \\
&layer7: \mathrm{k}_{t-1,7}(T_{t,6} - T_{t-1,7})Xa/dx
\end{aligned} \tag{20}$$

$$\begin{aligned}
&Q1 = \left(H(T_{oven} - T_{\mathrm{t}-1,1}) - K_{t-1,2}(T_{\mathrm{t}-1,1} - T_{t-1,2})/dx\right)Xa \\
&Q1 = \begin{pmatrix} 45\dfrac{W}{m^2K}\left(823.15K - 297.18K\right) - \\ \left(0.4909\dfrac{W}{mK}\left(297.18K - 297.15K\right)/4.28x10^{-4}m\right) \end{pmatrix} * 0.0375m^2 \\
&Q1 = \left(23936\frac{W}{m^2} - 36.52\right) * 0.0375m^2 = 896.24W
\end{aligned} \tag{21}$$

Next the second term of equation 11 must be evaluated and this is shown as equation 22. The equations to determine the change in reaction and the heat capacity of the volatiles are shown previously as equations 12 and 19, respectively. Mass flux for the n^{th} layer is the net mass flux away from the layer so it is the mass flux received from the more inner layers less the mass flux generated as a result of the reaction in that layer. Equation 22 shows that mass flux generated within a layer is simply the initial mass available for reaction multiplied by the overall extent of reaction for that layer.

$$\left(\dot{m}_g c_{p,g}\frac{\partial T}{\partial x}\right) = m_{o,pyr}\alpha_{rxn-N}c_{p,g}(T_{t-1,N})(T_{t,N-1}-T_{t-1,N})/\,\mathrm{dt} = \mathrm{Q}2$$

$$Q2 = 3.76\,\mathrm{g}*5.793x10^{-35}*0.846\frac{J}{g}*\left(823.15K-297.18K\right)/1x10^{-4}s \tag{22}$$

$$Q2 = 9.69x10^{-28}W$$

The third term in equation 11 is composed of three terms which are detailed in equation 23. The subscript *t-2* is used to indicate two time steps prior to the current one. For the first time step *t-2* and the *t-1* subscripts refer to the initial conditions, by the 3rd time step the *t-2* time step will be the result calculated in the first time step. The change in enthalpy of the layer and the volatiles are calculated as the integral of the respective heat capacities with respect to temperature multiplied by the mass under consideration.

$$\left(\frac{\partial\alpha}{\partial t}(-H+H_g-Q_{Rxn})\right) = \left(-\Delta H_N+\Delta H_{g-N}-Q_{RXN-N}\right)\Big/dt = Q3$$

$$\Delta H_N = c_{p_{t,N}}\left(T_{t-1,N}-T_{t-2,N}\right)m_{t-1,n}$$

$$\Delta H_N = 1.1\frac{J}{g\cdot K}\left(297.181K-297.178K\right)*25.52g = 0.0898J$$

$$\Delta H_{g-N} = \mathrm{m}_{o,\mathrm{RXN}}\mathrm{d}\alpha_{RXN}\int_{T_{t-1,N}}^{T_{t-1,N-1}} c_{p,g_N}(\mathrm{T})\,\mathrm{dT} \tag{23}$$

$$\Delta H_{g-N} = 5.18g*5.79\,\mathrm{x}10^{-35}\int_{297.179}^{823.15} c_{p,g_N}(\mathrm{T})\,\mathrm{dT} = 1.58x10^{-31}J$$

$$Q_{Rxn-N} = H_{RXN}d\alpha_{Rxn}m_{oRXN} = 2319J/g*5.79\,\mathrm{x}10^{-35}*3.135g = -4.21x10^{-30}J$$

$$Q3 = (-0.0898\,J+1.58x10^{-31}J+4.21x10^{-30}J)/1x10^{-4}s = 898W$$

The third energy contribution term to Q3 is heat generated by the pyrolysis or either oxidation reactions. As shown by equation 23 this is the product of the heat of reaction (measured by DSC), the change in α for that specific sub reaction and the initial mass available for reaction. The values for the heat of reaction term, Hrxn, are found in Table 31. Two different masses available for reaction are used during the pyrolysis process. First is the mass of resin that is volatilised; which is the difference in the initial mass of the composite and the mass at the end of the pyrolysis process. The mass available for reaction term is the mass of resin that gets converted into char. In this work it was assumed that all resin that wasn't volatilised would be turned into char. So the value for this mass is the mass of the composite at the end of the pyrolysis reaction minus the fibre weight. For char oxidation the mass available for reaction is the mass of char at the completion of the pyrolysis reaction. During fibre oxidation the initial mass available for reaction is simply the original mass of fibre in that layer which is the mass of the composite multiplied by fibre weight fraction. All of these masses available for reaction were described as the total mass for the whole composite; in the model the mass would be need to be adjusted to just be for the layer of composite in question.

The change in temperature for the current time step is calculated according to equation 11 which is reproduced with the worked out example as equation 24.

$$mc_p\frac{\partial T}{\partial t}=k\frac{\partial^2 T}{\partial x^2}-\dot{m}_g c_{p,g}\frac{\partial T}{\partial x}+\frac{\partial \alpha}{\partial t}(H-H_g-H_{Rxn})$$

$$mc_p\frac{\partial T}{\partial t}=Q1-Q2+Q3$$

$$\Delta T=\frac{Q1-Q2+Q3}{mc_p}dt \tag{24}$$

$$\Delta T=\frac{896.24W-9.69x10^{-28}W+898W}{25.55g*1.1\frac{J}{g\cdot K}}1x10^{-4}s$$

$$\Delta T=6.38x10^{-3}K$$

Once the temperature in layer 1 for the first time step has been determined the process is repeated for the subsequent layers. To prepare for the next time step the extent of reactions, compositions of the composite, and thermal constants must be recalculated. Equation 8 is used to calculate the extent of the reaction based on the current temperature and the values in Table 31. An example is shown as equation 25.

$$\frac{d\alpha_{pyr}}{dt}=Ae^{-E_a/RT}(1-\alpha)^n$$

$$d\alpha_{pyr}=2.52x10^{17}s^{-1}e^{\frac{-271 kJ/mol\cdot K}{300K*8.314J/mol}(1-0)^{2.9735}}*1x10^{-4}s \tag{25}$$

$$d\alpha_{pyr}=3.10x10^{-39}$$

Table 31. Reaction Constants

Reaction	**α Range**	**Pre Exponential Factor (1/s)**	**Activation Energy (J/mol·K)**	**Reaction Order (-)**	**Heat of Reaction (J/g)**
Pyrolysis	0-0.203	2.52×10^{17}	271,002	2.9735	2,319
Char Oxidation	0.203-0.3502	3.03×10^{5}	120,576	1.0158	5,365
Fibre Oxidation	0.3502-1.0	1.80×10^{3}	140,000	0.0068	5,435

Once the change in alpha for the specific reaction has been determined the overall alpha for the entire recycling process and the alpha for the reaction can be determined. The α for each subreaction scales from 0 to 1 as the overall α increases within each α range given in Table 31. Equation 26 shows how the overall reaction progress is tracked, where $\alpha_t = \alpha_{t-1}$ (alpha from previous time step) + $d\alpha_{rxn}$ (the change in α of a particular reaction).

$$
\begin{gathered}
\alpha_{t+1} = \alpha_t + d\alpha_{rxn} \\
\alpha_{pyr} = \frac{\alpha_t}{\alpha_{pyrToCharOx}} \\
\alpha_{CharOx} = \frac{\alpha - \alpha_{pyrToCharOx}}{\alpha_{CharOxToFibreOx} - \alpha_{pyrToCharOx}} \\
\alpha_{fOx} = \frac{\alpha_t - \alpha_{CharToFibreOx}}{1 - \alpha_{CharToFibreOx}}
\end{gathered}
\tag{26}
$$

9.4 Thermal Model Results and Discussion

The thermal model was used to simulate the recycling of a 6 mm thick composite at 550°C in a forced convection environment such as a tube furnace. The resin system assumed was MTM 44 with the kinetic parameters as previously described. The fibre mass fraction used was 0.67. Figure 87 shows the temperature in the first (outermost), 4th (quarter thickness), and 7th (middle) layers of the composite during recycling. The three stages of recycling (pyrolysis, char oxidation, and fibre oxidation) are clearly shown. The pyrolysis reaction is active for around the first 200 s, then char oxidation takes over for the next 12-15 s, before the fibre oxidation stage is triggered. Char oxidation taking only 15 s is clearly too fast and the cause of this will be investigated later in this section.

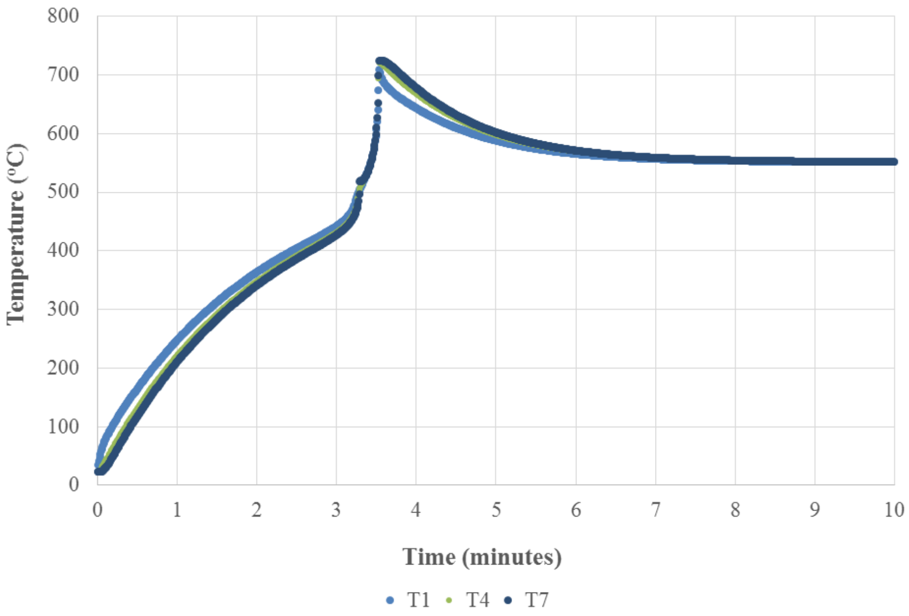

Figure 87. Temperature distribution during recycling generated from model

Fibre oxidation is the longest stage and Figure 88 shows that it is much slower than char oxidation and fibre oxidation. At 10 minutes the overall alpha has increased to 0.334 from 0.332 at 4 minutes.

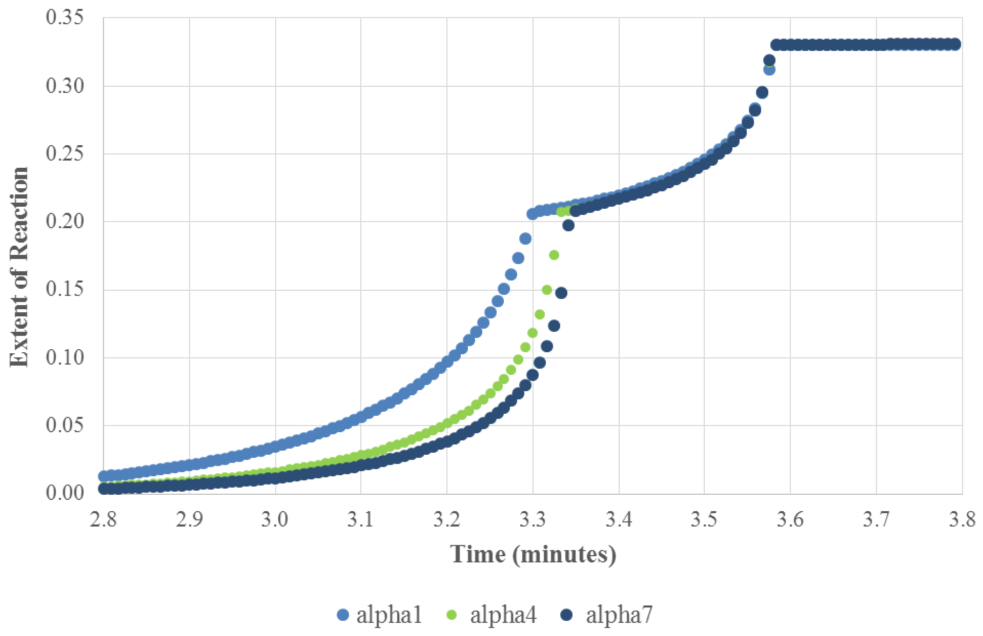

Figure 88. Overall reaction progress in 1st, 4th, and 7th layers of composite

The reaction progress equation has an exponential form which is reflected in Figure 88. As the pyrolysis and char oxidation reactions progress the more rapidly the reaction advances and thus disproportionate amounts of heat is released causing the temperature to increase rapidly. Figure 89 shows conductive heat flow from the recycling furnace, cooling convective heat flow from the generation of volatiles, and the heat released from the pyrolysis, char oxidation, and fibre oxidation reactions. Conductive heat flow clearly dominates through the entire recycling period while convective heat flow is two orders of magnitude smaller. The heat of reaction is fairly low for the first 3 minutes but towards the end of the pyrolysis reaction it picks up which explains the rapid increase of temperature seen in Figure 87. The transition from pyrolysis to char oxidation is seen at around 3.25 minutes in the Heat of Reaction curve where it elbows. The transition is not as noticeable in the Convective Heat Flow curve but the gaps in the curve show the reaction is progressing so quickly that a sampling rate of once per second is not sufficient to get a continuous curve. The pyrolysis to char oxidation transition is when the curve becomes continuous again (the end regime of the pyrolysis reaction being too fast for the sampling rate) and the char oxidation to fibre oxidation is around the 3.5 minute mark where the Heat of Reaction and Convective Heat Flow curves begin to level off and when the Conductive Heat Flow curve begins to drop.

Char oxidation is very exothermic as seen in Figure 89 and during the char oxidation reaction, as clearly demonstrated Figure 87, the temperature in each layer of the composite rapidly increases beyond the temperature of the recycling environment. During the fibre oxidation stage the temperature cools down and approaches 550°C, the temperature set as the recycling temperature. During fibre oxidation layer 7 is hotter than layer 1 which shows how the composite insulates its inner layers.

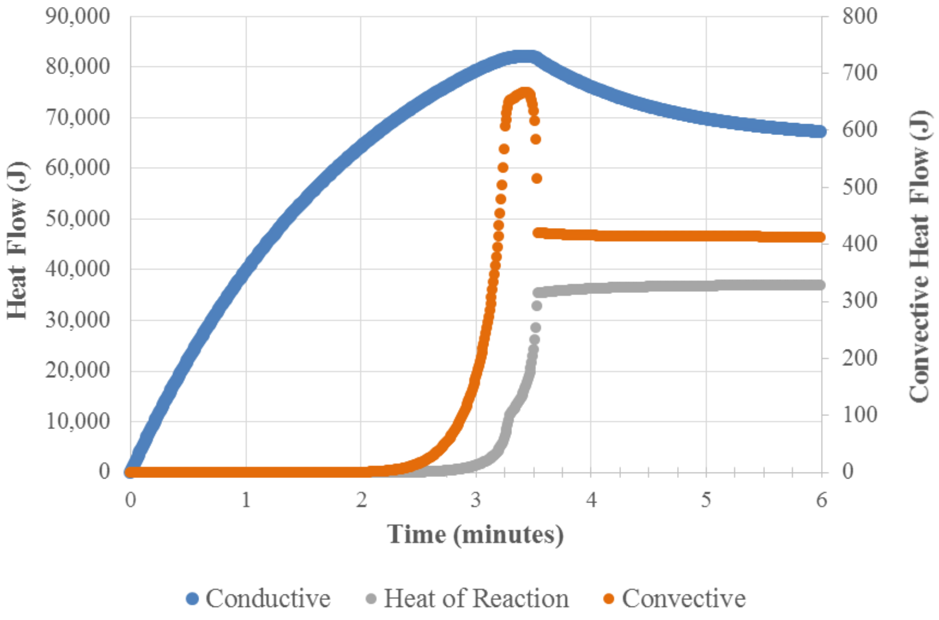

Figure 89. Sources of heat flow during recycling

The overall recycling time is short compared to physical experiments and further analysis of the kinetic parameters needs to be done to help match the model to real composite systems. The kinetic analysis for the resins was conducted with just the resin, not a composite. Adding fibres to the resin is not believed to affect the resin decomposition reactions. Experimentally, performing the resin kinetic analysis on a composite would be tainted by an imperfect measure of fibre mass which would reduce the accuracy of the location of the pyrolysis to char oxidation crossover point. In an effort to slow the model down the activation energies for pyrolysis and char oxidation were increased by 10% for subsequent model use. 10% was chosen as an upper limit of error or poorness of fit for the linear regressions used in Friedman's Method to determine the kinetic reaction constants for the resin. Figure 90 is a temperature distribution of the same composite as Figure 87 but with the pyrolysis and char activation energies increased by 10%.

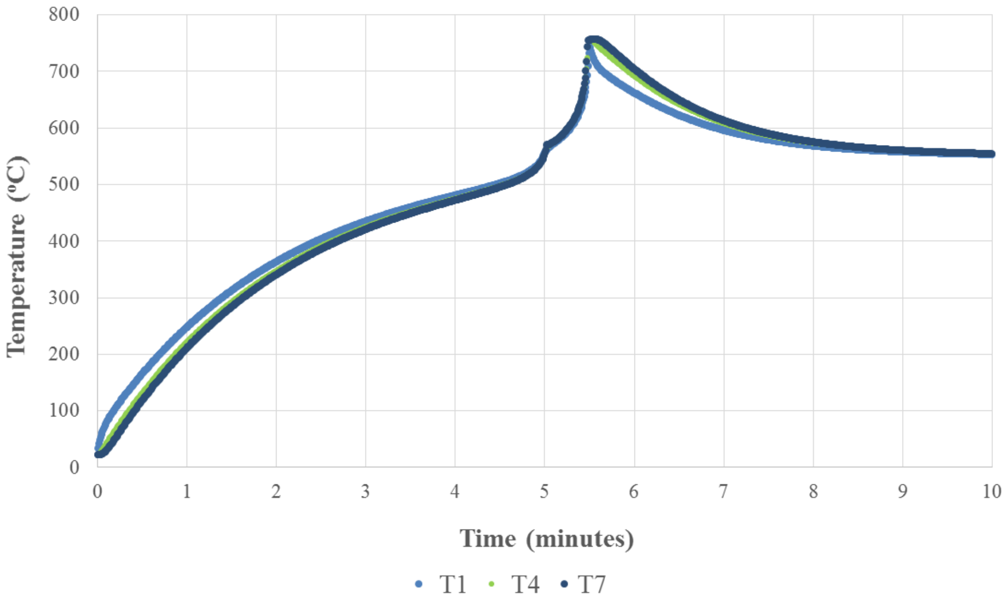

Figure 90. Model temperature distribution in 6 m thick laminate recycled at 550°C with activation energies for pyrolysis and char oxidation increased by 10%

Pyrolysis now takes place over five minutes and the char oxidation time has almost doubled to around 30 s in duration. The temperature in the centre of the composite (layer 7) increases up to 757°C in Figure 90 compared to 724°C in Figure 87. In this scenario the char oxidation stage was delayed until the average temperature in the composite was higher than in Figure 87 due to conduction from the recycling atmosphere, which meant the added heat from char oxidation increased the temperature at the centre of the composite to 757°C.

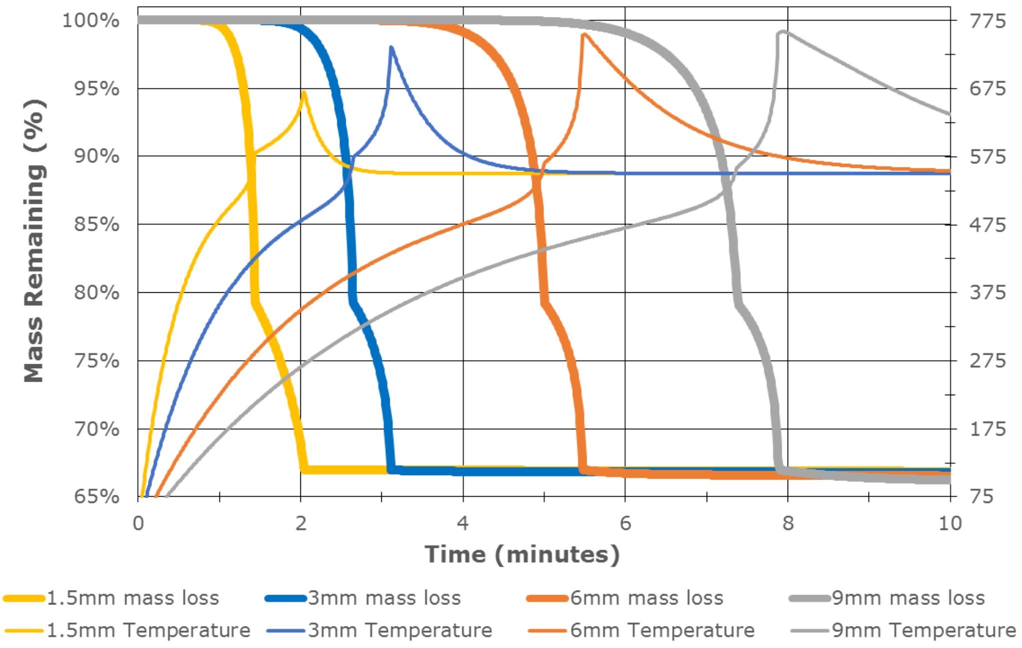

Figure 91. Mass loss over time at 550°C as a function of thickness. Temperature reported from ¼ thickness of composite. (Activation energies for pyrolysis and char oxidation are increased by 10%.)

The model predicts as seen in Figure 91, that more than half of the time of the recycling process results in very little mass loss (<2%). The reaction time of pyrolysis and char oxidation was calculated over a range of thicknesses from 1.5 mm to 9 mm. One concern for thick composites may be the level and uniformity of the oxygen concentration across multiple layers of the composite. This is not a concern during the pyrolysis reaction as it happens in the absence of oxygen anyway. During char oxidation and fibre oxidation this could be a concern. However, since as seen in Figure 88, the difference in how far along in the recycling process each layer is, is practically indistinguishable (albeit at a 6 mm thickness) during char oxidation and fibre oxidation, the concern is minimal. Secondly, the design of experiments shows oxygen concentration is not a significant factor on its own and the differences in oxygen concentration would be smaller than the differences tried in the DOE. Having two adjacent layers in the char oxidation stage at the same time may limit the amount of oxygen getting to the more inner of the two layers. In practice char oxidation is not perfectly uniform and some cracks or holes in the resin structure will develop during the recycling, allowing oxygen to penetrate to the next layer. A way to account for differing oxygen concentration levels for adjacent layers during their char oxidation period may help adjust the char oxidation period to more closely match experimental results. Obviously, once a layer is in the fibre oxidation phase, oxygen is able to fully distribute and penetrate that layer on a macroscopic basis. There may be some limitations to oxygen diffusion between adjacent filaments, but so far this limitation in the model does not appear to be a reason for significant departure from experimental results.

The time spent in the pyrolysis reaction increases with increasing thickness at close to a constant rate. In contrast to pyrolysis the amount of time the char oxidation reaction takes stays within a narrow range as demonstrated by Figure 92. The time depends on the thickness but is not a simple increase with increasing time. Initially, for thickness from 1.5 mm to 4mm the reaction time decreases with increasing thickness. From 4 mm to 6 mm the time increases, from 6 mm to 8 mm the time decreases, and then from 8 mm to 9 mm the time again increases. A decrease in the time spent in the char oxidation phase can be rationalized in that with increasing thickness there is more insulating of the inner layers, causing the temperature of the composite to reach in excess of the recycling operating temperature and thus higher temperatures drive the reaction faster. Evidence of the temperature insulation is seen in Figure 94. The argument for increased reaction time is it takes more time for heat to flow to the centre of the composite.

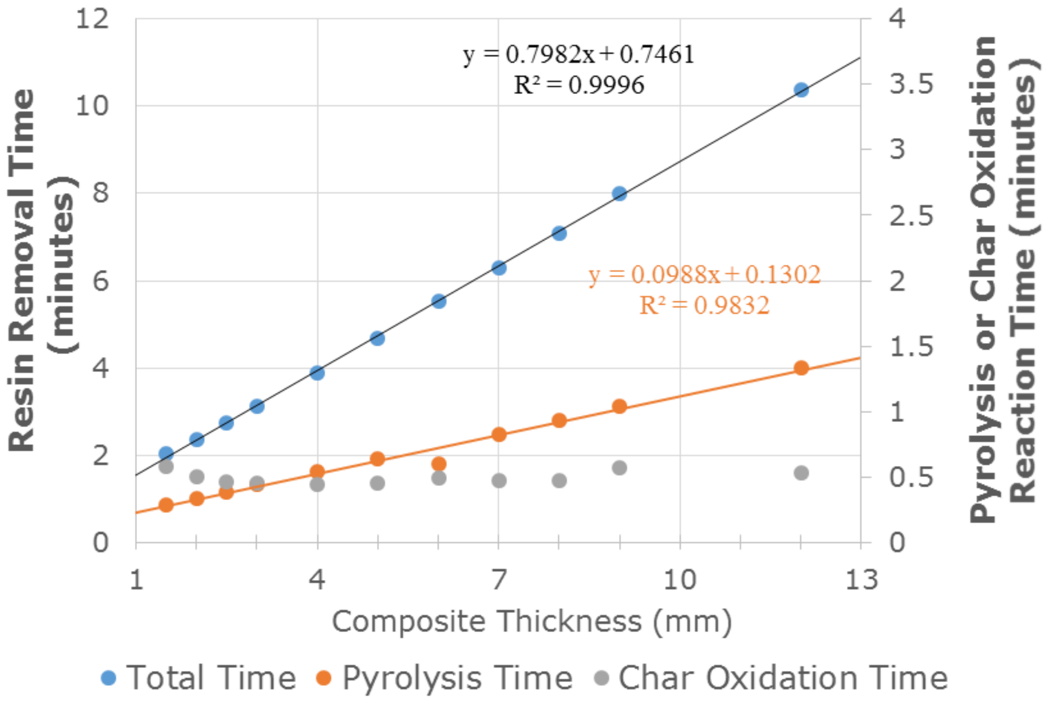

Figure 92. Recycling time as a function of thickness at 550°C. (Activation energies of pyrolysis and char oxidation increased by 10%)

There is competition between thicker composites causing higher temperature which in turn reduces recycling time and thicker composites needing more time to be recycled; sometimes this means the composite will undergo the char oxidation reaction for longer than would be predicted by the temperature insulation argument alone. Figure 93 shows the terms Q1, Q2, and Q3, as defined earlier, for three different thicknesses of composite: 5 mm, 6 mm, and 7 mm. Q1 and Q3 are a measure of the heat added to a layer while Q2 is the removal of heat by the volatiles. A 6 mm thick composite spends more time in char oxidation than a 5 mm composite or a 7 mm composite. Q1, Q2, and Q3 are normalized yet Q2 still increases with increasing thickness and perhaps at a certain thickness the magnitude of Q2 with respect to Q1 and Q3 is enough to slow the char oxidation reaction down.

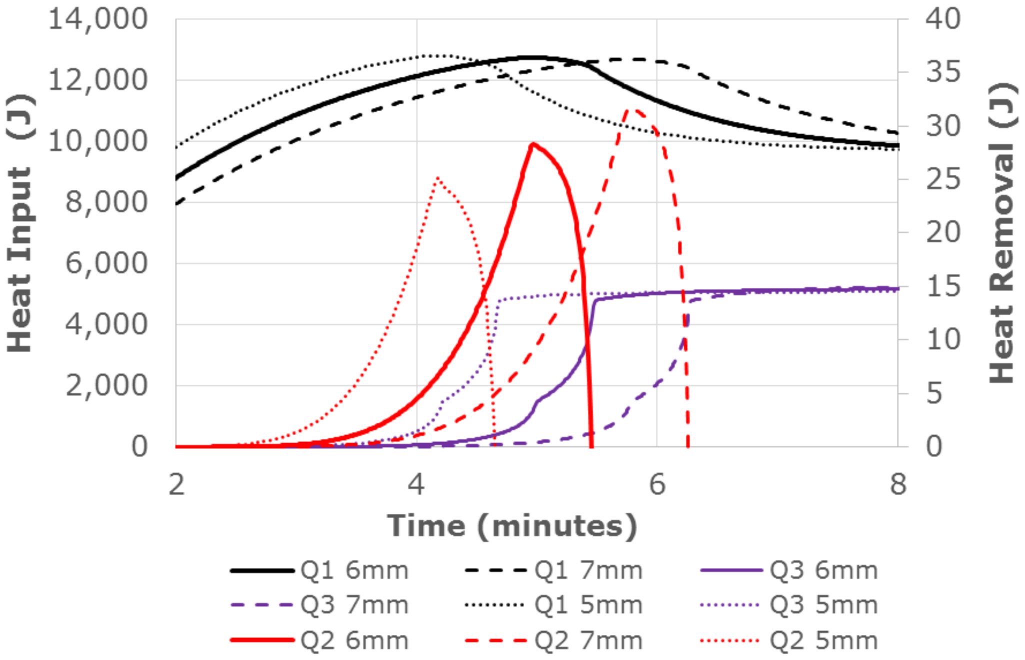

Figure 93. Sources of heat (normalized by thickness of composite)

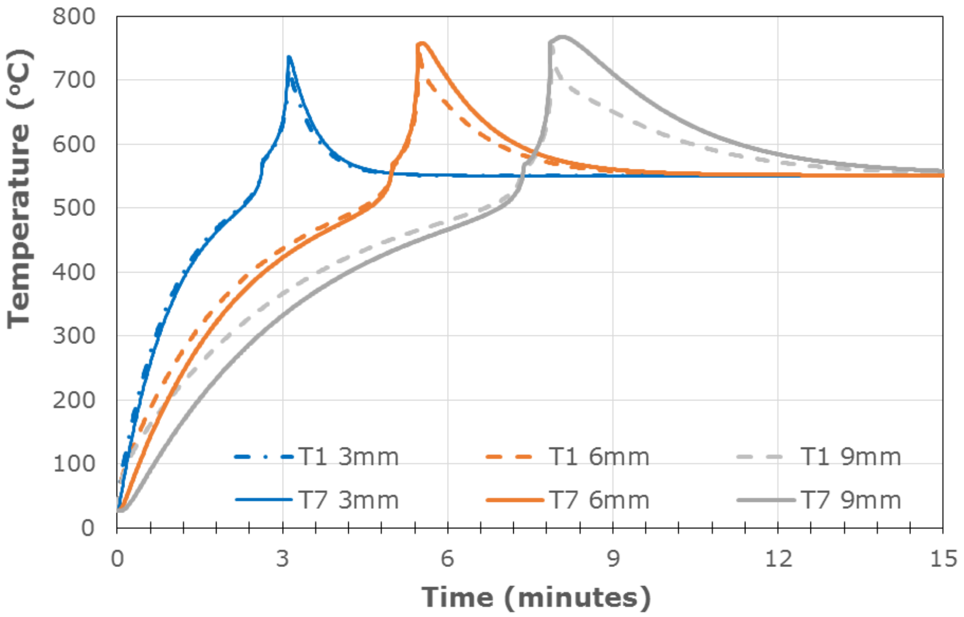

Figure 94. Temperature difference across the thickness (550°C operating temperature)

Figure 94 shows how the thickness affects the temperature distribution inside the composite. As the thickness of the composite increases both the maximum temperature inside the composite increases as does the difference between the outermost layer (T1) and the centre of the composite (T7). The transitions from one stage of recycling to the next are also smoother with increasing composite thickness and this is particularly true for the char oxidation to fibre oxidation transition.

Figure 95 shows for a 6 mm thick composite, the mass loss curves for operating temperatures between 540°C and 600°C. As expected, higher temperatures do make the process run quicker, although at the risk of more fibre damage. In order to remove all the resin from the fibre, the recycling process takes 4.2 minutes at 600°C, 4.7 minutes at 575°C, 5.1 minutes at 560°C, 5.45 minutes at 550°C, and 5.85 minutes at 540°C. The time spent in the char oxidation stage is 0.31 minutes at 600°C, 0.35 minutes at 575°C, 0.40 minutes at 560°C, 0.45 minutes at 550°C and half a minute at 540°C. From 540°C to 550°C and 550°C to 560°C increasing the operating temperature makes the process run faster at 0.05 minutes/10°C, but increasing the temperature above 560°C has diminishing returns.

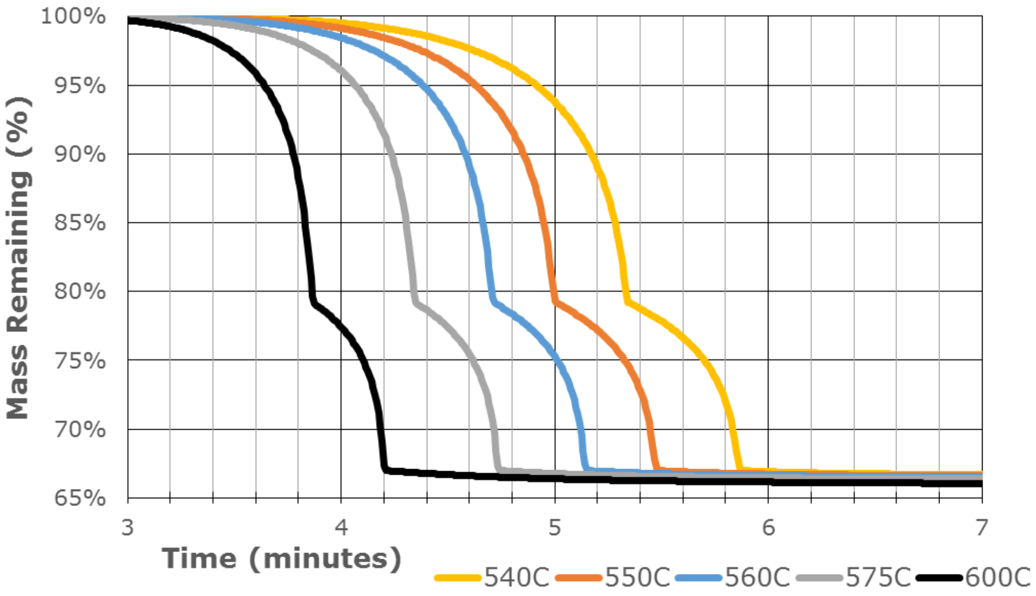

Figure 95. Mass loss rate depending on operating temperature

Given how increasing the pyrolysis activation energy resulted in higher temperatures during char oxidation, in part because the composite had more time to heat up, only increasing the char oxidation activation energy was tried. To best compare it to the experimental TGA data presented in Figure 86, an oven temperature ramp rate of 50°C/min to 550°C was included in the model. The temperature distribution is shown in Figure 96 and the mass loss curve is show in Figure 97. The temperature distribution of the composite appears very similar to how it has been previously, including almost no visible differences in the temperature from layer to layer and a temperature overrun during char oxidation. However the maximum temperature in the composite, which was again measured in the central layer, was 696°C which is less hot than in previous model iterations. Figure 97 is rather dissimilar to the TGA weight loss curve shown in Figure 86; however there are some promising elements of the plot. Overall, the shape of the curve in Figure 97 is much different to that measured by the TGA; for example the model mass loss curve has much more abrupt changes.

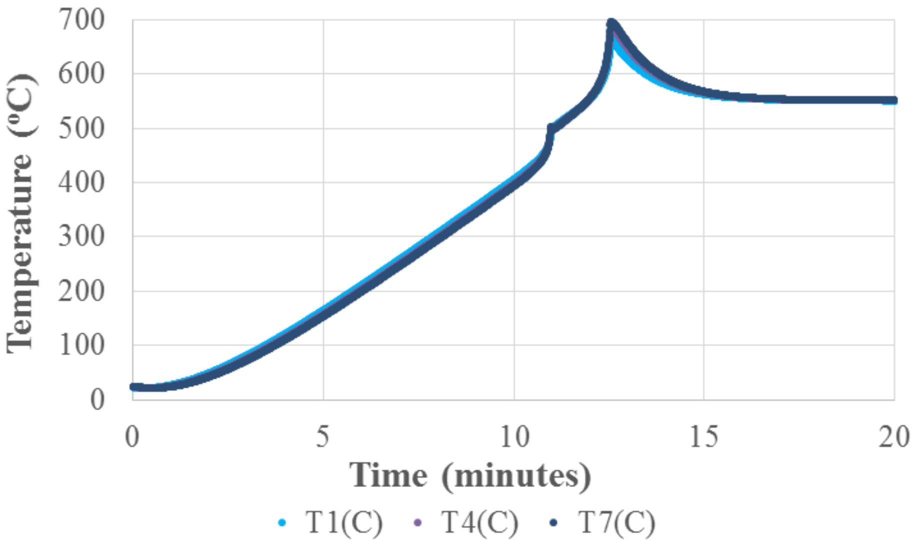

Figure 96. Model temperature distribution in 6 mm thick laminate recycled at 550°C with activation energies for char oxidation increased by 10%

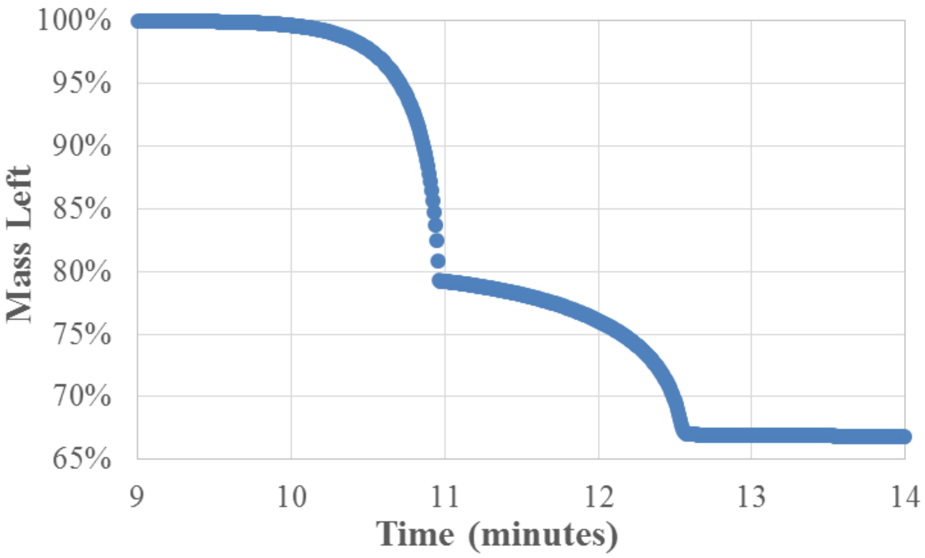

Figure 97. Model mass loss profile for recycling in 550°C with a 50°C/min ramp rate

Also according to the model, noticeable weight loss starts later (around 10 minutes) compared to 8 minutes from the TGA. In the TGA experiment char oxidation finishes at around 14.5 minutes, where as the model predicts it finishing at around 12.5 minutes. Increasing just the char oxidation activation energy by 10% results in both the time spent in pyrolysis and the time spent in char oxidation, increasing beyond the duration they had for an increase in both pyrolysis and char oxidation activation energies. In Figure 97 the pyrolysis time is about 1 minute and the char oxidation time is about 1.5 minutes. From the TGA work, the pyrolysis time is around 2 minutes and the char oxidation time is just under 5 minutes. The model now more accurately reflects that char oxidation takes longer than pyrolysis.

The thermal-kinetic model is a useful tool for considering how a change in the composite or a change in the recycling operating temperature affect each stage of the recycling process and what impact that has on mass loss and temperature distributions. In order to avoid certain temperature ranges or wanting to keep processing times within a given range for each part of the recycling process, the model can be used to make an informed decision over what type of thermal recycling process, to use and how to run it in order to balance productivity with fibre quality. The model has successfully integrated all processes happening during composite recycling, although there is still an opportunity for working on any and all parts of the model to help make the time scales and mass loss profiles more accurately match experimental results.

10 Thermal Modelling Validation

The thermal-kinetic model described in the preceding section is complex and requires the integration of topics from several disciplines. In this chapter the model is broken into smaller components and these components are analysed more thoroughly to prove they work as intended and to assess their accuracy.

10.1 Heat Flow Measurement Experimental Setup

In the thermal-kinetic model there are heat sources from: the recycling environment, chemical reactions within the material, and volatiles escaping from within the composite. At temperatures below the volatilisation temperature of the composite, the heat sources can be simplified to just the external heat from the recycling environment whether it be an oven, furnace, or some form of reactor. From TGA analysis the onset temperature for resin reacting to form char is around 400^{o}C, thus 200^{o}C was chosen as an appropriately low temperature at which to study conduction from the recycling atmosphere, to the outermost layer of the composite and then conduction within the composite laminate. When a cold composite is introduced to a hot recycling atmosphere, a temperature distribution through the thickness of the composite develops. The outer layers of the composite should be hotter than the inner layers. Additionally, the speed at which the temperature of the composite increases is related to the heat transfer coefficient (H_{trans}) and the thermal conductivity (K_c). Both of these parameters need to be measured directly or alternatively derived from a measured temperature distribution through the thickness of a composite as a function of time.

In order to measure this temperature distribution, a laminate with embedded thermocouples was prepared. The laminate used thirty unidirectional prepreg ply layers, to give a total anticipated cured thickness of 6 mm. The prepreg material was BMS8-276 from Toray which is a toughened epoxy resin with T800S carbon fibres. Ten thermocouples were embedded through the thickness of the composite which enabled the measurement of heat flow through the laminate. Table 32 shows the ply layup including where each of the ten thermocouples were placed and how that corresponded to the fourteen layer model written in Java. A schematic of how the thermocouples were laid out in the composite is shown in Figure 98 where the numbers on the left hand side are the thermocouple ID, and the numbers along the bottom are the ID number of the cell based on the thermal-kinetic model. Figure 99 shows the laminate placed in an air circulating oven.

Table 32. Thermocouple Placement

Ply Lay Up	Desired Layer in Model	Calculated Layer in Model	Thickness From Outermost Face (mm)	Thermocouple ID
Px1				
T/C x2	1	0.4669	0.2	1,2
Px6				
T/C	3	3.2667	1.4	3
Px4				
T/C	5	5.1333	2.2	4
Px4				
T/C x2	Centre	Centre	3.0	5,6
Px2				
T/C	6	6.0667	2.6	7
Px5				
T/C	4	3.7333	1.6	8
Px4				
T/C	2	1.8667	0.8	9
Px3				
T/C	1	0.4669	0.2	10
Px1				

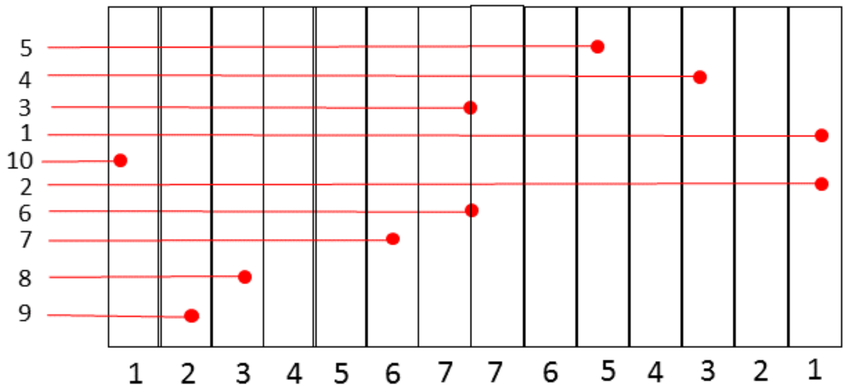

Figure 98. Thermocouple placement in laminate

Figure 99. Setup for heat flow measurements

The laminate pictured in Figure 99 is 250 mm tall by 150 mm wide and 6 mm thick. The thermocouples are embeded to the centre line of the composite to reduce any measurment variation caused by a non uniform temperure profile across the width of the laminate. The thermocouples are distrubuted symetrically through the length of the lamiante but shifted 50 mm to the top to allow room for the vice. The vice was used to position the laminate so that there would be equal air flow (leading to equal heat transfer) on both sides of the laminate. Breather fabric, used in vacuum bagging, was used to insulate the vice from the composite laminate.

In addition to the thermocouples in the laminate two more were used to measure the temperature of the oven. One was placed inside the oven while it heated up and the second was clamped in the vice along with the laminate. The first thermocouple is used to determine when the oven is at a steady temperature and provides a backup reading to the thermocouple held right next to the laminate. A Pico Technologies TC-08 USB thermocouple data logger was used to collect temperature data from eight thermocouples over a period of around twenty minutes. The thermocouples chosen for logging were: layer 1 (bag side), layer 1 (tool side), layer 2, layer 4, layer 6, layer 7 (centre thickness), and the two oven temperature measurements.

10.2 Derivation of Heat Transfer Coefficient and Thermal Conductivity

A simplified version of the thermal-kinetic model was used to model just conduction without any internal reactions and the resulting temperature distribution through the thickness of the laminate. By changing the heat transfer coefficient and thermal conductivity of the composite in the simplified model, the temperature distribution predicted by the model was able to match the temperature measurements from the thermocouples embedded in the laminate. The oven was allowed to preheat to 200°C and then the laminate clamped in a vice was placed in the oven as shown in Figure 99. Figure 100 shows the measured temperature distribution in the composite laminate as well as the oven temperature. Temperatures for intermediate layers between the first and the centre were slightly cooler than layer 1 and the temperature in each subsequent layer was slightly cooler than the previous while the laminate heated up to the oven temperature. By the 14-minute mark in Figure 100, all the layers were measuring ~200°C with layer 1 being slightly hotter; eventually all the layers saturated to a measured temperature of around 206°C within 18 minutes of being placed in the oven.

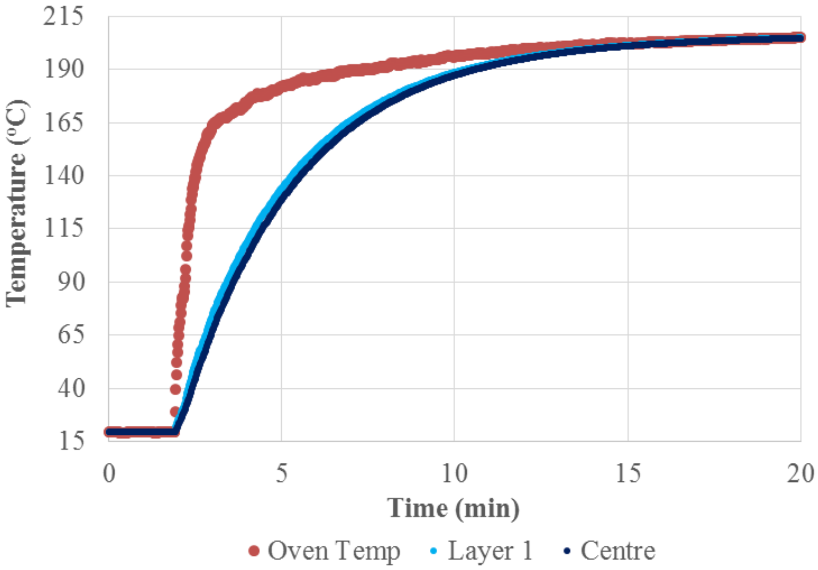

Figure 100. Measured temperature distribution

The oven temperature shown in Figure 100 was taken from the thermocouple clamped in the vice along with the laminate which is why the oven temperature is at room temperature for the first few minutes of the experiment. In the 12-17 minute range the temperature of the layers in the laminate are approaching the oven temperature. After twenty minutes all the layers have reached a homogeneous temperature and it is the same as the oven temperature. In Figure 100 only layer 1 and the centre layer are shown for clarity. Figure 101 takes a closer look at the difference in temperature between layers. As would be expected layer 1 is hotter than layer 2 which is hotter than layer 4 which is hotter than the centre layer. As time increases the difference in temperature between layers decreases. Similarly, as the layers get deeper into the laminate the difference in temperature between one layer and the next decreases. The temperature on each of the layers is very close together which is also consistent with the temperature distribution predicted by the simplified thermal kinetic model shown in Figure 102.

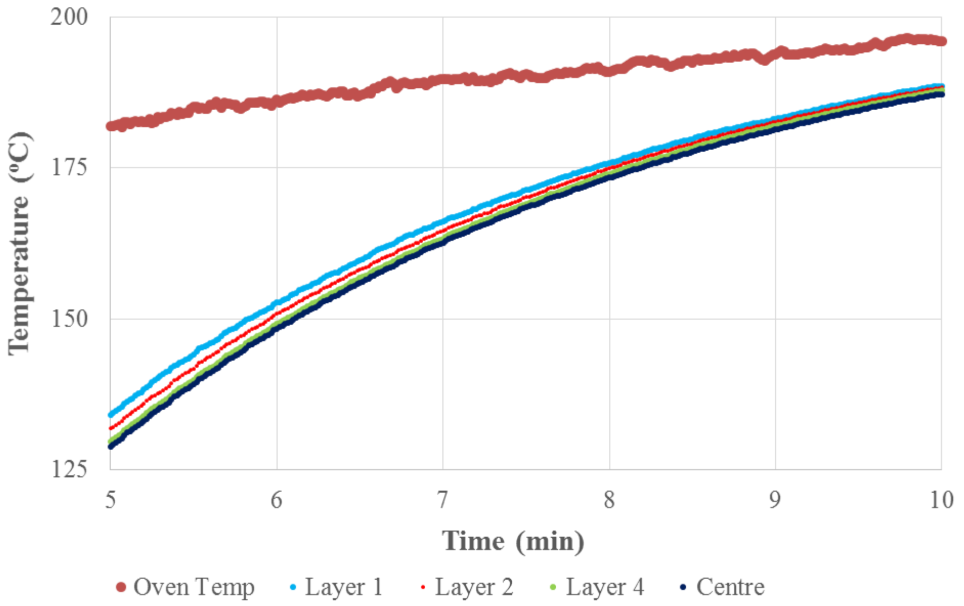

Figure 101. Expanded view of a selection from Figure 100

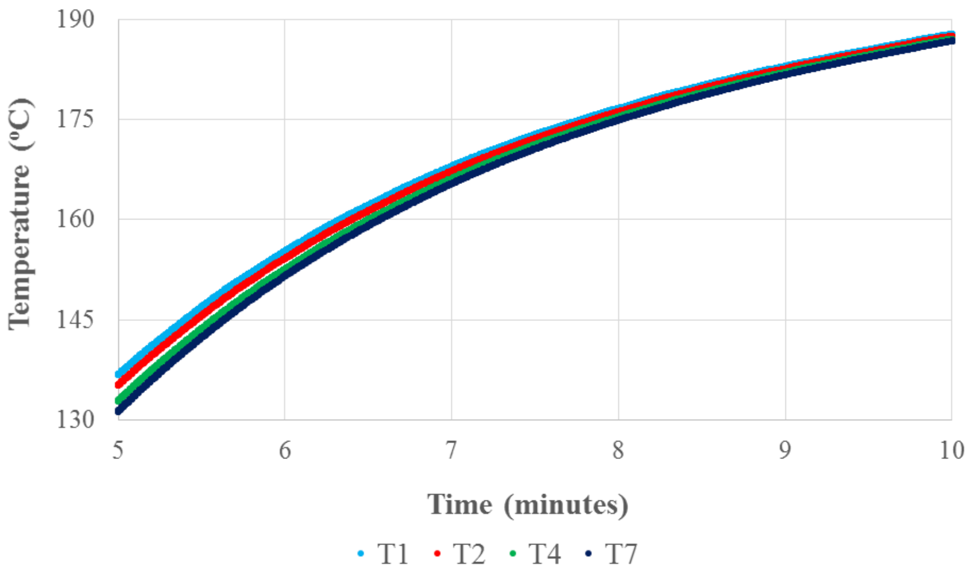

Figure 102. Conduction model temperature distribution

A measure of error of the model is calculated using the sum of squares method across layers 1, 2, 4, 6, and 7. By using the Solver add-in for Excel a non-linear optimization was carried out to find the best values of the heat transfer coefficient and thermal conductivity by minimising the error measurement. Error was expressed as the difference between the measured temperature distribution using the thermocouples embedded in the laminate and the temperature distribution calculated using a simplified version of the thermal kinetic model. In this case the model used the measured oven temperature (thermocouple clamped in vice with the laminate) instead of a constant value. The starting point for the optimisation was a heat transfer coefficient of 50 W/m^2·K and a thermal conductivity of 1 W/m·K. After error minimisation the heat transfer coefficient and thermal conductivity were determined to be 45.5 W/m^2·K and 0.498 W/m·K. The convergence was double-checked by using new starting points slightly above and slightly below these values. In both cases the heat transfer coefficient and thermal conductivity converged back to their originally optimised values. The solver routine used was “GRG Nonlinear” developed by Frontline Solvers [93].

The primary limitation in this methodology is the mismatch in thermocouple positions in the laminate with respect to the layers in the model. For example, as indicated in Table 32, the thermocouple for layer 1 is actually about half a layer away from layer 1 compared to the other thermocouples which are within a quarter layer of their intended position in the laminate. While the thermocouple for layer 1 is the most out of position with respect to the model it is needed to obtain a reliable measurement of the heat transfer coefficient. Table 33 shows that without including layer 1 in the error minimisation procedure the heat transfer coefficient decreases and the thermal conductivity increases to the maximum allowed by the constraints put on the error optimisation.

Table 33. Influence of excluding a given layer from h and k calculations

Total Error	***h* (W/m^{2}K)**	***k* (W/m-K)**	**Constraints**
10.5	45.5	0.498	None
8.87	45.5	0.498	layer 1 removed from total error summation[1]
8.72	44.74	0.600	$40<h<60$; $0.4<k<0.6$ Exclude layer 1
8.57	43.8	0.800	$35< h <55$; $0.35< k <0.8$ Exclude layer 1
8.45	42.6	2.00	$25< h <55$; $0.35< k <2$ Exclude layer 1
8.60	45.2	0.570	$25< h <55$; $0.35< k <1$ Exclude layer 2
8.30	45.6	0.484	$25< h <55$; $0.35< k <1$ Exclude layer 4

[1] *h* and *k* taken from above optimisation, but layer 1 removed from the total error summation

In the optimisation procedure there is also a trade-off between selecting the thermocouple positions that best match the model and having more data points over which to compute the heat transfer coefficient and thermal conductivity. Excluding layer 2 from the sum of squares error calculation results in a small change to the heat transfer coefficient but a large change in thermal conductivity. Without layer 2 there is a large distance between the first layer and the next layer used in the error minimisation procedure. Without layer 4 there is an even larger distance but because the gap is deeper in the laminate the overall effect is smaller. Layer 2 may have a stronger influence on the heat transfer coefficient than layer 4 since it closer to the surface of the laminate. The thermocouple for layer 4 is the second furthest out of place (Table 32) and by excluding it from the error minimisation routine, the overall error calculation was minimised while keeping the values for heat transfer coefficient and thermal conductivity close to the values determined using all layers. The values for heat transfer coefficient and thermal conductivity used in the thermal kinetic model are the average of the first and last entries in Table 33 and were previously listed in Table 29.

10.3 Conduction Validation

To verify the model correctly computes heat transfer, values for oven temperature and centre point temperature were compared to a Heisler chart for inverse Biot numbers of 5 and 10. A Biot number is a dimensionless indicator of the quality of the heat transfer coefficient. Mathematically the Biot number is

$$Bi = \frac{hL}{k} \qquad (27)$$

where h is the heat transfer coefficient, L, is the half thickness of the solid body, and k is the thermal conductivity of the solid body [94]. Biot numbers much greater than 1 indicate a very high heat transfer such that the outermost layer of the solid body approaches the temperature of the thermal fluid the solid body is in contact with. Heisler charts show the temperature at the midplane of a plate as a function of time [94]. The conditions for which Heisler charts are valid are: for an infinitely long plate, no internal heat generation (or consumption), the surroundings must be at a constant temperature, the heat transfer coefficient must be constant within the temperature regime considered, and the solid body must be at an initial uniform temperature. Heisler charts have multiple traces, one for each inverse Biot number (Bi^{-1}). To accurately read off midplane temperatures and time from a Heisler chart (such as the one shown as Figure 103), inverse Biot numbers of 5 and 10 were chosen. On the X-axis of Heisler charts, dimensionless time is represented by the Fourier Number. The Fourier Number is the ratio of heat transport rate to heat storage rate and is defined as equation 28 where α is thermal diffusivity in m^2/s, t is time in seconds, and L is the conduction length in meters. Thermal diffusivity is related to thermal conductivity as per equation 29.

$$F_o = \frac{\alpha t}{L^2} \tag{28}$$

$$\alpha = \frac{k}{c_p \rho} \tag{29}$$

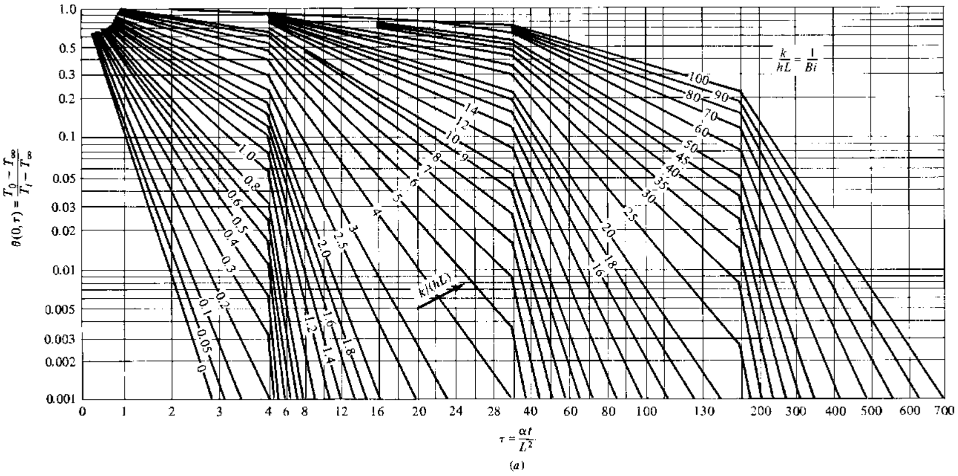

Figure 103. Heisler Chart for infinite plate [95]

To satisfy equation 27 for an inverse Biot number of 5 and a conduction length of 3 cm the heat transfer coefficient was taken as 60 $W/m^2 \cdot K$ and thermal conductivity was taken as 0.9 $W/m \cdot K$. For an inverse Biot number of 10 the heat transfer coefficient was taken as 30 $W/m^2 \cdot K$ and thermal conductivity was taken as 0.9 $W/m \cdot K$. Although the values for thermal conductivity and heat transfer coefficient are not the exact values measured for the BMS8-276 materials system, they are order of magnitude correct and result in inverse Biot numbers close to the actual value of 3.59. The model was compared to three time/temperature points taken on each inverse Biot number line. For an inverse Biot number of 5 and Fourier numbers of 18, 13, and 3.8 midplane temperature ratios were expected to be 0.035, 0.09, and 0.5. As shown in Table 35 the model is slightly fast (higher temperatures) compared to Figure 103. Some error could be from the limit of the resolution of picking out the exact expected values of the Heisler chart. Another way of determining the values of the Heisler chart is by computing the first six elements in the infinite series:

$$\frac{T(x,t)-\mathrm{T}_\infty}{T_i-\mathrm{T}_\infty}=2\sum_{n=1}^{\infty}\frac{\sin(a_n)}{a_n+\sin(a_n)\cos(a_n)}\cos\left(a_n\frac{x}{L}\right)\exp\left(-a_n^2\frac{\alpha t}{L^2}\right) \tag{29}$$

Table 34. First six roots of Equation 29[1]

β_i	a_1	a_2	a_3	a_4	a_5	a_6
0.1	0.3111	3.1731	6.2991	9.4354	12.5743	15.7143

[1] adopted from Ref. [94]

Table 35. Comparison of thermal conduction results

Heisler Plot		**Model**		**Heisler Plot**		**Model**	
β_i^{-1}=5				β_i^{-1}=10			
Fo	$\frac{T-T_\infty}{T_o-T_\infty}$	**Fo**	$\frac{T-T_\infty}{T_o-T_\infty}$	**Fo**	$\frac{T-T_\infty}{T_o-T_\infty}$	**Fo**	$\frac{T-T_\infty}{T_o-T_\infty}$
18	0.035	18	0.0339	20	0.15	20	0.145
		17.825	0.035			19.640	0.150
13	0.09	13	0.087	17	0.2	17	0.194
		12.848	0.090			16.684	0.20
3.8	0.5	3.8	0.501	10	0.4	10	0.384
						9.569	0.4

This comparison for an inverse Biot number of 10 is shown in Figure 104. The “Model” values were taken from the temperature values in layer 4 by computing the result of the term on the left hand side of equation 29 using T_t as the layer temperature at each time, T_i as the initial temperature, and T_∞ as the oven temperature which was set to 200ºC. A comparison for an inverse Biot number other than 10 was not possible as the roots to equation 29 for an inverse Biot number other than 10 were not available. Figure 104 also shows the model running slightly faster than expected based on the Heisler plot. However the error seems minimal.

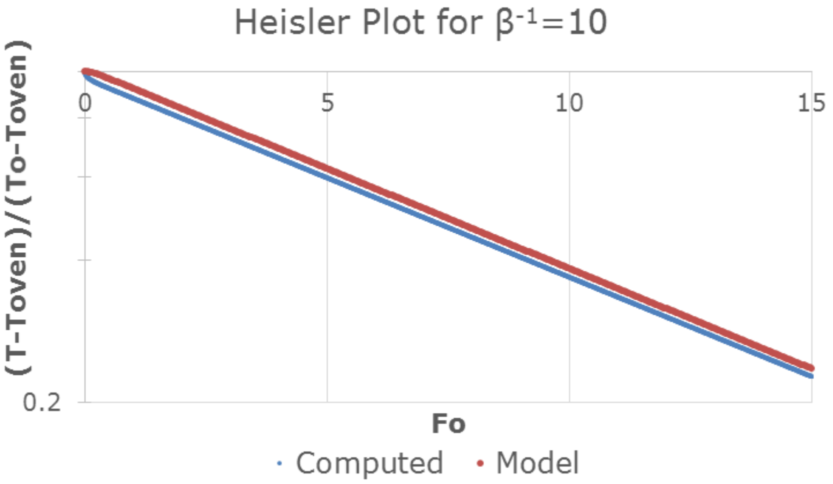

Figure 104. Heisler plot reconstruction to verify heat flow

11 Conclusions

A novel approach to studying carbon fibre recycling has been presented. The three most important elements are the microstructural analysis, the single fibre tensile test data, and the development of a thermal-kinetic model for simulating carbon fibre composite recycling.

The O/C ratio measured from XPS did not appear to reliably predict the severity of the recycling method. Deconvoluting the C1s and O1s peaks may reveal additional details. Alternatively, the use of contact angle measurement could provide an indication of fibre oxidation.

The microstructural analysis demonstrated the successful application of Raman and XRD techniques to recycled carbon fibres. Unfortunately these analyses were not conclusive enough to demonstrate a change in the fibre microstructure as a result of the recycling process. A larger data set of all the fibres used in this study, not just the T700 fibres, may show a more definitive correlation. Different Raman and X-ray equipment specifically designed for fibres or physically small samples may also increase the precision of the method to a point where differences between samples are significant. BET would be a useful method to determine if and how the surface of the fibres had become rougher or if voids inside the material had developed as a result of the recycling. Use of Krypton adsorption and a reliable BET machine is the clear path forward from the erratic results presented in this study. The use of TEM to investigate points of tensile failure could also be extremely useful in determining factors that control the strength of a recycled carbon fibre. Using TEM to measure local microstructure like d-spacing and crystal size would provide definitive evidence as to if recycling changes the structure of the fibre. Thicker cross-sections and stiffer embedding media will hopefully improve the sample preparation which in turn will be instrumental in improving the quality of the micrographs.

Mechanical testing using the large sample size and data reduction procedures developed for this work proved quite successful. High coefficient of variation for tensile data made most samples not statistically different from each other. Always testing enough samples so that 60^{+} results are included in the analysis may prove beneficial. Further work using the 3-parameter Weibull distribution or different ranking methods may also be a way of increasing the confidence of the test result. Compliance is a large part of the elastic modulus calculation. Efforts to lower the system compliance and to understand why there is so much variation from sample to sample would go a long way towards improving the SFTT technique.

Factorial models from the ANOVA were fit to the tensile strength and elastic modulus data sets. While the predictive power of these models was poor they were still extremely useful in identifying important interactions between factors. Tensile strength retention was usually around 90% for fibres recycled at 550^{o}C and at hotter temperatures there is an obvious drop in tensile strength. Fibres that are more resistant to oxidation do not show a significant drop until 650^{o}C; whereas fibres like Hexcel IM7 and AS4 show a small but significant drop in strength at 600^{o}C and are nearly destroyed at 650^{o}C. The Hexcel fibres are a good example of why the interaction between temperature and oxygen concentration is important but may not be significant until another factor, such as manufacturer, is considered. When considered in smaller data sets grouped by fibre type or by manufacturer, Pareto plots from the ANOVA analysis were able to show the recycling process affects different fibres differently. Therefore keeping track of composite pedigree and separating waste accordingly will allow recycled material to be of a higher quality and value.

A thermal-kinetic model for carbon fibre composite recycling has been developed with a very strong dependence on the kinetic characterisation of the resin system. The model is also highly customisable so it may be adapted to suit the material being recycled and the process itself. The mass loss profiles generated from the model are faster than those obtained from TGA. TGA may not be the most representative method to measure weight loss during recycling, rather recycling full thickness samples in a furnace and pulling them out at time intervals would be more appropriate. Some improvement in matching time scales was achieved by increasing the activation energy for the char oxidation reaction. Further review of the reaction kinetics for MTM 44 resin system needs to be conducted. Similarly, characterisation of the BMS8-276 resin system or another high Tg resin system should be pursued to see how much the difference in kinetic parameters changes the temperature distribution and weight loss profiles of the model. There may also be some differences in how well Friedman's method works under the range of heating rates used during TGA versus heating conditions during carbon fibre recycling, especially during char oxidation. Further work with the model could focus on the heat transfer of loose fibre bundles during fibre oxidation and fibre bundles during char oxidation. During char oxidation the fibre bundles are getting progressively more like loose fibre bundles and this may have significant implication on the reaction rate.

With respect to the fluidised bed; the model will be used to explore the effect on recycling time of different resins, thicknesses of composite, and operating temperatures. Optimisation of these parameters could also be pursued along with their eventual verification by using the same parameters on the actual fluidised bed setup. Expanding the model to 2D would allow the exploration of aspect ratio as a factor and if the size reduction process to prepare feed material for the fluidised bed needs to produce composite fragments within a certain aspect ratio range.

Writing the model in Java allows for future expansion and modification of the model without significant work to the framework of the model and also provides a platform where the model could easily be turned into an executable application to run on any machine.

Bibliography

[1] The European Parliment and the Council of the European Union: End of life vehicle (ELV); directive 2000/53/EC, September 2000.
[2] The European Parliment and the Council of the European Union: On the landfill of waste; directive 1999/31/EC, April 1999.
[3] S. Pimenta, S.T. Pinho, Environmental Implications of Alternative Materials in Construction and Treatment of Waste 31 (2011) 378-392.
[4] S.J. Pickering, Composites Part A-Applied Science and Manufacturing 37 (2006) 1206-1215.
[5] J.-M. Gosau, Recovering carbon fibre and more from scrap composite material, Carbon Fibre Recycling & Reuse Developing a supply chain for waste CFRP, Pira International/IntertechPira, Hamburg, Germany, 2009.
[6] ELG Carbon Fibre Ltd., Carbiso MF Data Sheet.
[7] K. Jiamjiroch, Developments of a Fludised Bed Process for the Recycling of Carbon Fibre Composites, Department of Mechanical, Materials, and Manufacturing Engineering, vol PhD, University of Nottingham, 2012.
[8] H.L.H. Yip, S.J. Pickering, C.D. Rudd, Plastics Rubber and Composites 31 (2002) 278-282.
[9] L.O. Meyer, K. Schulte, E. Grove-Nielsen, Journal of Composite Materials 43 (2009) 1121-1132.
[10] J.-M. Gosau, T.F. Wesley, R.E. Allred, Integrated composite recycling process, 38th SAMPE Fall Technical Conference: Global Advances in Materials and Process Engineering, Society for the Advancement of Material and Process Engineering, Dallas, TX, United states, 2006.
[11] C.A. Leon y Leon, X. Zhou, Carbon Fiber Mechanical Properties: Reconciling Models & Experiments, 2nd Innovative International Composites Summit, Paris, France, 2011.
[12] P. Bajpai, Update on Carbon Fibre, Smithers Rapra, Shawbury, Shrewsbury, Shropshire, SY4 4NR, United Kingdom, 2013.
[13] Toray Carbon Fibers America, Standard Modulus Carbon Fibers, 2008.
[14] Umeco Strucutural Materials, Umeco MTM 44-1 Matrix Resin, 2012, p. 7.
[15] Umeco Strucutural Materials, Umeco MTM 57 Series Prepreg System, 2012, p. 6.
[16] M.G. Northolt, L.H. Veldhuizen, H. Jansen, Carbon 29 (1991) 1267-1279.
[17] Nippon Graphite Industries, Graphite Characteristics- Crystal Structure, vol 2015, 2000.
[18] K. Smith, Carbon Fiber - From and Industrial Developer's Viewpoint, *Advanced Materials and Processes: Enabling the Future* 42nd International SAMPE Technical Conference, Society for the Advancement of Materials and Process Engineering, Salt Lake City, Utah, 2010.
[19] D.J. Johnson, Journal of Physics D: Applied Physics 20 (1987) 286.
[20] H. Kobayashi, Toray's Advanced Materials: Innovation by Chemistry, Toray Advanced Materials Symposium, 2006.
[21] J. Gregr, The Complete List of Commercial Carbon Fibres, 7th International Conference Textile Science 2010, Liberec, Czech Republic, 2010.
[22] Toray Carbon Fibre America, Quality Carbon Fibre: typical fibre properties, 2006, p. 2.

[23] E. Fitzer, M. Heine, carbon fiber manufacture and surface treatment, in: A.R. Bunsell (Ed.) Fiber Reinforcements for Composite Materials, Elsevier, Amsterdam, 1988.
[24] D.D.L. Chung, Carbon Fiber Composites, Butterworth-Heinemann, 1994.
[25] R.E. Reed-Hill, R. Abbaschian, Chapter 22 Fracture Mechanics, in: J. Plant, M. Thomas (Eds.), PhysicalMetallurgy Principals, vol 3, PWS Publishing Company, Bostonm, Ma, 1994, p. 772.
[26] W.N. Reynolds, R. Moreton, Philosophical Transactions of the Royal Society A: Mathematical, Physical & Engineering Sciences 294 (1980) 11.
[27] W.N. Reynolds, J.V. Sharp, Carbon 12 (1974) 103.
[28] D.J. Johnson, C. Frank, Philosophical Transactions of the Royal Society of London.Series A, Mathematical and Physical Sciences 294 (1980) 443.
[29] S.C. Bennett, D.J. Johnson, W. Johnson, Journal of Materials Science 18 (1983) 3337-3347.
[30] M.A. Janney, W.L. Newell, E. Geiger, N. Baitcher, T. Gunder, Manufacturing complex geometry composites with recycled carbon fiber, Spring Symposium Conference Proceedings: Changing Times. New Opportunities. Are You Prepared?, Soc. for the Advancement of Material and Process Engineering, Baltimore, MD, United States., 2009
[31] M. Mauhar, M. Janney, U. Vaidya, R. Johnson, Thermoplastic composites for transportation applications from recycled carbon fiber, Baltimore, MD, 2012.
[32] J. Davidson, P. Roy, Recycling Carbon Fibre, in: L. Milled Carbon (Ed.) Great Britian, 2009.
[33] S.H. Alsop, Pyrolysis off-gas processing, SAMPE 2009 Technical Conference Proceedings: Changing Times. New Opportunities. Are You Ready?, Soc. for the Advancement of Material and Process Engineering, Baltimore, MD, United states.
[34] G. Gardiner, Recycled Carbon Fiber Update: Closing the CFRP Lifecycle Loop, Composites Technology, vol December 2014, 2014.
[35] M.A. Janney, Recycled Carbon Fiber: Applications in Automotive and Other Industries, CAMX 2014: Combined Strength. Unsurpassed Innovation, CAMX – The Composites and Advanced Materials Expo, Orlando, Florida, 2014.
[36] K. Wood, Carbon Fiber Reclamation: Going Commercial, High Performance Composites, March 2010,.
[37] P.E. George, K. Hurley, Challenges To Successful Implementation of Composites Recycling and Suggested Solutions, CAMX 2014: Combined Strength. Unsurpassed Innovation, CAMX- The Composites and Advanced Materials Expo, Orlando, Florida, 2014, p. 13.
[38] B.E. Allen, M.L. Connor, J.P. Heil, J.J. Cuomo, P.E. George, W.L. Carberry, Recycled Carbon Fiber Analysis: Morphological and Chemical Characterization, Proceedings of the 38th SAMPE International Technical Conference, SAMPE, Dallas, TX, 2006, p. 15.
[39] M.L. Connor, J.P. Heil, J.J. Cuomo, P.E. George, W.L. Carberry, Recycled carbon fiber analysis: Mechanical properties, 38th SAMPE Fall Technical Conference: Global Advances in Materials and Process Engineering, Society. for the Advancement of Material and Process Engineering, Dallas, TX, 2006, p. 9.
[40] J.P. Heil, M.J. Hall, D.R. Litzenberger, R. Clearfield, J.J. Cuomo, P.E. George, W.L. Carberry, A comparison of chemical, morphological, and mechanical properties of various recycled carbon fibers, SAMPE 2009 Technical Conference Proceedings: Changing Times. New Opportunities. Are You Ready?, Society for the

Advancement of Material and Process Engineering, Baltimore, MD, United states, 2009, p. 17.
[41] J.P. Heil, D.R. Litzenberger, J.J. Cuomo, A Comparison of Chemical, Morphological, and Mechanical Properties of Carbon Fibers Recovered From Commercial Recycling Facilities, SAMPE 2010 Technical Conference Proceedings New Materials and Processes for a New Economy, Society for the Advancement of Material and Process Engineering, Seattle, Wa, 2010, p. 15.
[42] J.P. Heil, J.B. Gavin, P.E. George, J.J. Cuomo, Composite Panels made From the Wetlay Process Using Recycled Carbon Fiber, SAMPE 2011 Technical Conference Procedings: *State of the Industry: Advanced Materials, Applications, and Processing Technology*, Society for the Advancement of Material and Process Engineering, Long Beach, Ca, 2011, p. 15.
[43] G. Jiang, S.J. Pickering, G.S. Walker, K.H. Wong, C.D. Rudd, Applied Surface Science 254 (2008) 2588-2593.
[44] G. Jiang, S.J. Pickering, E.H. Lester, T.A. Turner, K.H. Wong, N.A. Warrior, Composites Science and Technology 69 (2009) 192-198.
[45] R. Piñero-Hernanz, J. García-Serna, C. Dodds, J. Hyde, M. Poliakoff, M.J. Cocero, S. Kingman, S.J. Pickering, E. Lester, The Journal of Supercritical Fluids 46 (2008) 83-92.
[46] R. Pinero-Hernanz, C. Dodds, J. Hyde, J. Garcia-Serna, M. Poliakoff, E. Lester, M.J. Cocero, S. Kingman, S. Pickering, K.H. Wong, Composites Part A: Applied Science and Manufacturing 39 (2008) 454-461.
[47] T.A. Turner, N.A. Warrior, S.J. Pickering, Plastics Rubber and Composites 39 (2010) 151-156.
[48] T.A. Turner, S.J. Pickering, N.A. Warrior, Composites Part B: Engineering 42 (2011) 517.
[49] K.H. Wong, G. Jiang, S.J. Pickering, C.D. Rudd, G.S. Walker, Characterisation of recycled carbon fibre: Mechanical properties and surface chemistry, 38th SAMPE Fall Technical Conference: Global Advances in Materials and Process Engineering, Society for the Advancement of Material and Process Engineering, p. 10.
[50] K.H. Wong, S.J. Pickering, T.A. Turner, N.A. Warrior, Compression moulding of a recycled carbon fibre reinforced epoxy composite, SAMPE '09 Spring Symposium Conference Proceedings, vol 54, Society for the Advancement of Material and Process Engineering, Baltimore, MD, United States
[51] S. Pimenta, R. Gutkin, S.T. Pinho, P. Robinson, Composites Science and Technology 69 (2009) 948-955.
[52] S. Pimenta, R. Gutkin, S.T. Pinho, P. Robinson, Composites Science and Technology 69 (2009) 956-964.
[53] S. Pimenta, S.T. Pinho, P. Robinson, K.H. Wong, S.J. Pickering, Composites Science and Technology 70 (2010) 1713-1725.
[54] M.E. Otheguy, A.G. Gibson, E. Findon, R.M. Cripps, A. Ochoa Mendoza, M.T. Aguinaco Castro, Plastics Rubber and Composites 38 (2009) 406-411.
[55] M. Szpieg, M. Wysocki, L.E. Asp, Plastics Rubber and Composites 38 (2009) 419-425.
[56] R.E. Allred, J.M. Gosau, J.M. Shoemaker, Recycling process for carbon/epoxy composites, 46th International SAMPE Symposium and Exhibition 2001: a Materials and Processes Odyssey, Soc. for the Advancement of Material and Process Engineering, Long Beach, CA, United states, pp. 179-192.
[57] J.-M. Gosau, T.F. Wesley, R.E. Allred, Integrated composite recycling process, 38th SAMPE Fall Technical Conference: Global Advances in Materials and Process

Engineering, vol Dallas, TX, Soc. for the Advancement of Material and Process Engineering, Dallas, TX, United states.
[58] J.-M. Gosau, State-of-the-Art 2nd Generation Aircraft Composites, SAMPE 2009 Technical Conference Proceedings: Changing Times. New Opportunities. Are You Ready?, Society for the Advancement of Material and Process Engineering, Baltimore, MD, 2009.
[59] V.P. McConnell, Reinforced Plastics 54 (2010) 33-37.
[60] Horiba Scientific, Raman Academy, vol 2013.
[61] F. Tuinstra, J.L. Koenig, The Journal of Chemical Physics 53 (1970) 1126-1130.
[62] A. Cuesta, P. Dhamelincourt, J. Laureyns, A. Martínez-Alonso, J.M.D. Tascón, Carbon 32 (1994) 1523-1532.
[63] A.C. Ferrari, J. Robertson, Physical Review B 61 (2000) 14095-14107.
[64] F. Tuinstra, J.L. Koenig, Journal of Composite Materials 4 (1970) 492-499.
[65] B.E. Warren, Physical Review 59 (1941) 693-698.
[66] M. Minus, S. Kumar, JOM 57 (2005) 52-58.
[67] R.B. Abernethy, The new Weibull handbook, R.B. Abernethy; Distributed by Gulf Pub. Co, North Palm Beach, Fla.; Houston, 1996.
[68] W. Weibull, Journal of Applied Mechanics-Transactions of the ASME 18 (1951) 293-297.
[69] B. Dodson, The Weibull analysis handbook, ASQ Quality Press, Milwaukee, Wis., 2006.
[70] H.L. Friedman, Journal of Polymer Science Part C: Polymer Symposia 6 (1964) 183-195.
[71] Y. Yin, J.G.P. Binner, T.E. Cross, S.J. Marshall, Journal of Materials Science 29 (1994) 2250-2254.
[72] S. Brunauer, P.H. Emmett, E. Teller, Journal of the American Chemical Society 60 (1938) 309-319.
[73] Quantachomre Instruments, Automated Software Assistant for the Proper Calculation of BET Area of Microporous Materials, Powder Tech Note, p. 4.
[74] N. Leddy, Surface Area and Porosity, Centre for Microscopy and Analysis, 2012.
[75] Quantachomre Instruments. , Low Surface Area Analysis by Krypton Adsorption at 77.4K, Powder Tech Note, p. 2.
[76] A. Deurbergue, A. Oberlin, Carbon 30 (1992) 981-987.
[77] Toray Carbon Fibers America, T800S Data Sheet, vol CFA-019, Toray Carbon Fibers America, Inc., Santa Anna, California, 2010.
[78] Toray Carbon Fibers America, T700S, Technical Data Sheet, 2010.
[79] Toray Carbon Fibers America, T600S Data Sheet, Technical Data Sheet, 2006.
[80] Toray Carbon Fibers America, M46J Data Sheet, Technical Data Sheet, 2010, p. 2.
[81] Hexcel Corporation, HexTow AS4 Carbon Fiber Product Data, Hexcel Corporation, Stamford, Connecticut, 2010.
[82] Hexcel Corporation. , HexTow IM7 Carbon Fiber Product Data, Hexcel Corporation, Stamford, Connecticut, 2010.
[83] Mitsubishi Chemical America , Dialead K1392U, Coal Tar Pitch-Based Carbon Fibres, 2010, p. 1.
[84] J. Davidson, P. Roy, Recycling Carbon Fibre, Great Britian, 2009, p. 18.
[85] A. Sleeper, Minitab Demystified, The McGraw-Hill Companies Inc., 2012.

[86] I.T. Laboratory, Tukey's method, Engineering Statistics Handbook, Information Technology Laboratory.
[87] A.J. Gao, S. Luo, X.Q. Wang, Y. Lan, L.H. Xu, Cailiao Kexue yu Gongyi/Material Science and Technology 20 (2012) 135-138+143.
[88] P. Morgan, Carbon Fibers and Their Composites, CRC Press, 2005, p. 1200.
[89] J.B. Henderson, J.A. Wiebelt, M.R. Tant, Journal of Composite Materials 19 (1985) 579-595.
[90] M.W. Chase Jr., Journal of Physical Chemistry Ref. Data, Monograph 9 (1998) 1-1951.
[91] Toray Carbon Fibre America. , T800H Data Sheet, Technical Data Sheet, 2010, p. 2.
[92] J.B. Henderson, M.R. Tant, G.R. Moore, J.A. Wiebelt, Thermochimica Acta 44 (1981) 253-264.
[93] F. Solvers, Excel Solver Help.
[94] A. Bejan, Heat Transfer, John Wiley & Sons, Inc., 1993.
[95] M.N. Ozisik, Heat Conduction, in: Figure 2A p. 92-93, (Ed.) John Wiley & Sons, In, 1993.
[96] J.L. Thomason, Composites Science and Technology 77 (2013) 74-80.

Appendix A Weibull Tensile Data

Weibull statistics were used an additional characterisation of the single filament tensile data. The following figures show the tensile data for each fibre sample tested, grouped by fibre, as histograms and Weibull probability plots. Overlaid on the histogram, in red, is the Weibull distribution for that fibre sample. This visual helps to show the appropriateness of the fitting of a Weibull distribution and where gaps in the data lay if it were assumed the data should follow a Weibull distribution. Minitab also provides a P-value for the fit, where P-values of <0.05 (for 95% confidence levels) suggest the data does not fit the Weibull distribution. Seven samples did not follow the Weibull distribution: T7_40min_550C_10% O_2, T7_30min_600C_15.5% O_2, T8_20min_650C_air, T8_40min_650C_10% O_2, AS4_20min_650C_10% O_2, V-IM7, and IM7_20min_550C_air. AS4_20min_600C_10% O2 only has seven filaments included in the analysis which is clearly too few. The remainder of the aforementioned samples were not overly short on the number of filaments included in the analysis.

An alternative way of showing the Weibull distribution is plotting it as a probability distribution function. This form of plotting, plus showing the bounds of the 95% confidence interval, is also included here. The size of the confidence interval and the deviation of the data points from the line showing the calculated failure probability help to show how good the fit is and can be used to compare the fit quality between samples. For a numeric comparison the Anderson Darling (AD) statistic is used. A lower AD number indicates a better fit however AD numbers that are close may have the same fit quality. AS4 and IM7 fibre samples, especially at

600°C and 650°C, show larger confidence intervals and more deviation from the computed Weibull probabilities than the other fibre samples.

There does not seem to be a pattern to which fibre samples do not follow the Weibull distribution. When a fibre sample does not fit a 2-parameter Weibull distribution additional filaments could be tested and or a 3-parameter model could be used in hopes of increasing the fit quality. The probability distribution plots seen below show the largest deviations at low tensile strength which was also reported by Thomason [96]. Thomason showed the use of a 3-parameter Weibull distribution to include a threshold stress below which fibres did not break would help identify which filaments are truly outliers and improve the fit quality. Outliers could then be removed from the analysis as long as a repeatable procedure for picking the threshold parameter and the removal of outliers is in place. Additional testing may be needed to maintain a high number of filaments in the analysis if outliers are being removed. To make the Weibull distribution fit better or to provide a more accurate indication of strength and variability it may be used with different ranking estimators or by the use of the three parameter distribution as already discussed. However, if this is not done for all fibre samples it may make comparisons between fibre samples more difficult.

The 2-parameter Weibull distribution may not always be the most appropriate distribution to use for reporting strengths based on single filament testing of carbon fibre especially as some fibres are so weak they break during sample preparation or the test setup, whereas the use of the 2-parameter Weibull distribution assumes that fibres with the full range of strengths are captured during the testing [96]. Further analysis using Weibull may show how one sample is significantly different from another or may show that there is a unique set of recycling conditions that result in the fibres not following the Weibull distribution. When in the future a recycling process is being optimised to provide fibres with the highest possible tensile strength the use of Weibull can be more critical and every aspect of the data reduction scrutinized to try and provide the most accurate value for fibre tensile strength. For comparative studies such as this one, Weibull can be used as a tool and guide without as much scrutiny or risk in false conclusions.

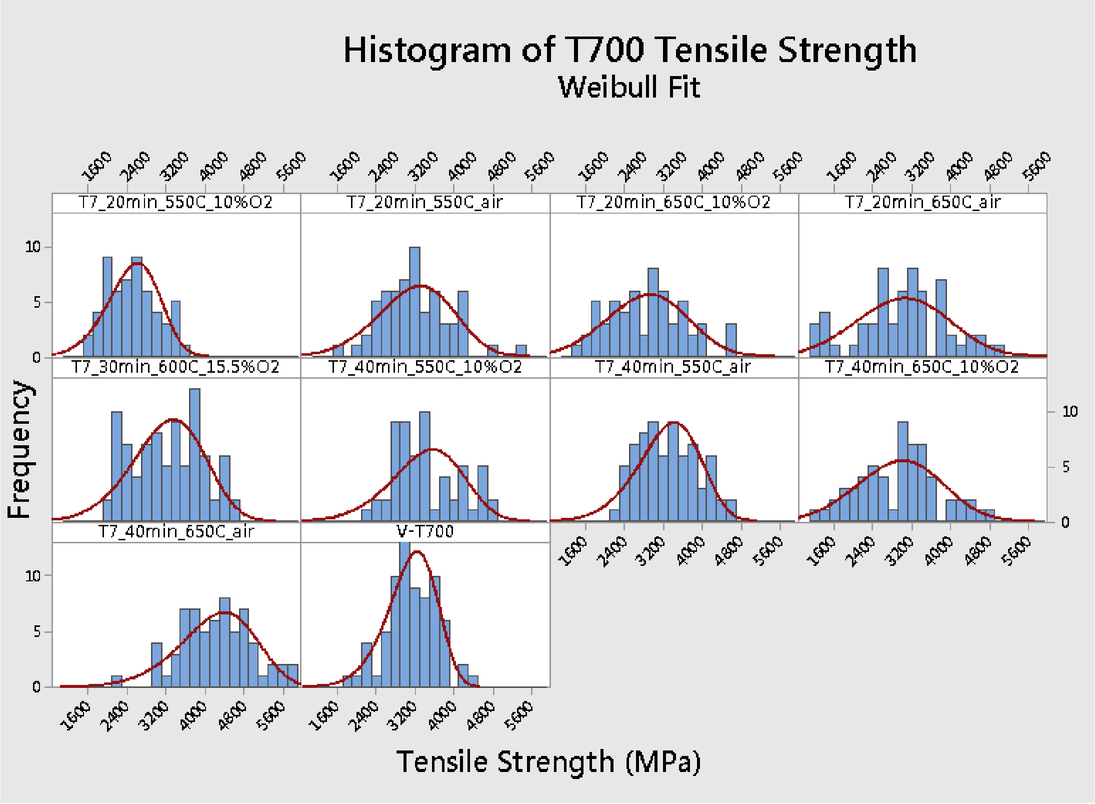

Figure 105. 2 parameter Weibull distribution overlaid on histogram of tensile strength for T700 fibres. Shape and Scale parameters as well as number of samples listed below in Table 36.

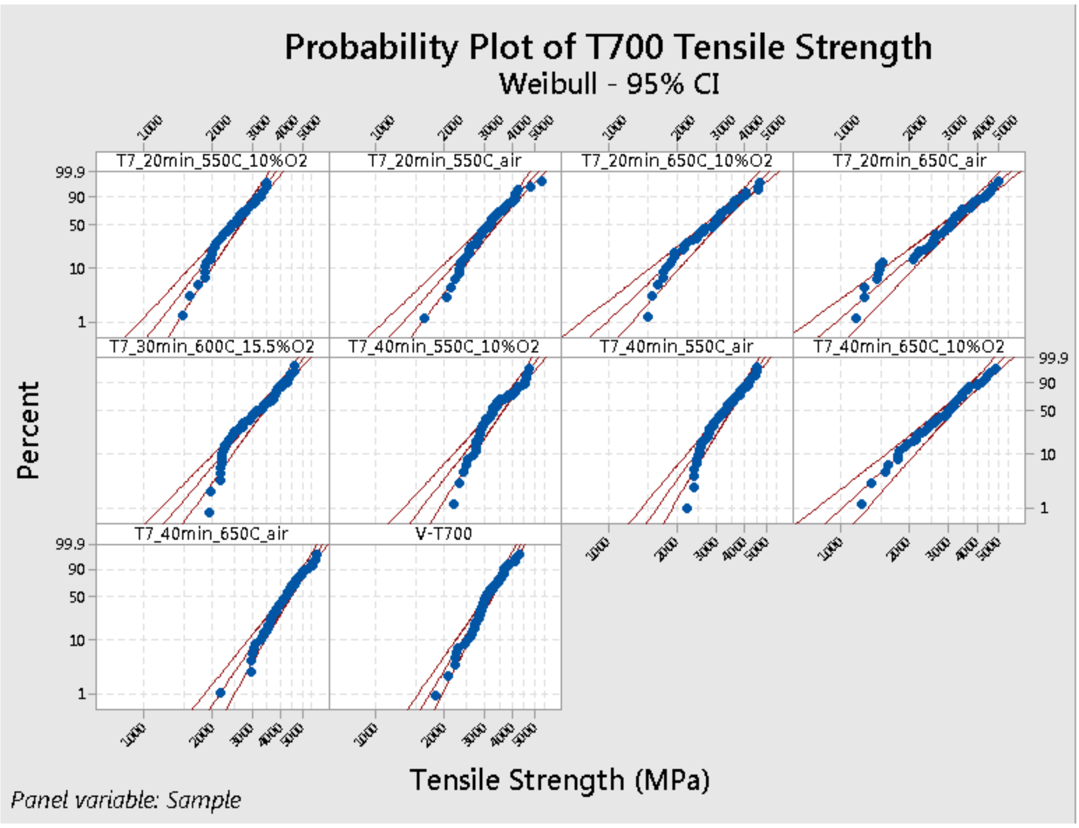

Figure 106. Weibull probability plots including confidence intervals for T700 fibres. Anderson Darling (AD) goodness of fit statistic and p-values shown below in Table 36. Lower AD values suggest better fits. P-values of <0.05 indicate data does not follow a Weibull distribution.

Table 36. Weibull Distribution fit summary for T700 fibres

20min_550C_10%O_2 Shape: 5.5 Scale: 2729 N: 56 AD: 0.462 P-value: 0.249	20min_550C_air Shape: 4.76 Scale: 3.498 N: 62 AD: 0.631 P-value: 0.096	20min_650C_10%O_2 Shape: 3.98 Scale: 3160 N: 58 AD: 0.338 P-value: >0.250	20min_650C_air Shape: 3.69 Scale: 3343 N: 62 AD: 0.412 P-value: >0.250
30min_600C_15.5%O_2 Shape: 5.06 Scale: 3519 N: 85 AD: 0.793 P-value: 0.039	40min_550C_10%O_2 Shape: 5.43 Scale: 3718 N: 59 AD: 1.486 P-value: <0.010	40min_550C_air Shape: 5.96 Scale: 3551 N:71 AD: 0.698 P-value: 0.068	40min_650C_10%O_2 Shape: 3.94 Scale: 3255 N: 59 AD: 0.261 P-value: >0.250
40min_650C_air Shape: 6.27 Scale: 4540 N: 65 AD: 0.362 P-value: >0.250	V-T700 Shape: 7.07 Scale: 3329 N: 77 AD: 0.687 P-value: 0.073		

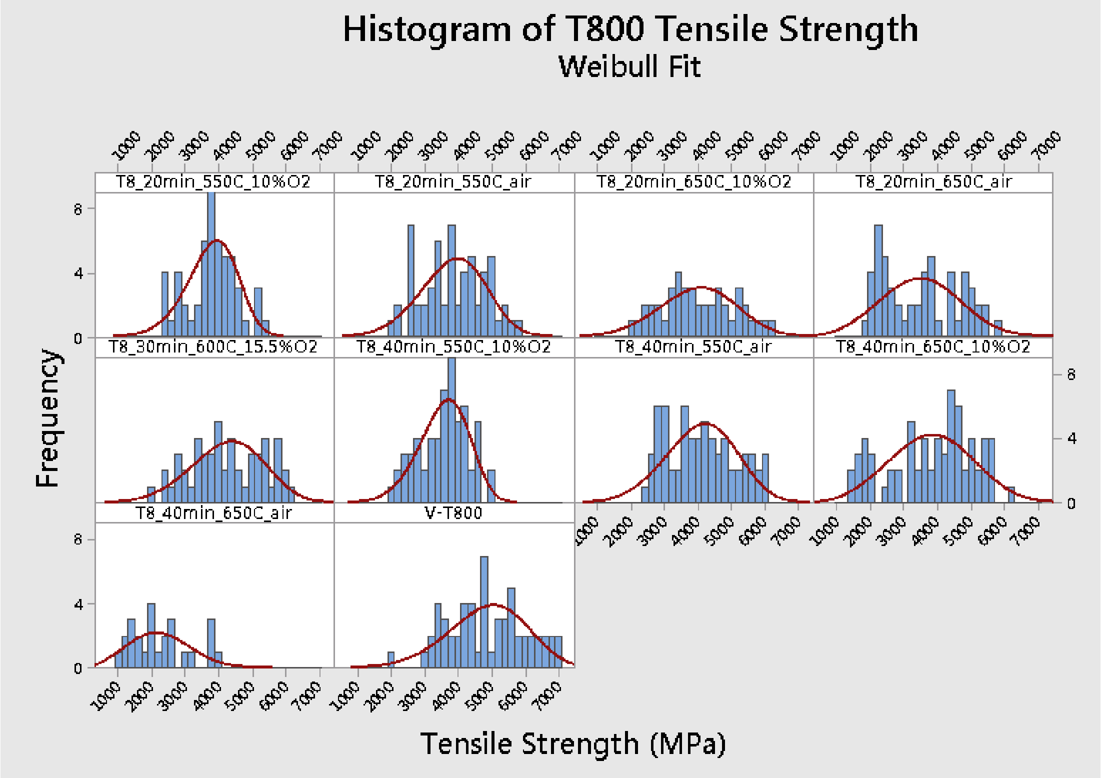

Figure 107. 2 parameter Weibull distribution overlaid on histogram of tensile strength for T800 fibres. Shape and Scale parameters as well as number of samples listed below in Table 37.

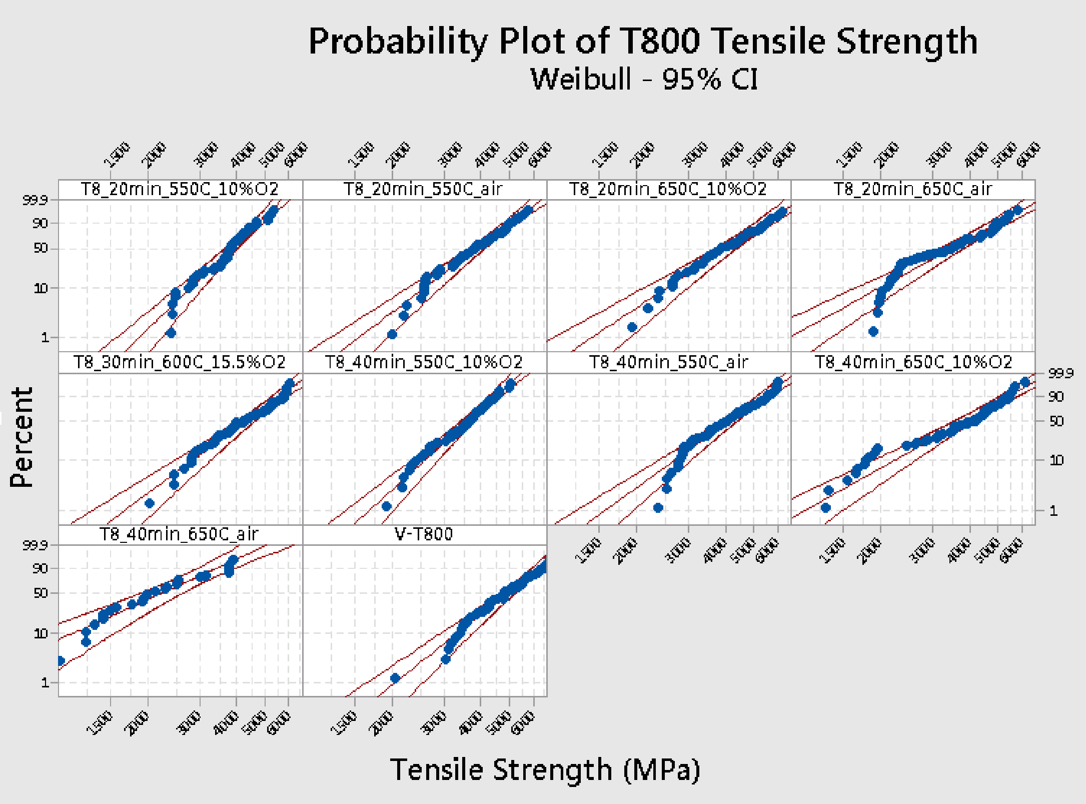

Figure 108. Weibull probability plots including confidence intervals for T800 fibres. Anderson Darling (AD) goodness of fit statistic and p-values shown below in Table 37. Lower AD values suggest better fits. P-values of <0.05 indicate data does not follow a Weibull distribution.

Table 37. Weibull Distribution fit summary for T800 fibres

20min_550C_10% Shape: 5.89 Scale: 4114 N: 56 AD: 0.642 P-value: 0.091	20min_550C_air Shape: 4.61 Scale: 4226 N: 59 AD: 0.304 P-value: >0.250	20min_650C_10%O_2 Shape: 4.070 Scale:4405 N: 43 AD: 0.246 P-value: >0.250	20min_650C_air Shape: 3.347 Scale: 3882 N: 54 AD: 1.20 P-value: <0.01
30min_600C_15.5%O_2 Shape: 4.52 Scale: 4694 N: 52 AD: 0.474 P-value: 0.238	40min_550C_10%O2 Shape: 5.59 Scale: 3880 N: 59 AD: 0.219 P-value: >0.250	40min_550C_air Shape: 4.45 Scale: 4478 N: 65 AD: 0.709 P-value:0.063	40min_650C_10%O_2 Shape: 3.45 Scale: 4256 N: 67 AD: 1.14 P-value: <0.010
40min_650C_air Shape: 2.783 Scale: 2538 N: 25 AD: 0.595 P-value: 0.117	V-T800 Shape: 4.852 Scale: 5333 N: 57 AD: 0.310 P-value: >0.250		

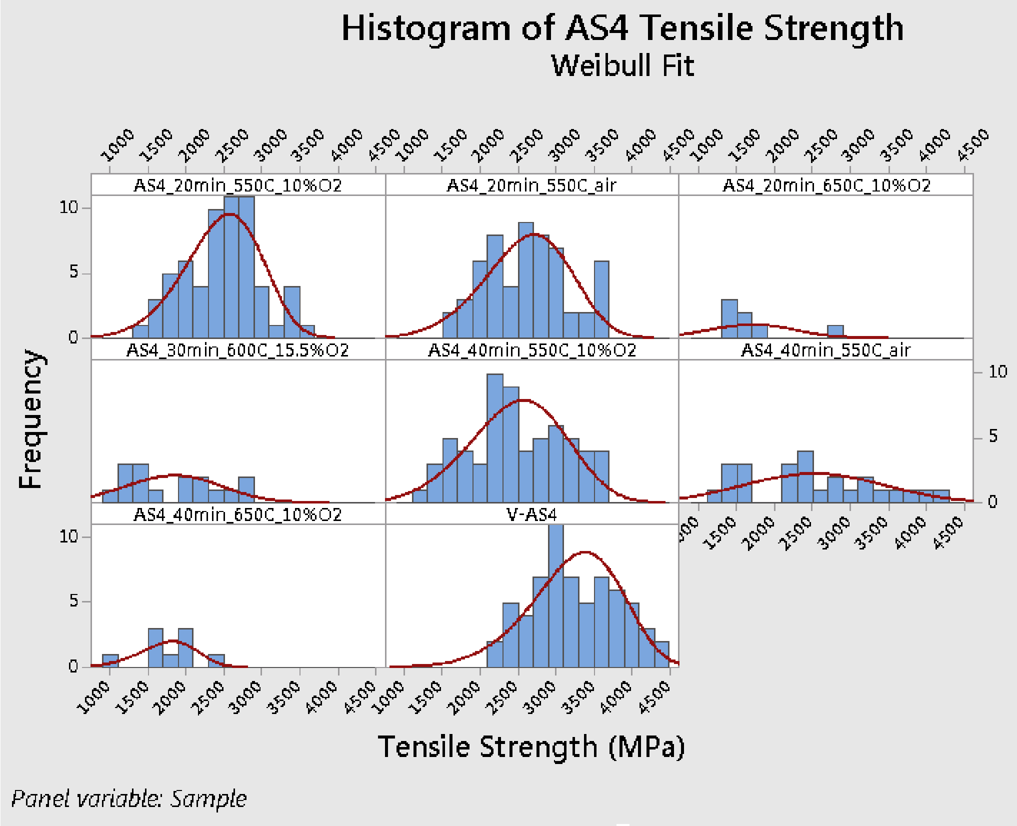

Figure 109. 2 parameter Weibull distribution overlaid on histogram of tensile strength for AS4 fibres. Shape and Scale parameters as well as number of samples listed below in Table 38.

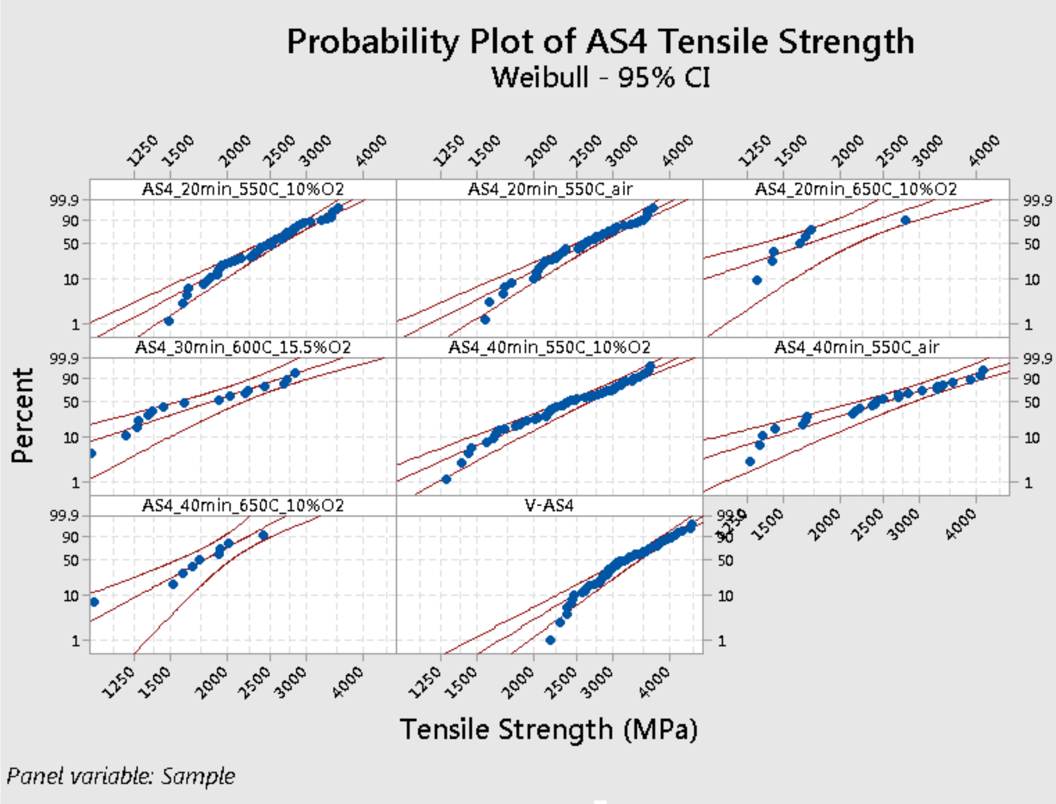

Figure 110. Weibull probability plots including confidence intervals for AS4 fibres. Anderson Darling (AD) goodness of fit statistic and p-values shown below in Table 38. Lower AD values suggest better fits. P-values of <0.05 indicate data does not follow a Weibull distribution.

Table 38. Weibull Distribution fit summary for AS4 fibres

20min_550C_10% Shape: 5.62 Scale: 2678 N: 61 AD: 0.424 P-value: >0.250	20min_550C_air Shape: 5.286 Scale: 2832 N: 57 AD: 0.518 P-value: 0.197	20min_650C_10%O_2 Shape: 3.583 Scale: 1890 N: 7 AD: 0.870 P-value: 0.020
30min_600C_15.5%O_2 Shape: 3.46 Scale: 2057 N: 16 AD: 0.532 P-value: 0.172	40min_550C_10%O_2 Shape: 4.53 Scale: 2727 N: 63 AD: 0.489 P-value: 0.224	40min_550C_air Shape: 3.243 Scale: 2840 N: 25 AD: 0.299 P-value: >0.250
40min_650C_10%O_2 Shape: 5.55 Scale: 1900 N: 9 AD: 0.248 P-value: >0.250	V-AS4 Shape: 6.3 Scale: 3488 N: 66 AD: 0.617 P-value: 0.105	

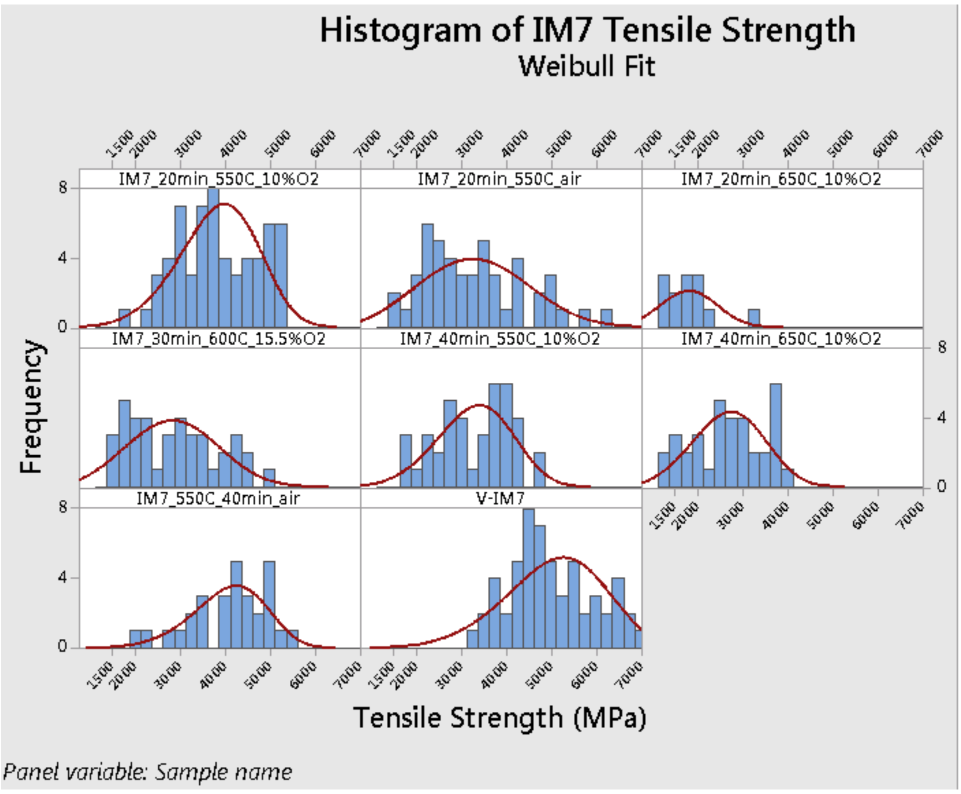

Figure 111. 2 parameter Weibull distribution overlaid on histogram of tensile strength for IM7 fibres. Shape and Scale parameters as well as number of samples listed below in Table 39.

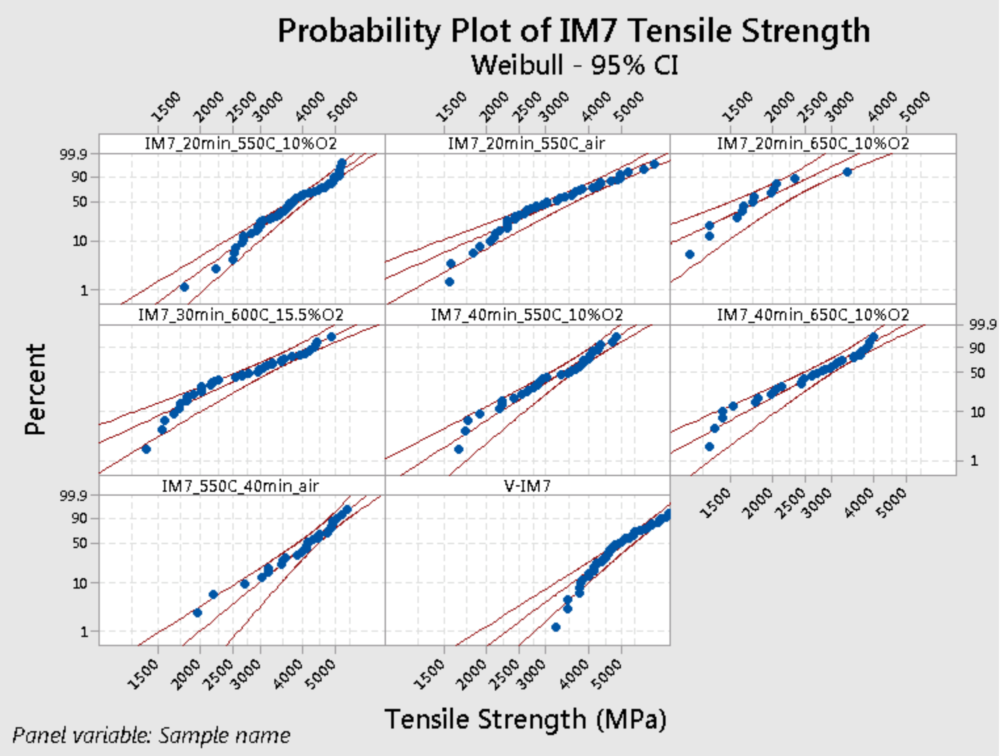

Figure 112. Weibull probability plots including confidence intervals for IM7 fibres. Anderson Darling (AD) goodness of fit statistic and p-values shown below in Table 39. Lower AD values suggest better fits. P-values of <0.05 indicate data does not follow a Weibull distribution.

Table 39. Weibull Distribution fit summary for IM7 fibres

20min_550C_10%O_2 Shape: 5.03 Scale: 4186 N: 63 AD: 0.756 P-value: 0.046	20min_550C_air Shape: 3.12 Scale:3707 N: 48 AD: 0.591 P-value: 0.127	20min_650C_10%O_2 Shape: 3.37 Scale: 2024 N: 13 AD: 0.642 P-value: 0.083
30min_600C_15.5%O_2 Shape: 3.23 Scale: 3191 N: 39 AD: 0.621 P-value: 0.098	40min_550C_10%O_2 Shape: 4.5 Scale: 3610 N: 40 AD: 0.611 P-value: 0.106	40min_650C_10%O_2 Shape: 3.86 Scale: 2979 N: 35 AD: 0.403 P-value: >0.250
40min_550C_air Shape: 5.79 Scale: 4410 N: 29 AD: 0.328 P-value: >0.250	V-IM7 Shape: 5.25 Scale: 5511 N: 58 AD: 0.882 P-value: 0.022	